Coorong nutrient cycling and fluxes

Jianyin (Leslie) Huang, David Welsh, Dirk Erler, Angus Ferguson, Justin Brookes, Chris Keneally, Daniel Chilton, Sabine Dittmann, Orlando Lam-Gordillo, Matilda Southgate, Stuart Simpson, Luke Mosley

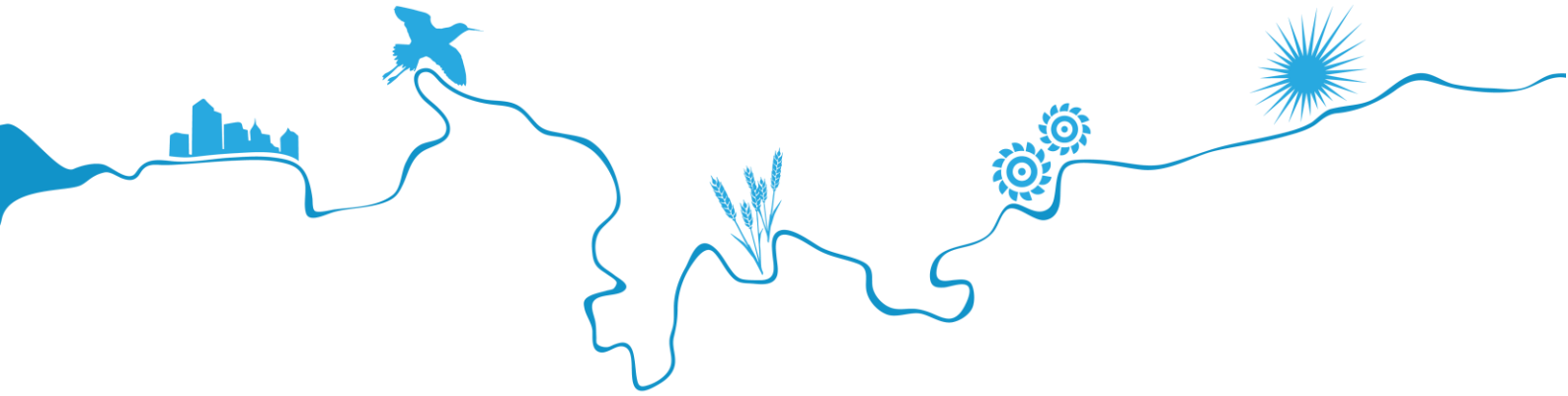

Goyder Institute for Water Research
Technical Report Series No. 22/07

GOYDER INSTITUTE FOR WATER RESEARCH

www.goyderinstitute.org

Goyder Institute for Water Research Technical Report Series ISSN: 1839-2725

The Goyder Institute for Water Research is a research alliance between the South Australian Government through the Department for Environment and Water, CSIRO, Flinders University, the University of Adelaide and the University of South Australia. The Institute facilitates governments, industries, and leading researchers to collaboratively identify, develop and adopt innovative solutions for complex water management challenges to ensure a sustainable future.

This program is part of the South Australian Government's Healthy Coorong, Healthy Basin Program, which is jointly funded by the Australian and South Australian governments.

Enquires should be addressed to: Goyder Institute for Water Research
The University of Adelaide (Manager)
209A, Level 2 Darling Building, North Terrace,
Adelaide, SA 5000
tel: (08) 8313 5020
e-mail: enquiries@goyderinstitute.org

Citation

Huang J, Welsh D, Erler D, Ferguson A, Brookes J, Keneally C, Chilton D, Dittmann S, Lam-Gordillo O, Southgate M, Simpson S, Mosley LM (2022) *Coorong nutrient cycling and fluxes.* Goyder Institute for Water Research Technical Report Series No. 22/07.

Disclaimer

This report has been prepared by the University of South Australia, the University of Adelaide, CSIRO and Flinders University and reviewed in accordance with the publication protocols of the Goyder Institute for Water Research. The report contains independent scientific/technical advice to inform government decision-making. The independent findings and recommendations of this report are subject to separate and further consideration and decision-making processes and do not necessarily represent the views of the Australian Government or the South Australian Department for Environment and Water. The Goyder Institute and its partner organisations do not warrant or make any representation regarding the use, or results of the use, of the information contained herein about its correctness, accuracy, reliability, currency or otherwise and expressly disclaim all liability or responsibility to any person using the information or advice. Information contained in this document is, to the knowledge of the project partners, correct at the time of writing.

Contents

Figures

Tables

Respect and reconciliation

Aboriginal people are the First Peoples and Nations of South Australia. The Coorong, connected waters and surrounding lands have sustained unique First Nations cultures since time immemorial.

The Goyder Institute for Water Research acknowledges the range of First Nations' rights, interests and obligations for the Coorong and connected waterways and the cultural connections that exist between Ngarrindjeri Nations and First Nations of the South East peoples across the region and seeks to support their equitable engagement.

Aboriginal peoples' spiritual, social, cultural and economic practices come from their lands and waters, and they continue to maintain their cultural heritage, economies, languages and laws which are of ongoing importance.

Executive summary

The Phase One Trials and Investigations (T&I) Project of the Healthy Coorong, Healthy Basin (HCHB) Program consists of a series of integrated components that will collectively provide knowledge to inform the future management of the Coorong. *Component 1 – Understanding Coorong nutrient dynamics* forms part of the T&I Project. There are four activities within Component 1. The aim of Component 1 Activity 1.3 described in this report was to investigate "nutrient cycling and fluxes" in the Coorong, via:

- a sediment quality survey to assess the distribution of key parameters
- experiments (*in* and *ex situ*) to determine the influence of different environmental conditions on nutrient cycling and fluxes
- developing an understanding of the microbial ecology, in particular the role of denitrification (a key nitrogen loss pathway in healthy systems)
- an assessment of the influence of benthic macroinvertebrates on nutrient dynamics and redox conditions
- assessing the impacts of sediment resuspension on nutrient dynamics.

Prior to this investigation there was a large knowledge gap on the fate and cycling of nutrients within the system. This final report provides substantial new information on how nutrients are cycling in the Coorong, and interactions with environmental and ecological components of the Coorong.

Multiple lines of evidence confirm that the sediment quality and nutrient cycling processes are currently in an 'unhealthy' state, due to a combination of factors. Key findings of the investigations from 2020-2021 that supported this conclusion were:

- High total nutrient and organic carbon concentrations in the sediment and water of the South Lagoon and southern region of the North Lagoon
- High ammonium levels in sediment pore water and high flux rates to the water column from the South Lagoon, which provides the "fuel" for algal growth
- Limited nitrate availability and a lack of coupled nitrification-denitrification activity, which removes nitrogen from the system (in gaseous form)
- High levels of sulfide in both shallow and deeper sediments of the South Lagoon, indicative of highly anoxic conditions
- High sediment oxygen demand in deeper sites of the South Lagoon
- An absence of macroinvertebrates in the South Lagoon, which can burrow and oxygenate sediment
- Rapid (weeks) recolonisation by burrowing invertebrates and a large improvement in sediment quality following an experimental translocation of hostile (hypersaline and sulfide-rich) sediment from the South Lagoon to the North Lagoon
- Resuspension of organic-rich deeper sediments increasing water column turbidity and total nutrient concentrations during strong wind events in the South Lagoon, while dissolved nutrient release was low.

Overall these findings are symptomatic of highly eutrophic (organic and nutrient-enriched) sediment and water conditions with impaired nutrient cycling processes. Coupled with the limited flushing of the South Lagoon, the current state of nutrient cycling processes is promoting nutrient retention and eutrophication. A consequence of longer water residence times currently observed in the Coorong when compared to natural (I.e. higher River Murray inflow) conditions, is an increase in the relative importance of various internal biogeochemical processes. This results in enhanced sediment:water flux and rapid recycling of bio-available nutrients under eutrophic and anoxic sediment conditions. This appears to be the case in the Coorong as there are very high total nutrient and algal levels, but low dissolved nutrients.

There was evidence of improved sediment quality and nutrient cycling where *Ruppia* was present in the South Lagoon, and where bioturbating macroinvertebrates were present in the North Lagoon. This suggests that if South Lagoon water quality can be improved sufficiently (e.g. salinity < 60 PSU) to enable these ecosystem components to thrive, then the functions they provide (e.g. oxygenation of sediment, nitrification-denitrification) will be able to further assist to restore healthier water and sediment conditions.

The findings of the investigation help to resolve current uncertainties in nutrient cycling and fluxes in the Coorong. The studies have provided key nutrient flux and process data to parameterise the biogeochemical model of the T&I Project *Component 7 - Integration*. By reducing key uncertainties on nutrient flux rates and processes the biogeochemical model can be used to more confidently assess scenarios to achieve a 'regime shift' back towards an aquatic plant dominated ecosystem, rather than the current algal dominated ecosystem. Ecosystem restoration options involving *Ruppia* and macroinvertebrates will also be better informed. Another related key output will be scientifically defensible advice on how to reduce nutrient availability to algae which will be provided as part of Activity 1.4 'Assessment of nutrient removal options in the Coorong'.

Acknowledgments

This project is part of the South Australian Government's Healthy Coorong, Healthy Basin Program, which is jointly funded by the Australian and South Australian governments.

We acknowledge the Coorong fishermen Garry Hera-Singh and Glen Hill for assistance with boating operations and sharing their expert local and historical knowledge for this research.

This report is dedicated to the memory of our dear colleague Prof. Peter Teasdale who was leading this project component until he unfortunately passed away. He is sorely missed but leaves an ongoing legacy in the hearts and minds of those of us fortunate to know and work with him.

Prof. Peter Teasdale on the Coorong during this project (Photo: Luke Mosley)

1 Introduction

1.1 Background

The Coorong is culturally, environmentally and economically important at local, national and international scales but has experienced a long-term decline in its ecological condition due to reductions in inflows. Whilst there has been recovery of some elements of the Coorong ecosystem associated with increased inflows since the Millennium Drought, the South Lagoon has not recovered to the levels expected. There has been a switch of the ecosystem from being dominated by aquatic plants to algae associated with eutrophication (nutrient enrichment), with subsequent impacts on invertebrates, fish and waterbirds. These changes in the ecosystem and the lack of recovery is likely caused by a number of complex, interacting factors, which are not well understood. This is limiting the capacity to forecast the ecological response to future management scenarios and therefore the capacity of water managers to identify management interventions required to improve the health of the Coorong.

The Phase One Trials and Investigations (T&I) Project of the Healthy Coorong, Healthy Basin (HCHB) Program consists of a series of integrated components that will collectively provide knowledge to inform the future management of the Coorong. *Component 1 – Understanding Coorong nutrient dynamics* forms part of the T&I Project. Through assessments of the relative importance of external and internal nutrient sources and processes within the Coorong, the research aims to provide a holistic understanding on how the nutrient load in the Coorong could be lowered to improve management. T&I Component 1 comprises four main activities as shown in Figure 1. The main research activities and linkages in the *Understanding Coorong nutrient dynamics* component of the Healthy Coorong, Healthy Basin Trials and Investigations Project..

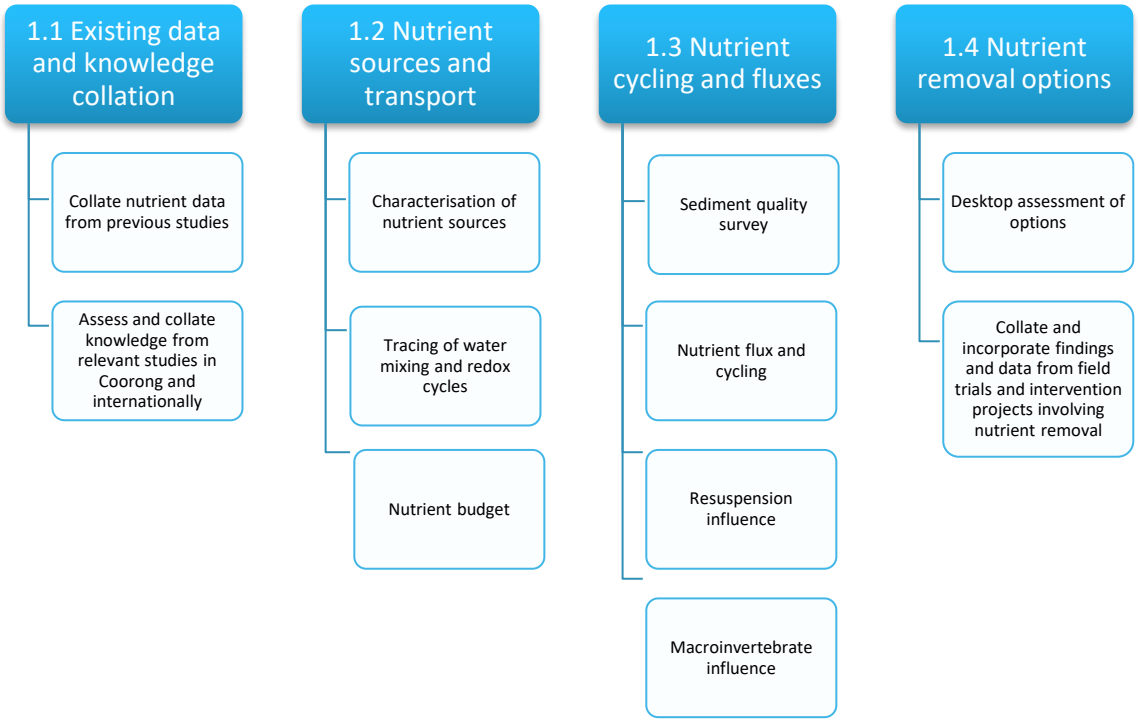

Figure 1. The main research activities and linkages in the *Understanding Coorong nutrient dynamics* component of the Healthy Coorong, Healthy Basin Trials and Investigations Project.

1.2 Aims

The shift from aquatic plants such as *Ruppia* sp. to algae in the Coorong is considered to be partly due to elevated nutrient levels in the water column and sediments (Mosley et al. 2020). While there is a reasonable

understanding of surface water sources of nutrients, there is limited understanding of the fate and cycling of nutrients within the system. The relative importance of external and internal nutrient sources and sinks, and the role of internal nutrient cycling influencing the availability of nutrients to algae and aquatic plants, is currently unclear. While concentrations of dissolved nutrient levels are typically low, it is thought that this may be because of rapid nutrient recycling and uptake by algae, which contributes to the maintenance of a nutrient and organic enriched "eutrophic" state. Nutrient cycling is likely to be strongly influenced by macroinvertebrates and microbes (Welsh 2003), but little is known about how these parts of the ecosystem are functioning in the Coorong.

The aim of Activity 1.3 '*Nutrient cycling and fluxes*' was to investigate the nutrient cycling and flux dynamics in the Coorong, via assessments of:

- sediment quality;
- nutrient cycles and fluxes under different environmental conditions;
- the influence of different ecological communities on nutrient cycling and fluxes;
- the influence of benthic macroinvertebrates on nutrient dynamics and redox conditions; and
- impacts of sediment resuspension on nutrient dynamics.

The aim of Activity 1.3 is to resolve current uncertainties in nutrient cycling and fluxes in the Coorong. In doing so it will provide key nutrient flux and cycling data to parameterise the biogeochemical model of the T&I Project *Component 7 - Integration*. This will reduce key uncertainties on nutrient flux rates and processes so that the model can be used to more confidently assess scenarios to achieve a "regime shift" back towards an aquatic plant dominated ecosystem, rather than an algal dominated ecosystem.

All the activities in Component 1 are interlinked. A synthesis of historical data and literature was provided in Activity 1.1 (Mosley et al. 2020). External sources and transport of nutrients was assessed in Activity 1.2 (Priestley et al. 2022a). Another key output is scientifically defensible advice on how to reduce nutrient availability to algae, provided as part of Activity 1.4 'Assessment of nutrient removal options' in the Coorong (Mosley et al. 2022).

2 Methods

2.1 Bulk sediment quality

A surface bulk sediment survey was undertaken from 11–13 March 2020. A total of 50 sites were surveyed along the Coorong North and South lagoons (Figure 2). Most sites were underwater at the time of sampling, which occurred in water depths ranging from approximately 0.5–4.5 m. Sediment cores were collected from submerged sites with a Russian D auger attached to an aluminium extension pole. The auger was pushed vertically into the sediment to a depth of approximately 0.5 m, where possible, and rotated to collect the core sample. Sub-samples for detailed laboratory analysis were collected only from the 0–5 cm surface layer of the sediment core, placed in a plastic vial with no air gap, immediately stored in an ice box, and frozen within 8 hours of sampling.

Additionally, some shallow shoreline samples (e.g. < 0.7 m depth) were collected with an acrylic tube pushed into the sediment. At a shoreline site at Noonameena, additional sediment layers were sampled to approximately 0.3 m depth to correlate to benthic macroinvertebrate sampling at this site. The sub-samples were homogenised and immediately placed in sealed vials with no air gap and cooled on ice. Upon return to the laboratory, samples were frozen at -20 °C until analysis.

Immediately after collection, each sediment core was described using visual indicators from the Rapid Assessment Protocol (RAP) of Hallett et al. (2019). The RAP assigns scores from 1 to 5 based on sediment colour, texture and odour criteria (Table 1). These criteria and score categories are based on common sediment quality indicators relating to sediment nutrient enrichment. Low scores indicate poorer sediment

quality for each criterion. The scores for individual criteria were summed to produce a total RAP score. The apparent redox potential discontinuity was also measured in each core to estimate the depth of the oxic and sub-oxic zones in the sediment. This was based on the depth of yellow-brown colouration at the top of the sediment, indicating the likely presence of iron oxides.

Table 1. Rapid Assessment Protocol criteria (from Hallett et al. 2019) used for sediment samples.

CRITERIA	SCORE				
	5	4	3	2	1
Colour	Yellow/brown to depth of core	Yellow/brown overlying grey	Yellow/brown overlying black	Grey to depth of core	Black to depth of core
Texture	Coarse grainy	Fine grainy		Smooth and silky	Oozy and slick/sticky
Odour	No H_2S odour	Mild H_2S odour		Moderate H_2S odour	Strong H_2S odour

A sub-set of 26 of the 50 samples received detailed laboratory analysis at the Environmental Analysis Laboratory, Lismore, Australia; a NATA accredited laboratory. Total phosphorus was measured via the total acid extractable phosphorus method (Rayment and Lyons 2011). Total carbon and nitrogen were measured via high temperature combustion and infra-red detection using a LECO CNS TruMAC Analyser. Total organic carbon (%Corg) was measured using the same analytical method following pre-treatment of the sample with dilute hydrochloric (HCl) acid added to remove inorganic carbon. Electrical conductivity (EC) and pH were measured on a 1:5 soil:water extract using methods from Rayment and Lyons (2011) (4A1 and 4B1 methods respectively). Wet samples were analysed for Acid Volatile Sulfur (AVS; iron monosulfide and free sulfides) using the methods of Sullivan et al. (2018), and adjusted to dry weight using the moisture content measured by loss of mass via drying at 105 °C. The hydrometer analysis method was used to determine the sediment texture (percentages of sand, silt and clay) using the method of Gee and Bauder (1986). A texture classification was made based on the hydrometer results and the appropriate texture triangle.

Total metals were determined following aqua regia digestion (1:3 concentrated nitric/HCl - standard method APHA 3125) (APHA 1992) of dried sediment samples with metals analysed by inductively coupled plasma mass spectrometry (ICP-MS). A significant portion of the total metal concentration (extracted using these concentrated acids) may not be bioavailable to organisms. Hence the 'maximum bioavailable metal concentration' was also determined by dilute-acid (1 mol/L HCl) cold extraction, see Simpson and Batley (2016) on a separate wet sediment sample. The samples were also analysed via ICP-MS.

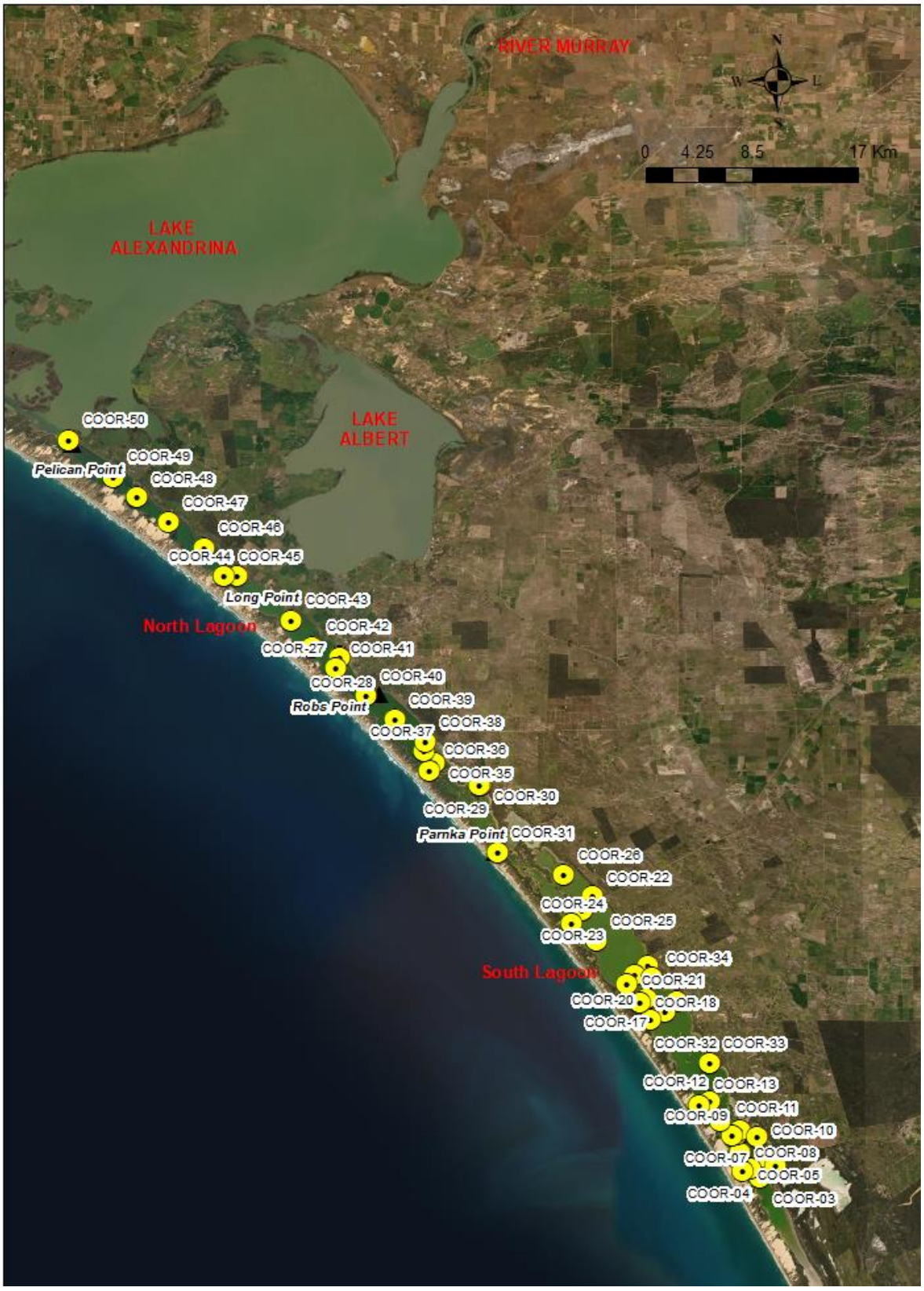

Figure 2. Sediment quality survey (March 2020) sampling sites in the Coorong. Yellow circles indicate sampling sites and black text within white background are corresponding site names.

2.2 Nutrient cycling and fluxes

2.2.1 Passive samplers to determine sediment quality across sediment types and seasons

Sediment sampling and experimental set up

Between November 2020 and March 2021, sediment cores were collected from various sites covering the diversity of sediment types and ecosystems in the North and South lagoons (Table 2 and Figure 3). At each site, 5–10 sediment cores (100 mm internal diameter (internal diameter) × 250 mm depth) were collected in PVC tubes. Sediment cores were closed top and bottom with lids and transported to either a greenhouse at the University of South Australia, Mawson Lakes campus within 5–6 hours of sampling, or a local research base (Cantara homestead) within 2 hours of collection. The sediment cores were transferred into 50 L plastic tubs, the top lids of the cores were removed, and tubs were filled with surface water from the respective sampling sites so that the sediments were immersed to a depth of 5 cm. Water was continually aerated to maintain oxygen saturation and water circulation, simulating natural conditions in the Coorong. The sediments were maintained under natural light-dark conditions, except for those from deep sites, which were covered by black plastic sheets to simulate the constant dark conditions that occur at these depths. The cores were incubated for at least 24 hours and allowed to stabilise before diffusive gradients in thin films (DGT) and diffusive equilibrium in thin films (DET) deployment.

For the field trip conducted at Woods Well in November 2021 changes in porewater chemistry and sediment water column fluxes were measured using *in situ* benthic chambers. The DET probes were also deployed *in situ* in the field.

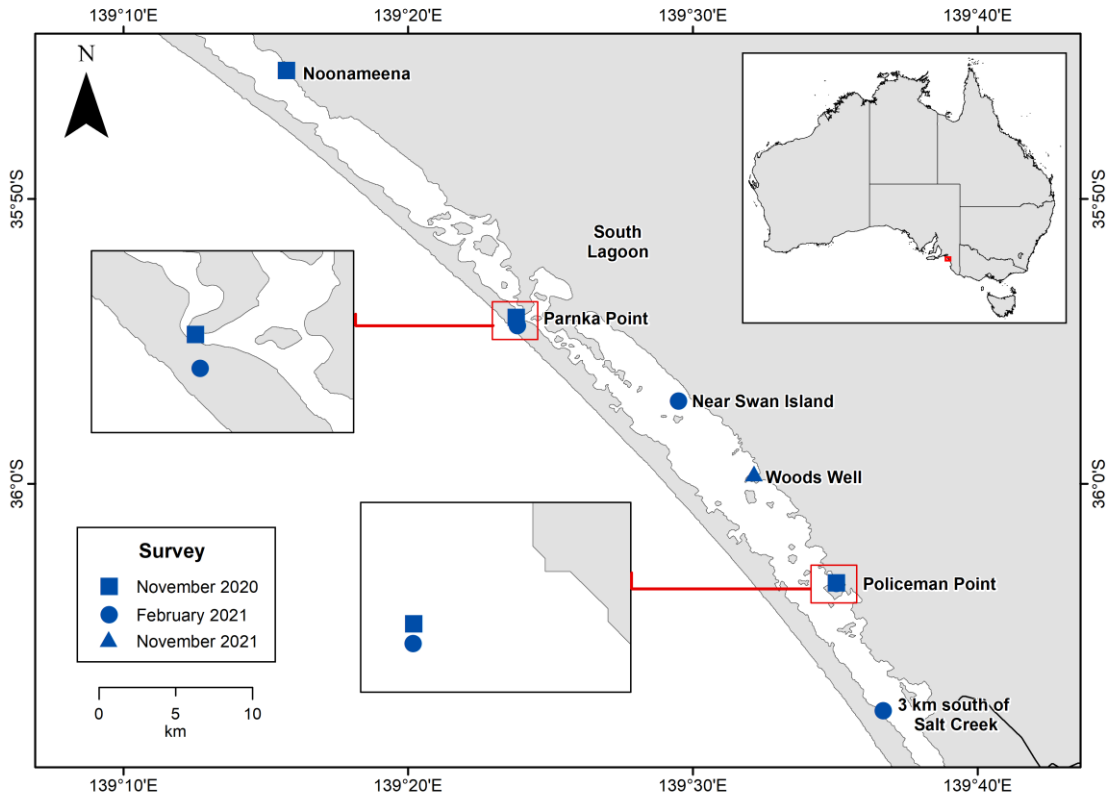

Figure 3. Site locations for passive sampler sediment collection and *in situ* experiments.

Table 2. Information for the sampling sites, time, water depth, sediment condition and experimental set up. DGT: diffuse gradients in thin films technique. DET: diffuse equilibrium in thin films technique.

SITE	MONTH	WATER DEPTH	SEDIMENT DESCRIPTION	EXPERIMENT	LATITUDE	LONGITUDE
Noonameena	November 2020	Shallow, ≤0.05 m	Sandy, burrowing organisms	DGT/DET	-35.7581	139.2621
Parnka Point	November 2020	Shallow, 0.1–0.4 m	Colonised by *Ruppia*, 1–2 cm hard shell grit layer in the middle, muddy at the bottom	DGT/DET and core incubations for oxygen and nutrient fluxes	-35.9026	139.3967
Policeman's Point	November 2020	Shallow, 0.4–0.5 m	Colonised by *Ruppia*, muddy sediment	DGT/DET	-36.0578	139.5840
Parnka Point	February 2021	Shallow, 0.4–0.5 m	Muddy sediment, 1–2 cm hard shell grit layer in the middle. Many cores with more than 5 cm jet black layer	DGT/DET and core incubations for oxygen and nutrient fluxes	-35.9073	139.3974
Policeman's Point	February 2021	Shallow, 0.4–0.5 m	Fine sand and no *Ruppia*. Sediment cores have 0.5–1 cm yellow oxic layer, followed by 3–5 cm jet black colour sediment, then grey colour to the bottom	DGT/DET and core incubations for oxygen and nutrient fluxes	-36.0582	139.5840
South of Salt creek	February 2021	Deep, 1.5 m	Black muddy sediment and very soft	DGT/DET and core incubations for oxygen and nutrient fluxes	-36.1328	139.6114
Near Swan Island	February 2021	Deep, 1 m	Black muddy sediment and very soft	DGT/DET and core incubations for oxygen and nutrient fluxes	-35.9516	139.4917
Woods Well	November 2021	Shallow, 0.4–0.5 m	Colonised by *Ruppia*, sandy sediment	*In situ* DET deployments and benthic chamber determination of oxygen and nutrient fluxes over a diel cycle	-35.9939	139.5358

Passive sampler probe preparation, deployment, retrieval and processing

DGT and DET techniques were deployed to study sediment pore water chemistry in the sediment cores. These are well-established *in situ* passive sampling techniques that are useful for obtaining high resolution measurements of porewater solutes, applied here *ex situ* (Davison et al. 1997; Davison et al. 1991; Huang et al. 2019; Kankanamge et al. 2020; Krom et al. 1994; Pagès et al. 2012; Robertson et al. 2008). All sediment DGT and DET probes were purchased from DGT Research (Lancaster, UK). The sediment probes have dimensions of 5 x 240 x 40 mm, with an open window of 18 x 150 mm. Combined DET-DGT probes were applied for simultaneous sulfide and iron measurements. The DET-DGT probes consisted of 0.2 mm silver iodide (AgI) binding gel layer, and 0.8 mm diffusive gel layer, which also served as the iron DET, made from bisacrylamide, followed by a 0.1 mm polyethersulphone filter membrane with 0.45 µm pore size. For the *in situ* experiment conducted at Woods Well, the DET-DGT probes were replaced by the combined DET-DET probes for sulfide and iron (Kankanamge et al. 2020), which consisted of two 0.6 mm diffusive gel layers made from bisacrylamide and 0.1 mm polyethersulphone filter membrane with 0.45 µm pore size. The DET probes, which are used for nutrient measurement (ammonium, nitrate and phosphate), consisted of 1.2 mm agarose gel layer and a 0.1 mm polyethersulphone filter membrane. The preparation of the different gel

layers was conducted following the protocols described in previous studies (Huang et al. 2016; Pagès et al. 2012; Robertson et al. 2008).

Before deployment, probes (including blanks) were de-oxygenated in a 1 mol/L sodium chloride (NaCl) solution or water from the specific sampling site overnight by sparging with pure nitrogen gas. The DGT and DET probes were deployed in the sediment cores with 2–3 cm of the open window above the sediment-water interface (SWI) and 12–13 cm under the SWI (Figure 4). The DGT and DET probes were deployed for 6–8 hours and 10–12 hours under natural light and dark conditions, respectively.

Figure 4. Photo of diffuse gradients in thin films (DGT) and diffuse equilibrium in thin films (DET) being deployed in sediment cores.

For the *in-situ* study carried out from 8 to 11 November 2021 at Woods Well, the DET probes were deployed in the field, approximately 50–100 m away from the benthic chambers (Figure 4. Photo of diffuse gradients in thin films (DGT) and diffuse equilibrium in thin films (DET) being deployed in sediment cores.). All of the DET probes were deployed randomly in a 1 × 2 m area between 3 pm to 6 pm on 9 November, allowing at least 15 hours of equilibrium before initiating the retrieval of replicate probes at 4 hour intervals for the next 24 hour diel cycle. The first set of DET probes were retrieved at 6 am on 10 November and the last set of probes were collected at 6 am on 11 November.

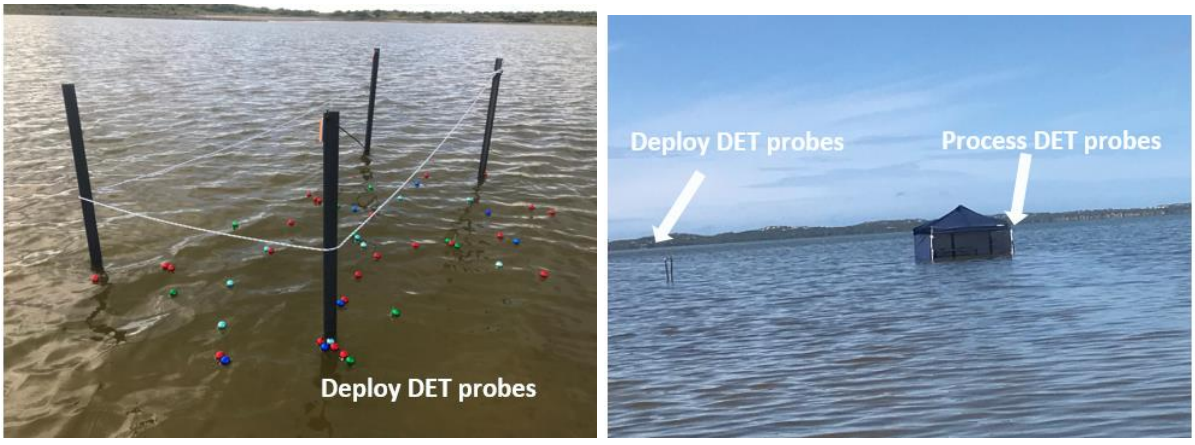

Figure 5. Diffuse gradients in thin films (DET) probes were deployed *in situ* in sediment at Woods Well and processed immediately in the field.

At the end of the respective deployment periods in core or *in situ*, the DGT and DET probes were pulled out gently from the sediment and rinsed immediately with ultra-pure deionised water to remove any sediment residues. The gels were cut from the probe window using a scalpel blade and the filter membrane was removed. The diffusive (colorimetric DET) gels for iron determinations were placed onto a ferrozine staining gel layer (Pagès et al. 2012, Robertson et al. 2008), stained, scanned and the images were processed as

described by Bennett et al. (2012) using GIMP software (version 2.8.22). Iron concentrations, two-dimensional distributions, and mean depth profiles were calculated as per the methods described by Pages et al. (2012) and Robertson et al. (2008). The AgI sulfide-binding gel layers from the DGT-DET probes were scanned immediately and the images were processed. Sulfide concentrations, two-dimensional distributions, and mean depth profiles were calculated as described by Robertson et al. (2008). For the experiment conducted at Woods Well, AgI DGT was replaced by the colorimetric DET for sulfide (Kankanamge et al. 2020). The sulfide DET gels were placed onto a mixed diamine reagent staining gel layer (Cline, 1969; Reese et al. 2011), stained, scanned, and the two-dimensional distributions and mean depth profiles were calculated as described by Kankanamge et al. (2020). Nutrient DET gels were laid on top of a clean PVC sheet and sliced into different depths (5 or 10 mm thickness). The DET gel layers were sliced in layers with 5 mm thickness from the overlying water to 3 cm below the SWI to capture any nutrient transformations in this area. This method was particularly focussed on nitrogen because nutrient transformations can occur in narrow biogeochemical zones near the SWI, ranging from less than a millimetre to a centimetre in thickness. From 3 cm below the SWI, the DET gel layers were sliced into layers of 10 mm thickness as the nutrient changes may not be as significant compared to near the SWI. Each piece of gel was transferred into a 5 mL plastic vial and eluted in 3 mL 0.1 mol/L HCl. The eluents were neutralised and analysed according to standard methods for waters and wastewater (4500-NH_3 H, 4500-NO_3^- F, 4500 P G, 4500 N C and 4500 P I) using a Seal AA3 segmented flow analyser (Seal Analytical, USA).

Statistical analyses

To explain the influence of time and depth on porewater dissolved solute concentrations (i.e. ammonium, phosphate, sulfide and iron) multiple Generalised Additive Models (GAM) were performed using the packages “mgcv” (Kassambra 2020) and “ggplot2” (Wickham 2016) in R software (R Core Team 2017). For assessing differences in concentration of nutrient between times (light, dark) and depths, several univariate PERMutational ANalysis Of VAriance (PERMANOVA) were performed with Euclidean distance for the single variables (Anderson et al. 2008) using PRIMER v7 with PERMANOVA add on.

2.2.2 *Ex* and *in situ* techniques to determine sediment water column oxygen and nutrient fluxes

Ex situ core incubation

Sediment sampling and experimental set up

Sediment cores were collected between November 2020 and March 2021 from various sites covering the diversity of sediment types and ecosystems in the North and South lagoons (Table 2 and Figure 3). At each site, ten cores for flux incubations were collected by hand or using pole corers to a sediment depth of 15–20 cm, using 40 x 7.8 (internal diameter) cm perspex core tubes. Additionally, 200–300 L of water was collected for core maintenance and incubation.

The cores were transported to a greenhouse on the University of South Australia, Mawson Lakes campus within 5–6 hours of sampling or to a local research base (Cantara homestead) within 2 hours of collection. Cores for flux incubations were submerged within a custom-built incubation chamber (Figure 6) containing site water. Water within the chamber was maintained at *in situ* temperature (19 ± 1 °C) by circulating the chamber water through an aquarium heater/chiller unit using an inline water pump. Dissolved oxygen (DO) concentrations were maintained at saturation with an aerator. Water within the cores was mixed with the overlying water using magnetic stirrers suspended in each individual core 10 cm above the sediment surface, which were driven by a central electric motor. The cores from the shallow sites were equilibrated under natural ambient light/dark conditions for 24–36 hour prior to the flux incubations. The cores from the two deep sites were equilibrated under dark conditions by covering black plastic sheets for the same period before flux incubations.

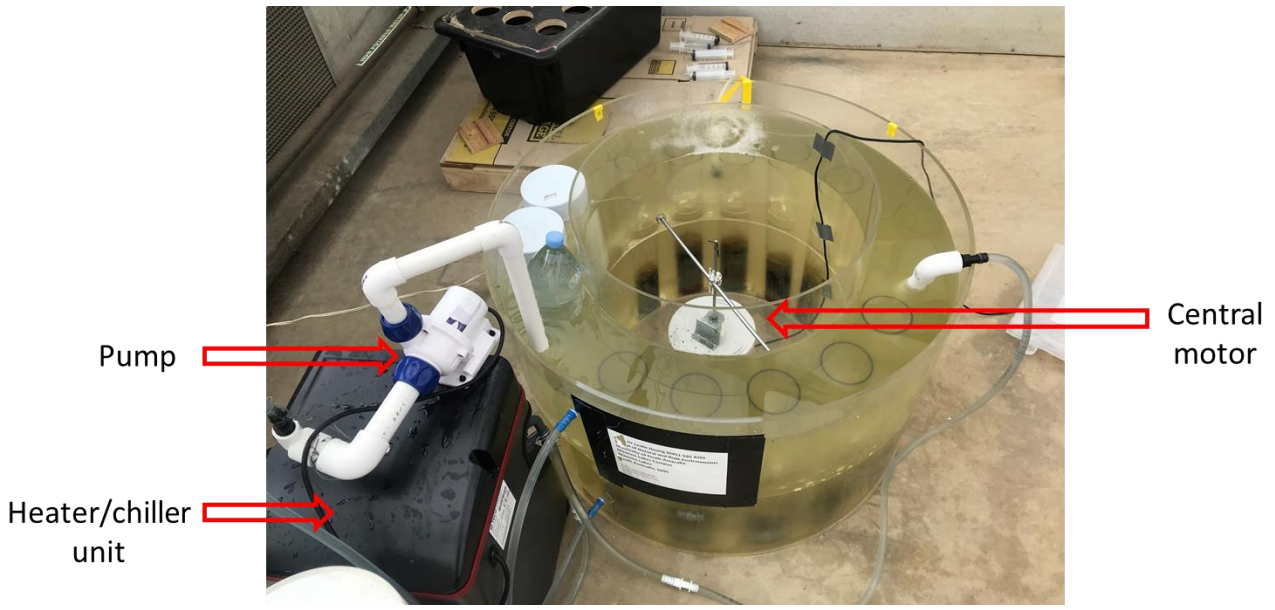

Figure 6. Core incubation system used in this study. Shown are the pump, heater/chiller unit and central motor.

Determination of sediment-water column fluxes of oxygen, nutrients and other solutes

Prior to the core incubations, the water in the incubation chamber was refreshed with Coorong site surface water to maintain near *in situ* dissolved nutrient concentrations. The water within each individual core was then exchanged with the overlying water by suspending an aerator within each core for ~1 min, whilst the cores were still submerged. To initiate incubations, the water level in the tank was lowered to below the core tops. The water column Dissolved Oxygen (DO) concentration was measured and initial water samples were collected for the determination of dissolved nutrient concentrations and other solutes. The cores were then sealed with floating plexiglass lids to prevent gaseous exchange with the atmosphere. The time of the incubation depended on the oxygen consumption/production rates determined in preliminary incubations using the same set up, in order to maintain oxygen concentrations within ±20% of the initial air saturation concentration. At the end of the incubation period, the floating lids were removed and water samples collected for the determination of the final DO, dissolved nutrient and other solutes concentrations. For the sediments collected from Parnka Point on 10 November 2020, DO and dissolved nutrient concentrations were measured as per the above method. For the sediments collected between February and March 2021 from Parnka Point, Policeman's Point, 3 km south of Salt creek and near Swan Island, DO, dissolved organic carbon (DOC) and inorganic nutrients were determined as described by Welsh et al. (2000).

For the sediment cores collected from Parnka Point in November 2020, after the dark incubations, the water level in the incubation chamber was raised to above the core tops and the cores allowed to re-equilibrate overnight. The procedure above was then repeated under natural (ambient) light conditions to determine the fluxes of solutes under these conditions.

The fluxes of DO, dissolved nutrients and other solutes were calculated as the difference between final and initial concentration of the target solute in the water column according to the following equation (Nizzoli et al. 2007)

$$Fx = \frac{(Cf - Ci) \times V}{A \times t}$$

where,

Fx = flux of the *x* species (µmol/m^2/h)

Cf = final concentration of *x* (µmol/L)

Ci = initial concentration of *x* (µmol/L)

V = volume of the water inside to core (L)

t = incubation time (hours)

A = sediment surface area inside the core (m^2)

Benthic community respiration (CR) was estimated as the benthic oxygen consumption during dark incubations and benthic net primary production (NPP) as the oxygen production during light incubation. The benthic gross primary production (GPP) represents the total quantity of oxygen produced during photosynthesis and was estimated as CR + NPP.

In situ benthic chamber determinations of sediment-water column nutrient fluxes over a diel light cycle

Experimental set up

Three benthic chambers with a pump controller system were used to determine the impact of the presence of *Ruppia tuberosa* on oxygen and nutrient fluxes between the sediment and water column *in situ*, over a diel light cycle. Each chamber consisted of two matching halves of 10 mm thick clear acrylic, a clear lid, a pair of stainless-steel cutter plates with a 200 mm deep cutting edge, a flushing pump, a mixing pump, a float switch, a one-way valve and a spray bar. The chambers were 850 mm high and wide, and they sit within a pair of stainless-steel cutter plates (Figure 7). The DO (miniDOT) and light (miniPAR) loggers, which were purchased from PME, USA, were attached to the inside and outside walls of the chambers, respectively. The loggers sat in the water column approximately 20 cm above the *Ruppia*/seagrass (10-15 cm), which was about 35 cm above the sediment.

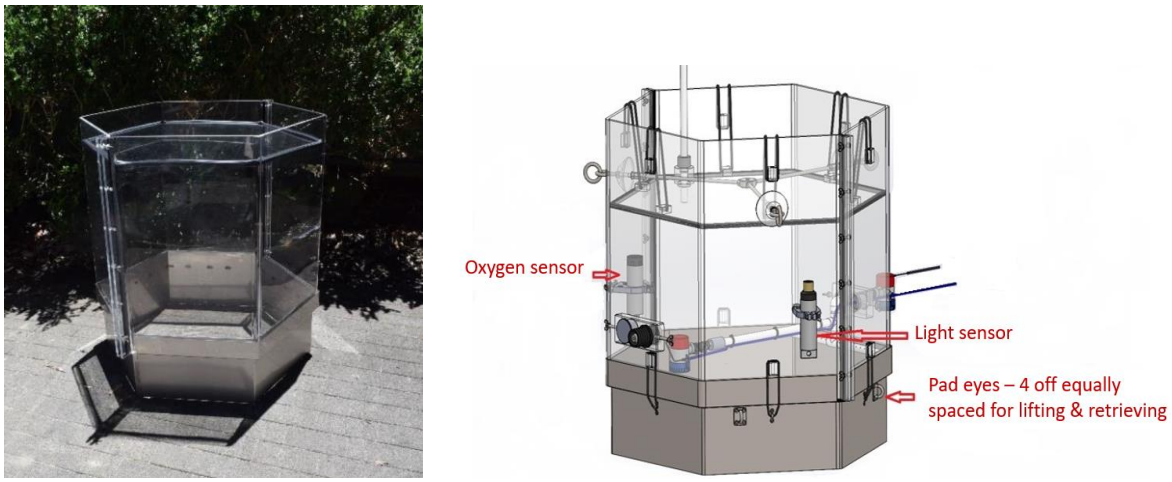

Figure 7. Photo and image of the benthic chamber system used in this study.

The *in situ* experiment was conducted from 8 to 11 November 2021 at Woods Well. The chambers were assembled, with the stainless-steel cutter plates of the chambers pushed into the sediment to ensure the chamber volume was isolated from the ambient environment. DO and light loggers were activated before deployment, with data recorded every minute. The three chambers were deployed within a 5 m diameter of the pump controller system (Figure 8). Lids with rubber gaskets were adjusted to remove air bubbles and isolate the enclosed water from the atmosphere. The pump regulation system was activated at 5:30 pm on 8 November, 36 hours before the initiation of sample collection. This system consisted of a mixing pump within each chamber connected to a spray bar, which continuously pumped water to ensure the water within the chambers was efficiently mixed. The flushing pumps were activated for a period of 3 min at 4 hour intervals, during which external water was pumped into the chambers with excess water exiting via the one-way valve. These pumps ensured that the water within the chambers remained oxygenated and nutrient concentrations were similar to those in the external water column at the start of each chamber incubation.

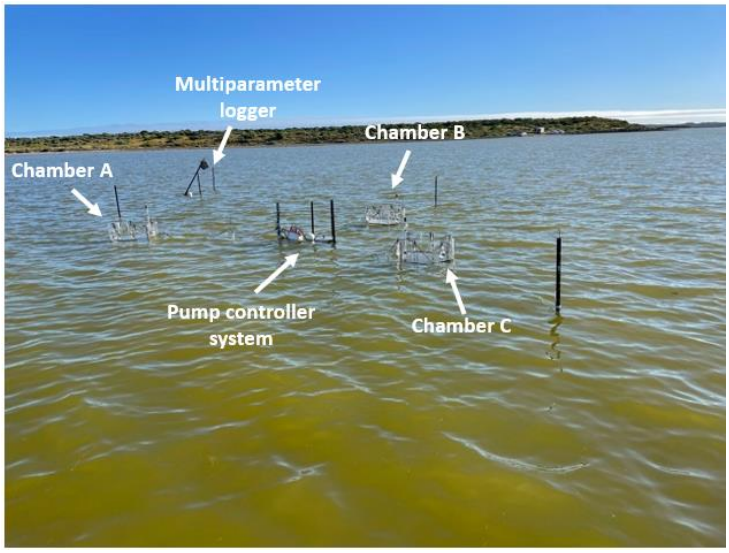

Figure 8. Photo of deployed benthic chambers with a pump controller system at Woods Well.

Determination of sediment-water column fluxes of oxygen and nutrients

The oxygen fluxes were calculated based on the above equation using the slope of the DO concentration over sequential 3 hour incubation periods (6–9 am, 10 am–1 pm, 2–5 pm, 6–9 pm, 10 pm on 10 November–1 am on 11 November, and 2–5 am on 11 November 2021) to time the volume of the water inside to core, then divide the sediment surface area inside the core. To measure nutrient fluxes, water samples were collected from the three chambers via sampling ports in the period between each flushing cycle. Initial samples were collected ~0.5 hour after the chambers had flushed and end samples were collected ~3 hours later, prior to initiation of the next chamber flushing cycle. Sampling commenced at 6 am on 10 November 2021 and followed the same incubation periods as listed above for oxygen fluxes, with the final samples collected at 5 am on 11 November 2021. Three replicates of water samples were collected from each chamber at each sampling time. The dissolved nutrient fluxes were calculated from the difference in solute concentrations between the initial and end time samples, as described for the core incubations.

Determination of seagrass biomass

For the sediment core experiment, five sediment cores were collected on 10 November 2020 from Parnka Point. The core contents were sieved through a 0.5 mm mesh to collect the seagrass biomass (shoots and roots) after the flux incubations. For the *in situ* experiment conducted from 8 to 11 November 2021 at Woods Well, a 40 x 7.8 cm (internal diameter) perspex core tube was used to collect seagrass samples close to the benthic chamber and the DET probes after the experiment. Ten biomass samples were collected at each site. The core contents were sieved through a 0.5 mm mesh to collect the seagrass biomass. Fresh biomass was separated, briefly rinsed with tap water to remove salts and oven dried at 80 °C to a constant dry weight.

Analytical methods

Water samples for dissolved nutrient and organic carbon (DOC) concentrations were collected using 50 mL syringes with fitted with silicon tubing, filtered through 0.45 µm pore size polyethersulphone membrane filters. Nutrient samples were stored frozen until analysis for ammonium, nitrate and phosphate concentrations using a Seal AA3 segmented flow analyser following APHA Standard Methods 4500-NH_3 H, 4500-NO_3^- F, and 4500-P G (APHA, 1992). DOC samples (~20 mL) were fixed with 0.25 mL of 15.2 mol/L phosphoric acid and stored at 4°C. In the laboratory, DOC concentrations were determined according to standard method 5310 C (APHA 1992).

Statistical analyses

The fluxes of oxygen, inorganic nutrient and other solutes under light and dark conditions from the core incubator were compared using a Student T-test. The sediment water column oxygen and inorganic nutrient fluxes from the benthic chamber were compared using ANOVA.

2.3 Microbial ecology

2.3.1 Sampling method

Sediments were sampled at seven sites (Table 3) using custom plexiglass cores (18 cm diameter) between 2 and 3 December 2019. The top 10 cm of each core was sliced and placed in sterile zip-lock bags and preserved with RNALater solution (ThermoFisher), then stored at -20 ˚C overnight prior to weighing and nucleic acid extractions. Overlying water was analysed *in situ* for pH, temperature, DO, salinity water column profiles, and total/dissolved nutrients. Sampling was performed at varying water depths over the two days, including wading and boat sampling at ~0.5m and ~1m depths to assess sediments in deeper channels.

Table 3. Site information for microbial DNA sampling.

SITE NAME	SITE CODE	LAGOON	MONTH	LATITUDE	LONGITUDE
Salt Creek	*SC1*	South	Dec 2019	-36.16333	139.647875
Jack Point	*JP2*	South	Dec 2019	-36.03157333	139.5694333
Villa Dei Yumpa	*VD3*	South	Dec 2019	-35.93736333	139.4885333
Parnka Point	*PP4*	North/South*	Dec 2019	-35.90077	139.3962333
Noonamena	*NM5*	North	Dec 2019	-35.7793275	139.28335
Long Point	*LP6*	North	Dec 2019	-35.695812	139.16252
Mark Point	*MP7*	North	Dec 2019	-35.62539333	139.0763667
Parnka Point	*PA*	North/South*	Feb 2021	-35.907383	139.397432
Near Swan Island	*NSI*	South	Feb 2021	-35.9516	139.4917
Policeman's Point	*PO*	South	Feb 2021	-36.0582662	139.5840172
3km South of Salt Creek	*SSC*	South	Feb 2021	-36.1328	139.6114

* Parnka Point site is located directly at the exchange point between North and South lagoons.

Additional sediment samples were taken during the November 2021 sampling trip described in section 2.2. Four sites (PA, NSI, PO and SSC; Figure 3 and Table 2), were sampled to cover a diversity of sediment types and ecosystems across the South Lagoon and to provide ecological context to complement the biogeochemical analyses detailed in section 2.2.1. Sediments were sampled in triplicate with plexiglass cores (18 cm internal diameter). Upon return to the shore, the top 10 cm of core was then mixed and subsampled in triplicate with a sterilised metal spatula into 15 mL plastic centrifuge tubes. Three volumes of LifeGuard (Qiagen) preservation solution were added to the sediment sample, which was immediately stored at -20 ˚C for maximum of three weeks until extraction.

2.3.2 Molecular and bioinformatic method

Total deoxyribonucleic acid and ribonucleic acid (DNA/RNA) was extracted and then quantified with both a Nanodrop spectrophotometer and a Qubit fluorometer. Gene abundance and expression of *nirK* (encoding nitrite reductase, the rate-limiting enzyme of denitrification) was quantified with quantitative polymerase chain reaction (qPCR) and Reverse-transcriptase (RT)-qPCR, respectively, against standard curves generated with synthetic gene fragments of known concentration and abundance. True positive signals in the data were identified with a melt curve analysis. Cell activity ratios were calculated, assuming one copy of *nirK* per genome and five genomes per cell, where A is cell activity, as follows:

$$A = \frac{transcript\ copies}{(gene\ copies/5)}$$

For microbial community structure analysis, extract DNA replicates were pooled, then the V3-V4 region of the 16S rRNA gene was amplified and sequenced.

Bioinformatic analysis was performed with QIIME2, DADA2, MAFFT, fastree2 and Bayesian taxonomy classification against the Greengenes 13_8 99% OTU reference library (McDonald et al. 2012). Functional roles of the community were inferred with Phylogenetic Investigation of Communities by Reconstruction of Unobserved States (PICRUSt) software (Langille et al. 2013).

2.3.3 Statistical analyses

Statistical analyses were performed in RStudio (R Core Team, 2013, version 4.0.0 – 2020-04-24) for the purposes of visualising microbial community sequence data and taxonomy in the context of environmental variables. Operational taxonomic unit (OTU) tables, taxonomy tables, and phylogenetic trees were imported to a phyloseq object, for each dataset. Phyloseq objects were transformed to relative abundance and agglomerated at phylum-level taxonomic classifications, phyla <1% relative abundance were grouped, and data were plotted to analyse the overarching phylum composition of prokaryotic communities. Phyloseq objects were transformed by rarefication at minimum read counts to normalise prior to weighted unifrac distance metric application. Environmental variables were each checked for normality with a Shapiro-Wilk test and transformed with Tukey's Ladder of Powers where necessary. To test beta diversity (differences in between-site community) principal coordinates analysis (PCoA) and non-Metric Multidimensional Scaling (nMDS) ordinations were performed on each dataset, with unifrac distances, to visualise phylogenetic dissimilarity between samples, and Bray-Curtis distances to visualise abundance dissimilarity between samples. A correspondence analysis was also employed, to better visualise the effect of the salinity gradient. PERMANOVA was employed to statistically confirm community dissimilarities visualised with ordination. Prior to this, testing with 'betadisper' was performed to assess homogeneity of beta dispersion and contextualize results with the potential contribution of dispersion. To test the contribution of continuous variables to identified changes in community diversity, constrained correspondence analysis (CCA) was performed with the optimal explanatory formula of continuous variables, forward-selected with the vegan package's 'ordistep' function. To analyse inter-variable relationships, a series of single regressions were conducted with Spearman's rank-order correlations on gaussian × gaussian variable pairs.

2.4 Macroinvertebrate influences on nutrient dynamics

To investigate the influence of macrobenthic fauna on sediment nutrient concentrations and biogeochemistry, two experiments were conducted *in situ* at various sites in the Murray Mouth and Coorong North and South lagoons (Figure 9).

2.4.1 Macroinvertebrate evaluation 1: Salinity gradient survey

The first experiment was carried out in spring 2020. Seven sites across the Coorong were selected and surveyed based on access logistic and available historical and environmental information from other ongoing projects. All sites were surveyed at low tide, when the mudflats were exposed and accessible from shore.

Macroinvertebrate fauna sampling

Sediments for macrobenthic fauna were sampled using a handheld PVC corer (100 mm internal diameter), with five replicates randomly taken per site. All sediment samples were sieved through 500 µm mesh size in the field and preserved in ethanol (70%) until further processing. In the laboratory, sediment samples were sorted, and all organisms were identified to the lowest possible taxonomic level and counted.

Environmental conditions

Water quality variables (temperature, salinity, pH) were measured during the macroinvertebrate sampling. Sediment samples were taken for analysing organic matter content, sediment grain size, and chlorophyll-*a* concentration. Organic matter (OM) content was determined by drying the sediment samples to constant weight using an Ohaus MB45 Moisture Balance (controlling the temperature profile at 80 °C). When a constant weight was achieved, sediment samples were burnt in a furnace at 450 °C for 5 hours. Grain size was determined by laser diffraction using a particle size analyser (Malvern Mastersizer 2000). Average values for grain size fractions for each site were entered into the GRADISTAT program v8.0 (Blott and Pye 2001) to obtain the median (D50 µm) and coefficient (sorting σG). Chlorophyll-a (g/m^3) was determined using a spectrophotometer (Thermo Scientific, Spectronic 200) following protocols of Ritchie (2008).

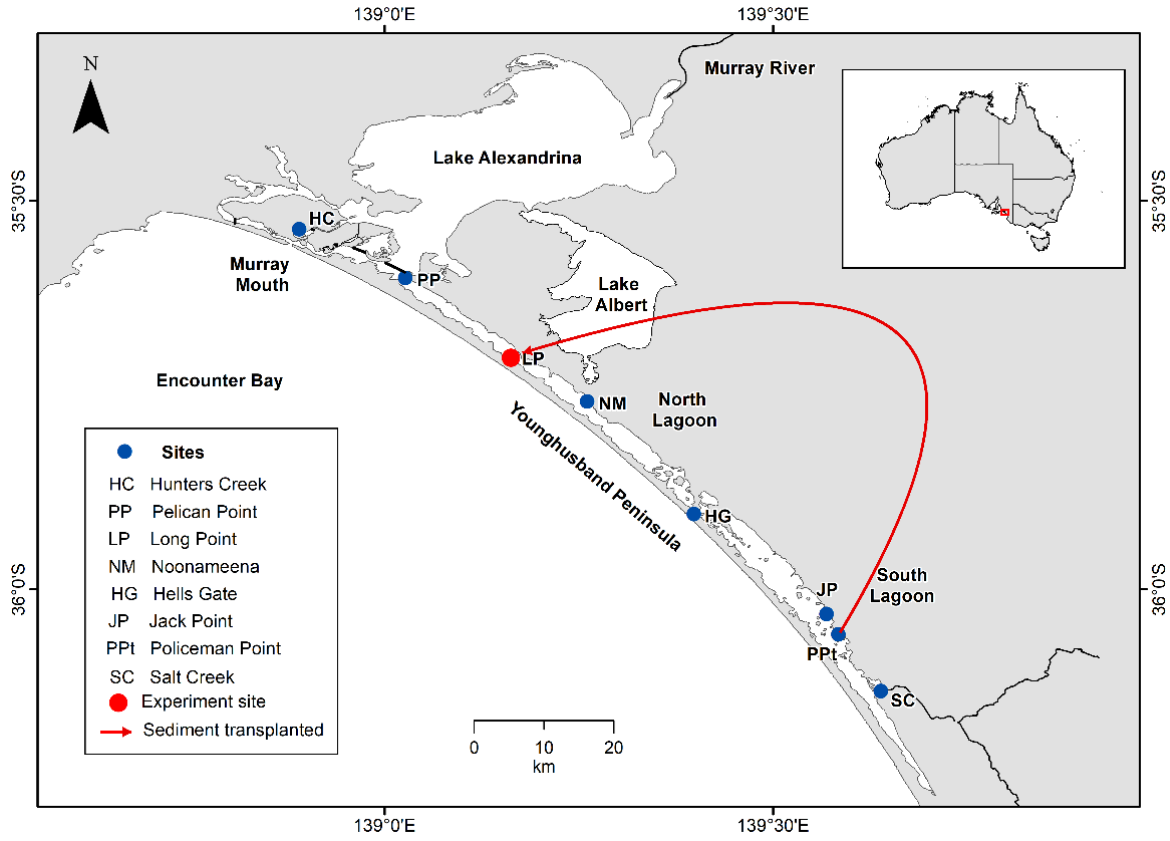

Figure 9. Sampling and experimental sites for investigating the influence of macroinvertebrates on nutrient cycling in the Coorong. Sites for experiment 1: Hunters Creek, Pelican Point, Long Point, Noonameena, Hells Gate, Jack Point, and Salt Creek. Sites for experiment 2: Long Point and Policeman Point.

Sediment pore water and sediment samples (depth layers: 0-2 cm, 2-10 cm, and 10-20 cm) were collected for analysing nutrient concentrations. Porewater nutrient concentrations (mg/L) of nitrate, nitrite, ammonium, and phosphate were determined using a Skalar SAN ++ SFA segmented flow analyser. Sediment pH, conductivity, total phosphorus, carbon and nitrogen concentrations were determined by LECO by the Environmental Analysis Lab at Southern Cross University.

Organic matter degradation

Five rapid organic matter assessment (ROMA) plates (Figure 10) were deployed at each of the seven sampling sites, 11 days prior the sampling, following a design of O'Meara et al. (2017). Using this approach, depths of the holes in the ROMA plates were selected based on rapid changes in redox conditions in marine sediments and vertical distributions of fauna (Lohrer et al. 2010; Hewitt et al. 1996; Thrush et al. 1996). Holes in ROMA plates were filled with a 0.029 g C/ml mixture of food grade agar, microcrystalline cellulose (CAS 9004-34-6; Thermofisher) and powdered bran. Ratios were adapted from bait lamina recipes and optimised for estuarine ecosystems (O'Meara et al. 2017). After 11 days, the ROMA plates were retrieved from the sediment and carbon consumption was measured by the change in agar volume in each hole on the ROMA plate following the approach of O'Meara et al. (2017).

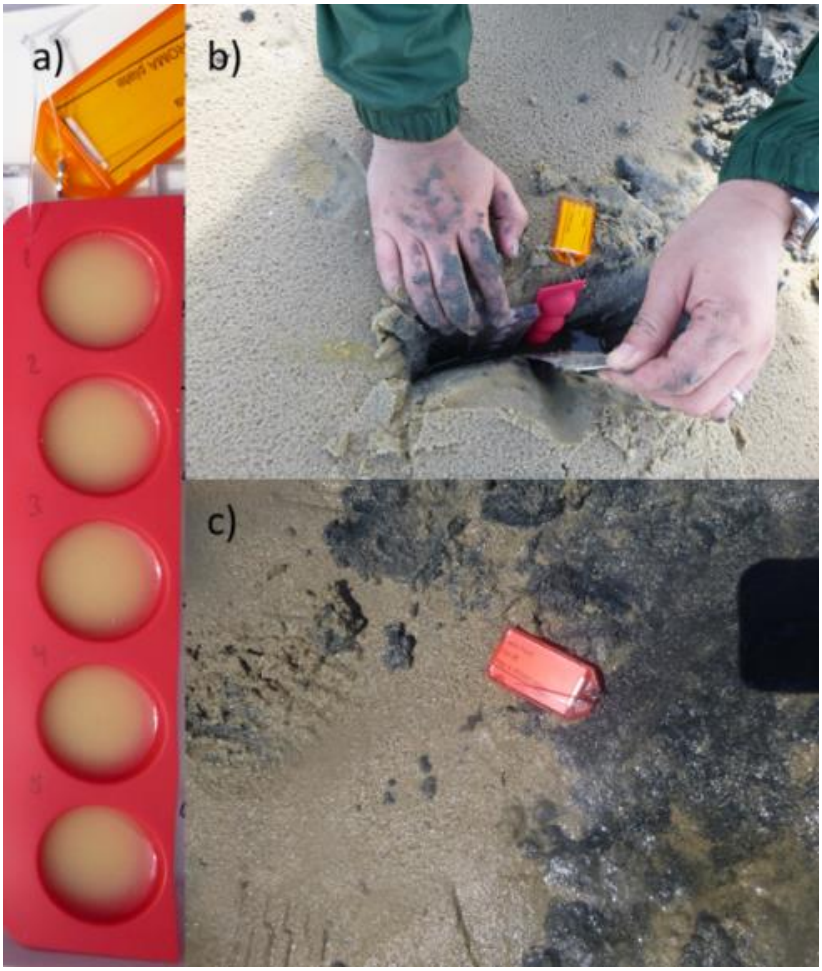

Figure 10. Deployment of rapid organic matter assessment (ROMA) plates. (a) ROMA plate before deployment. (b) Placing of the plate vertically against the sediment surface with a wedge created using a spade. (c) Sediment replaced gently to reduce disturbance to the plate.

Data analysis

Macroinvertebrate data were analysed for diversity (as species richness) and abundance (individuals per m^2). To assess community structure, a nMDS analysis was performed using a Bray-Curtis similarity matrix. Differences across sites in species richness, abundance, community structure and organic matter degradation (also testing for differences across depths) were analysed using PERMANOVA. For univariate tests for the single variables, the tests were based on Euclidean distance similarity. PERMANOVA were run with 9999 permutations (Anderson et al. 2008) in PRIMER v7 with a PERMANOVA add on.

To elucidate the macroinvertebrate influence on the nutrient concentrations, multiple Generalised Additive Models (GAM) were performed using the same packages as in section 2.2.1 in R software (R Core Team 2017).

2.4.2 Macroinvertebrate evaluation 2: Sediment and macroinvertebrates translocation

To investigate whether the bioturbating activity of macrobenthic fauna can improve biogeochemical conditions in sediments from the South Lagoon, a second experiment was conducted in the field. The experiment involved the transplantation of "hostile" (hypersaline, sulfide-rich) sediments from the South Lagoon into the North Lagoon (Figure 9), where historical monitoring has shown salinities are low enough for macroinvertebrates to occur as well as manipulating the densities of deeper dwelling bioturbating polychaetes (*Simplisetia aequisetis*).

Experimental design

Long Point (North Lagoon) was selected as the experimental site because it had low salinity with the mean value of 28 PSU, with sediment for transplanting taken from Policeman Point (mean salinity 131 PSU) at the southern end of the South Lagoon (Figure 9). The experiment was carried out between April and May (autumn) 2021 (Figure 11). The sediment was extracted using PVC corer (100 mm internal diameter) to 20 cm depths, defaunated (through freezing), and implanted in the lower intertidal zone of the mudflat at Long Point. The PVC corer had openings at the bottom and top ends with a lid of 0.5 mm mesh size, to retain the organisms and allow the flux of water and matter.

This experiment was carried out *in situ* and included the analysis of several factors (Figure 11Figure 12):

(i) Sediment source – sediment from the South Lagoon was transplanted into the North Lagoon to elucidate whether bioturbation by macroinvertebrates can change the nutrient concentrations and improve nutrient fluxes. Sediment from Long Point in the North Lagoon was also used to assess whether changes in the density of a bioturbating polychaete will affect the nutrient concentrations.

(ii) Density – deep burrowing macrobenthic fauna was added using the polychaete *Simplisetia aequisetis*. The polychaetes were collected from Pelican Point in the Murray Mouth where they are very abundant. As the density of bioturbation can affect nutrient concentrations and fluxes, four levels of density were used, simulating four Coorong scenarios from low densities during drought to higher densities after longer periods with high flow: 0x – azoic (i.e. no organisms) sediments; 0.5x – half of the natural density; 1x - natural density, and 2x –double the natural density, where dendity is defined as the number of organisms per core. Natural density was based on long-term data from ongoing monitoring (Dittmann et al. 2018). Long Point sediments were used as procedural control (LP in Figure 9) and sediment which was not affected by any experimental manipulation was also collected at the North Lagoon site.

(iii) Time – the influence of adding bioturbators on sediment nutrient concentrations and fluxes was assessed over four weeks, with weekly analysis of three replicate experimental units per treatment (Figure 11Figure 12).

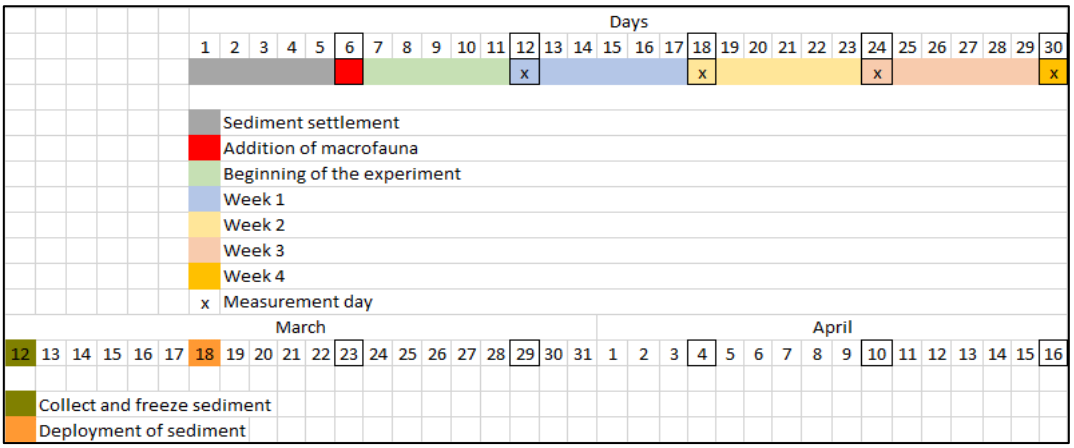

Figure 11. Timeframe and design for the *in situ* experiment to investigate the effects of bioturbation by macrobenthos on biogeochemical conditions in Coorong sediments.

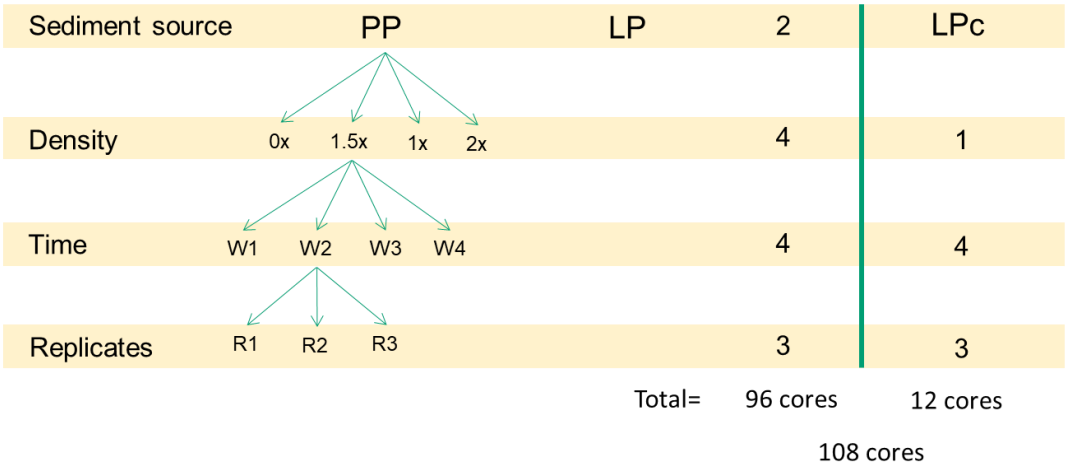

Figure 12. Experimental design for Experiment 2. Levels are illustrated just once for each factor for clarity. These three factors resulted in 108 core units for measurements, 96 experimental units (2 Sources × 4 Densities × 4 Times × 3 Replicates) and 12 control units (1 Source × 1 Density × 4 Times× 3 Replicates) PP: Policeman Point, LP: Long Point procedure control, LPc: Long Point Control. X: times; W: week; R: replicates.

Macroinvertebrate and environmental conditions measurements

Each of the 108 experimental units (i.e. cores) for this design was analysed for porewater salinity, porewater nutrients, sediment grain size, and macrobenthic fauna (Table 4).

Upon retrieval of each experimental unit, samples for porewater salinity and nutrients (ammonium, nitrate, nitrite and phosphate) were collected using Rhizon samplers (Seeberg-Elverfeldt 2005) at different depths (0–2 cm, 2–10 cm, 10–20 cm). Sediment was divided into different depths and samples for sediment grain size and nutrients were also taken. Diffusive Gradients in Thin-films (DGT) and Diffusive Equilibrium in Thin-films (DET) techniques were used as they are well-established *in situ* passive samplers for obtaining high resolution porewater profiles of solutes concentrations (Pagès et al. 2012, Huang et al. 2016, Kankanamge et al. 2017, Huang et al. 2019). DET-DGT probes were applied for sulfide (S) and iron(Figure 13 for details of the process).

Table 4. Summary of dates in 2021, activities and measurements taken for Experiment 2. W: week; M: measurement.

WEEK		WEEK 0		WEEK 1		WEEK 2	WEEK 3	WEEK 4	
Date	18/03	22/03	23/03	30/03	30/03	4/04	10/04	15/04	16/04
Activity	Trans.	Collect worms	Add worms	M1		M2	M3	M4	
DGT/DET		x		x				x	
Porewater	x				x	x	x		x
Bulk sediment	x				x				x
Grain size	x				x	x	x		x
Salinity	x				x	x	x		x
Macrofanua	x				x	x	x		x

Figure 13. Experimental design and measurement process for evaluation 2. a) Collection, b) transportation and freezing of sediment, c) addition of mesh lids and tags to each of the experimental units, d) deployment of experimental units, e) illustration of experimental unit in the sediment under water, f-g) aerial view of the complete grid of experimental units deployed at Long Point, h-i) deployment of DGT (diffusive gradients in thin films)/DET (diffusive equilibrium in thin films) probes, j-k) i*n situ* area for processing and analysing the DGT/DET probes, l) extraction of pore water using rhizon samplers for analysing salinity and nutrients at different depths, m) division of sediment at different depths, n) multi-tasking process of sediment collection for nutrient and sediment grain size, and o-p) sediment sorting for macrobenthic fauna and deposition of samples in tubs for further analyses.

Laboratory analysis

Porewater nutrient samples were collected using rhizon samplers (Rhizosphere Research Products) and concentrations of nitrate, nitrite, ammonium and phosphate were determined using a Skalar SAN ++ SFA segmented flow analyser. Sediment grain size was determined by laser diffraction using a particle size analyser (Malvern Mastersizer 2000). Average values for grain size fractions for each site were entered into the GRADISTAT program v8.0 (Blott and Pye 2001) to obtain the median (D50 µm) and sorting coefficient (σG), and percentage of fine sand (%FS). Sediment total organic carbon (TOC) and nitrogen (TN) were determined by LECO analysis by the Environmental Analysis Lab at Southern Cross University. The DET gel layers were eluted in 3 mL 0.1 mol/L HCl for 24 hours and then neutralised by addition 0.28-0.3 mL 1 mol/L NaOH before analysis. The DET eluents were analysed for (µmol/L) ammonium, phosphate, and nitrate using a Seal AA3 segmented flow analyser (Seal Analytical, USA).

Data analysis

To test for differences in macrobenthic fauna density and fixed treatment factors (sediment source, added *S. aequisetis* density, depth, and time), univariate PERMutational ANalysis Of VAriance (PERMANOVA) tests were conducted, using Euclidean distance for the single variables and 9999 permutations in PRIMER v7 with PERMANOVA add on software (Anderson et al. 2008). To evaluate the influence of *S. aequisetis* and other benthic macrofauna on porewater nutrients and sediment biogeochemical characteristics, non-parametric multiple regressions were performed with the DISTLM routine, using Euclidean distances, 9999 permutations (McArdle and Anderson, 2001). To test for significant differences between the sediment source, *S. aequisetis* density (organisms added), depth, and time, and their influence on sulfide, dissolved ferrous iron(II) and nutrient (DET-DGT measured) concentrations, Generalised Additive Models (GAM) were performed using the same packages as in section 2.2.1 in R software (R Core Team 2017).

2.5 Sediment resuspension effects on water column nutrients

The purpose of this work was to investigate the influence of wind-induced sediment resuspension on water column nutrient concentrations in the Coorong South Lagoon. Two sampling routines were carried out to capture an increase in wind speed from relatively quiescent conditions. An initial sampling routine (see Section 2.5.2 Intensive single-point sampling 1–3 March 2021) was performed by taking continuous measurements at a single point over time. After analysis of this data (see Section 3.5.2 Intensive single-point sampling 1–3 March 2021), it was deemed a more spatially complex sampling design incorporating sediment sampling was required and a second sampling routine was conducted (see Section 2.5.2 Multi-point sampling 21–24 June 2021).

2.5.1 Study site

Sampling for investigating the effects of wind-induced resuspension events on water column nutrients took place at Villa dei Yumpa (Figure 14) in the northern end of the South Lagoon. This site was chosen based on previous observations of the resuspension of sediments under strong wind conditions (pers. comm. Herra-Singh, February 2021), accessibility to the shoreline to launch a boat and proximity to on-site accommodation.

Thirteen sampling locations were established, twelve of these along three transects (T1-3) covering the width of the Coorong, with an additional sampling location established in the channel between Hack Point and Cow Island (HP, Figure 14). Sampling locations were determined based on the depth of the water at the initial time of sampling (shallow (S) ≤ 0.6 m water depth, and deep (D) > 0.6 m water depth) and their proximity to each shoreline of the South Lagoon (Younghusband Peninsula or the mainland). The spatial coverage of the survey method was designed to capture variation in physical sediment qualities which may affect their erodibility. Notably between deeper organic-rich sediments in the middle of the main channel and sediments closer to both shorelines as previously mapped by Sharma et al. (2009).

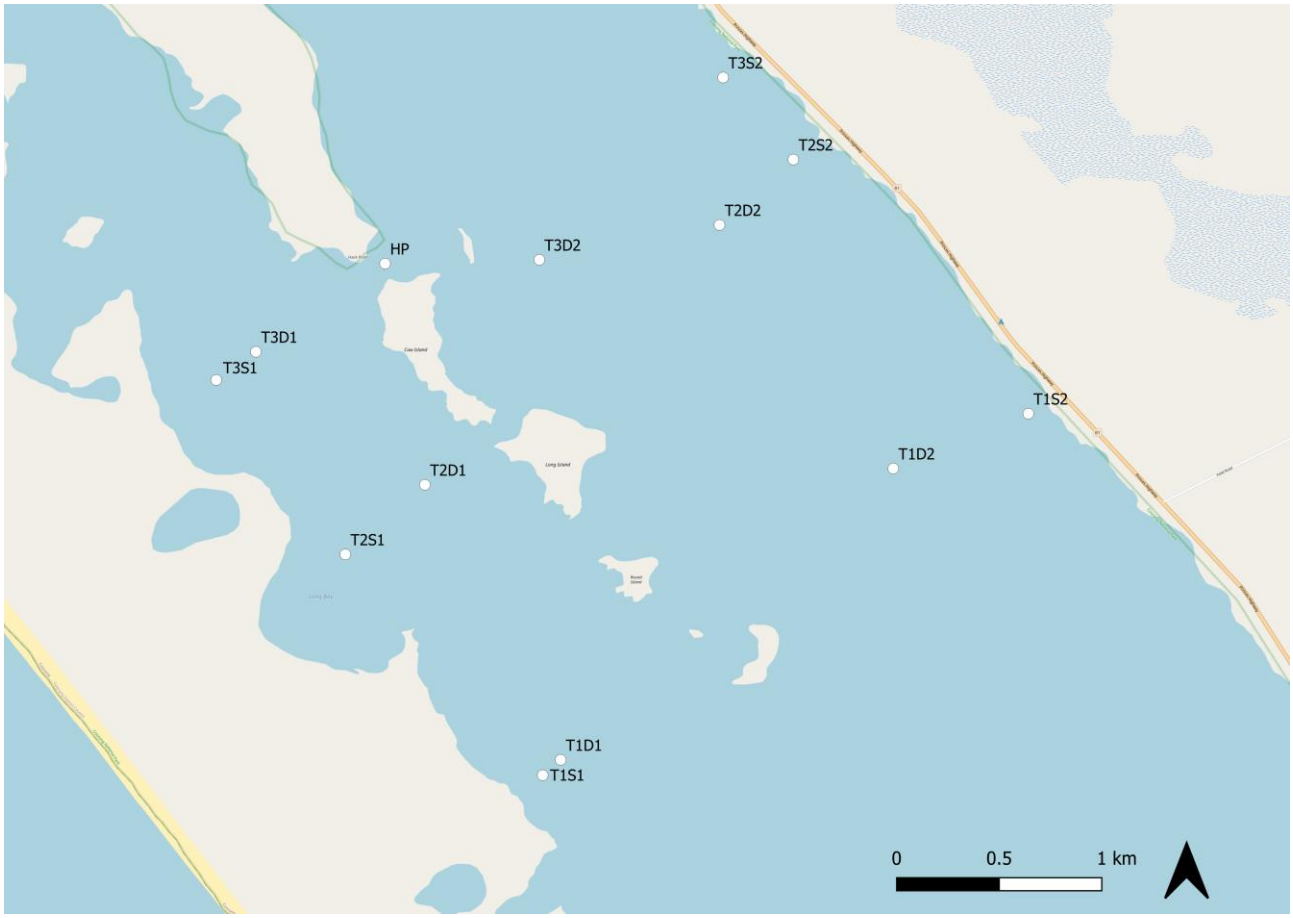

Figure 14. The sampling site at Villa dei Yumpa for investigating the effects of sediment resuspension on water column nutrients. Villa dei Yumpa is located at the northern end of the Coorong South Lagoon, immediately south of Parnka Point. The 13 sampling locations are denoted by transect (T1-3), water depth (shallow (S) ≤ 0.6m; deep (D) > 0.6 m) and proximity to each shoreline (1 Younghusband Peninsula, 2 the mainland) except for sampling location HP, which was established due to its proximity to the eddy covariance tower established at Hack Point.

2.5.2 Sampling methods

Intensive single-point sampling 1–3 March 2021

Intensive field measurements were made at sampling location T1S2 (Figure 1) over a 46 hour period beginning on 1 March 2021 at 11 am and concluding on 3 March 2021 at 9 am. These dates were selected based on Coorong weather predictions from the Bureau of Meteorology to maximise the chance of capturing a sediment resuspension event (e.g., strong southerly winds). Wind speed and direction were measured continuously during the sampling period (averaged over 5 minute intervals) from the shoreline using an Atmos-22 wind sensor (MEA, Adelaide, South Australia). Water samples (~500 mL) were taken at 20 time points (1 March: 12:15 pm, 2:30 pm, 4 pm, 6 pm, 8:30 pm, 10:15 pm; 2 March: 6 am, 8 am, 10 am, 12 pm, 2 pm, 4 pm, 5 pm, 6 pm, 7 pm, 8 pm, 9 pm, 10 pm; 3 March: 6:30 am, 8:30 am). Samples were taken from a single point along the transect, 0.15 m above the sediment using a bespoke water sampler consisting of a rule bilge pump (Xylem Australia, NSW) attached to a 30 m garden hose. The pump was operated remotely by attaching power cables running from the pump to a 12V battery located in a remote field lab on the shoreline.

Water samples were immediately processed for total nitrogen (TN), total phosphorus (TP), and dissolved nutrients (ammonium, oxidised nitrogen (nitrate + nitrite) and filterable reactive phosphorus). An 80 mL subsample was filtered through a pre-washed 0.45 µm filter with a pre-filter attached. The filtrate was stored in the dark at -18 °C. A second 80 mL subsample of raw water sample was stored in the dark at -18 °C. These subsamples were transported to the Australian Water Quality Centre (AWQC, Adelaide South Australia, NATA accredited) on 3 March 2021 for analysis of dissolved nutrients, TN and TP.

Turbidity was measured at the same time intervals stated above using a YSI EXO2 Sonde multiparameter probe (Xylem Australia, NSW). A 20 L bucket, pre-rinsed in site water, was filled using the bespoke water sampler immediately after the previous 500 mL water sample was taken. The EXO2 Sonde was submersed far enough into the bucket so that the measuring instrumentation was fully inundated. Once the readings had stabilised, triplicate measurements of water quality were taken 10 s apart and averaged for each time interval.

Multi-point sampling 21–24 June 2021

Sediment sampling, in addition to water sampling, was performed during the June 2021 sampling component to investigate the effect of varying sediment physical properties (bulk density, mean grain size, organic matter content, particle size distribution and water content) on water column turbidity and nutrient concentrations with varying wind conditions, as sediment physical properties can have an effect on their susceptibility to being resuspended (Grabowski et al. 2011).

Sediment cores were taken at all 13 sampling locations outlined in Figure 14 between 21 and 24 June 2021. Sediment cores (length ~30 cm, internal diameter 5.7 cm) were collected using a cylindrical PVC corer by pushing the corer into the sediment, followed by raising it vertically out of the sediment and plugging the bottom with a rubber stopper to prevent sediment loss. Overlying water was siphoned off using a syringe and the sediment was extruded from the core with the topmost 4 cm sliced off and placed into a plastic zip-lock bag. Sediment samples were stored in the dark at -18 °C until they were returned to the laboratory, where they were defrosted and homogenised prior to processing.

Triplicate aliquots of fresh sediment (~100 mg) were diluted for analysis of sediment particle size distribution (PSD) using a laser *in-situ* scattering transmissometer (LISST-100, Sequoia Scientific, Washington USA) fitted with a 115 mL mixing chamber. Sediment samples were suspended in 100 mL of deionised water and shaken to disaggregate weakly flocculated particles and then added to the mixing chamber. Twenty measurements of PSD were made at five-second intervals under constant mixing conditions. Sediment particles measured by the LISST (diameter 2.5-500 µm) are categorised into 32 size class bins, with size class 1 having a median diameter of 2.73 microns and size class 32 having a median diameter of 462 microns). Particle size distribution data were reported as the proportion of the total volume concentration.

Additional triplicate fresh sediment aliquots (~12 g) were taken from each sample for analysis of water content (WC), organic matter content (OM) and bulk density (ρ). Each fresh sediment aliquot was weighed, dried to a constant weight at 60°C, then combusted to a constant weight at 400°C. The WC was determined as the percentage difference in weight after drying at 60°C and the OM was determined as the difference in weight after combustion, reported as the percentage of dry weight or wet weight for use in bulk density calculations. Bulk density (ρ, g/cm^3) was calculated from WC and OM according to Håkanson and Jansson (1983):

$$\rho = 100 \times \rho_m / (100+(WC + IG_0) \times (\rho_m - 1)$$

where ρ_m is the density of inorganic particles (taken to be 2.6); and

IG_0 is the OM reported as percentage of fresh weight.

Water samples were taken at six time intervals from 21 to 24 June 2021. Samples were taken at locations T1D2, T2D2 and T3D2 (Figure 14) from 21 to 23 June 2021 and at HP (Figure 14) on 24 June 2021. Sampling was divided into two time intervals per day (~8–11 am and ~1–4 pm). Only an afternoon sampling was possible on 21 June due to transportation time to the site. Sampling locations were accessed by boat, marked on site by deploying a buoy and with a GPS. Strong wind conditions prevented sampling by boat on 24 June, resulting in sampling at HP by wading into the water. An additional three samples were taken during a manual resuspension event created by repeatedly driving the boat in circles until bottom sediments were visibly resuspending, replicating resuspension conditions previously observed from a boat in deeper water under strong wind conditions in March 2021. This was repeated at three sampling locations (T1D1, T2D1 and T3S1, Figure 14) on the afternoon of 23 June 2021.

1 L grab water samples were taken ~0.3 m below the surface in pre-rinsed grey polyethylene bottles and stored in the dark on ice until they were processed on the shoreline for total and dissolved nutrients as described above. A YSI EXO2 Sonde multiparameter probe (Xylem Australia, NSW) was used to measure turbidity at the same depth the grab water sample was taken. Once the readings had stabilised, triplicate measurements were taken 10 seconds apart and averaged for each time interval.

Wind speed and direction were measured continuously throughout the duration of the sampling period (averaged over 30 min intervals) from an eddy covariance tower (LI-COR, Lincoln, NE, USA) fitted with an anemometer (Gill Windmaster Pro 3-D) erected at Hack Point (HP in Figure 14).

Longer-term data

Longer-term continuous turbidity and wind data was obtained from the Department for Environment and Water (available at www.water.data.sa.gov.au) for the monitoring station on the main lagoon near Woods Well (A4261209) and the monitoring station near Parnka Point (A4260633), respectively. Analysis of Woods Well (turbidity) data was performed with wind speeds from Parnka Point for the period 16 December 2019 to midnight 26 February 2021. Parnka Point wind speed was recorded as the average wind speed over 10 min intervals. Woods Well turbidity was recorded every 5 minutes.

2.5.3 Statistical analyses

Data were analysed in R studio v4.1.3 using the R stats v4.1.3 and Performance Analytics v2.0.4 packages. Numerical summaries (mean, standard error of mean, maximum and minimum values) of measured variables were produced to allow comparisons of recorded variables with other results within this study and to results from previous studies. Variables were tested for their normality using the Shapiro-Wilk test and by visual inspection of a histogram of their distribution. Correlation analyses were performed to test for relationships between the variables. Spearman Rank-order correlations were used to test the relationship between the variables as all variables were non-normally distributed. The Kruskal-Wallis test was used to test for differences in continuous variables between categories. Post Hoc testing was carried out using the Wilcoxon rank sum test to reveal which categories significantly differed. Statistical significance was given when the *P*-value was < 0.05. All plots of measured variables were created using the ggplot2 v3.3.5 package and in Microsoft Excel 2021.

The results of the nutrient analysis from water sample from 8 pm 2 March 2021 were removed from the analysis due to a large discrepancy with all other values recorded (TN and TP below detectable levels). The cause of this error is unknown. All statistical analyses investigating the relationship of wind speed to turbidity and nutrients (total and dissolved) did not include the manual resuspension events created on 23 June 2021.

PSD statistical analyses were performed using the software package GRADISTAT (v9.1) using the Folk and Ward graphical method to calculate grain size parameters, such as the mean grain size (MGS, µm), the median grain size (D_{50}), and the sand and mud fractions (%). This method is relatively insensitive to samples with a large particle range in the tails of the distribution and provides a robust tool to compare compositionally variable samples (Blott and Pye 2001).

3 Results

3.1 Bulk sediment quality

The results of the March 2020 sediment quality survey indicate varying degrees of sediment health in the Coorong, with three main sediment types (Figure 15):

(A) Sediments with a visible oxic zone in the top approximately 5–10 cm of sediment, sometimes overlying black ooze sediments. These characteristics would normally signify healthy sediment

conditions; however, no benthic organisms were visible in these South Lagoon sediment samples, presumably due to the hypersalinity or other factors (e.g. high sulfide as discussed further below).

(B) Black organic-rich oozes (0–10 cm) grading to thick sulfide-rich (10–50 cm) black sediments with no or minimal (< 1 mm) oxic layer. These black oozes are considered unhealthy sediment conditions. No benthic organisms were present in these samples, presumably due to the hypersalinity and/or high sulfide content.

(C) Variable texture sediments with an oxidised layer (approximately 5–10 cm) and visible benthic organisms. These are considered healthy sediment conditions but were mostly only found in the northern region of the North Lagoon.

Seagrasses such as *Ruppia* sp. uptake nutrients from both the surface water and sediment pore water, but cycle nutrients more slowly than rapidly growing phytoplankton and filamentous algae. There is evidence that the roots of *Ruppia* sp. oxygenate the black ooze sediment in the Coorong (Figure 16), which is a known feature of seagrasses (Borum et al. 2007).

The poor sediment quality in much of the Coorong was reflected in very low total RAP scores; approximately 80% of samples had a RAP score ≤4 (Figure 16), particularly where *Ruppia* and macroinvertebrate species were not present. This is also reflected in the apparent Redox Potential Discontinuity (aRPD) being < 1 cm in most samples. This is consistent with observations of sulfide-rich (anoxic) black oozes present across wide areas of the lagoons. However, the aRPD data suggests a mixture of results, likely signifying some uncertainties in estimating the oxic to sub-oxic transition and the sub-oxic to anoxic transition with this semi-qualitative method.

Figure 15. Photos summarising key visual observations of sediments across the Coorong.

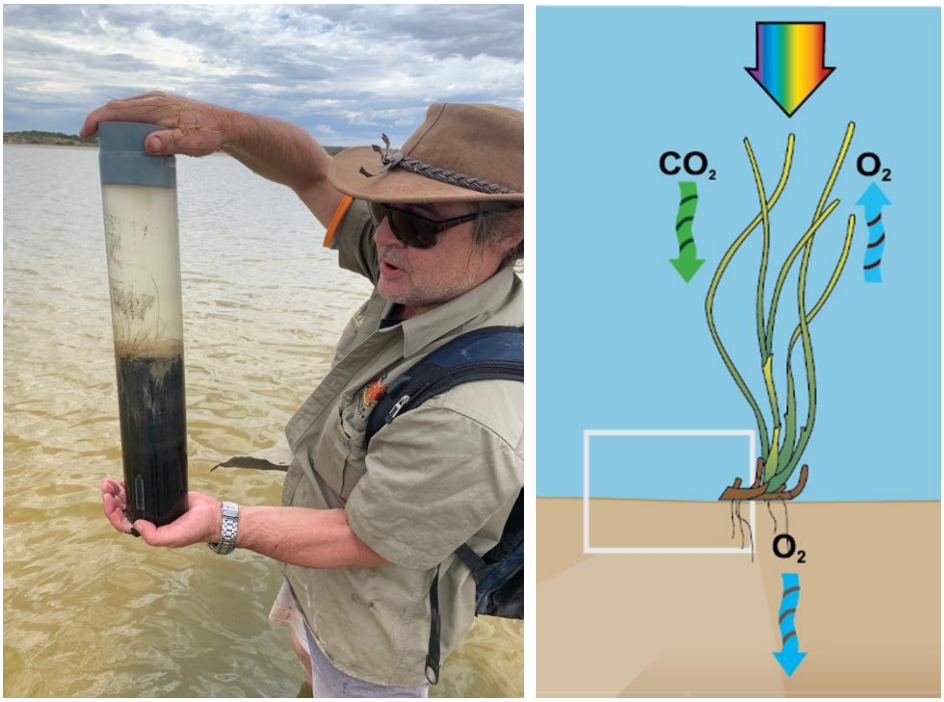

Figure 16. Evidence of the influence of aquatic plants (*Ruppia* sp.) on sediment quality. The influence of oxygen in the zone of root influence (rhizosphere) is visible by the lighter brown colouration (presumed to be iron oxides) adjacent to the plant roots. The conceptual model to the right illustrates this process can occur under light conditions via photosynthetically driven oxygen release from roots of aquatic plants.

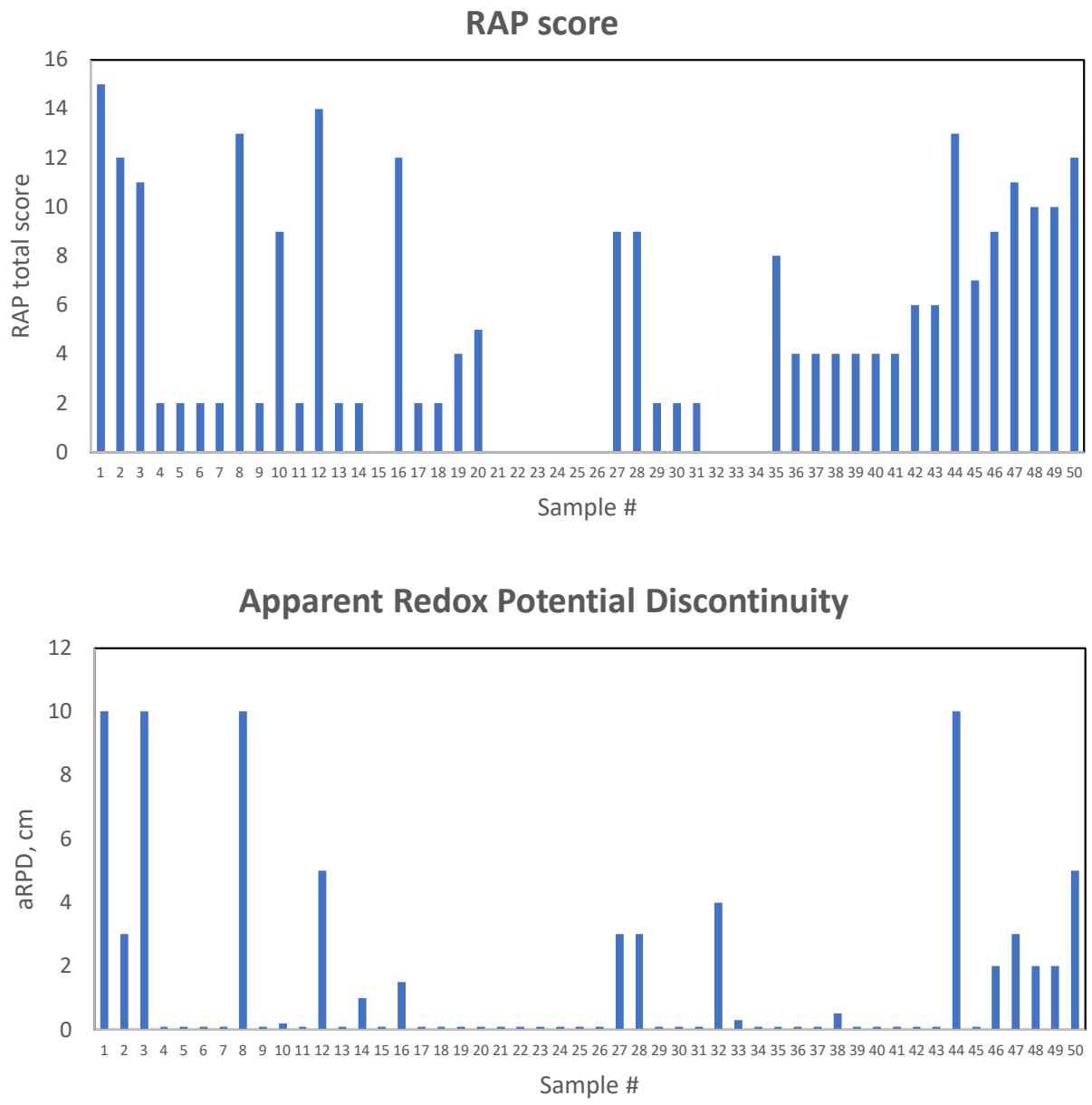

Figure 17. Rapid Assessment Protocol (RAP) total scores (top), and apparent Redox Potential Discontinuity depth (aRPD; bottom) for different sites (samples) across the site. The sample numbers (#) on the x axis correspond to the COOR-X numbers in Figure 2.

Generally, TN, TP, TOC and Acid Volatile Sulfide (AVS) concentrations increased in a gradient towards the South Lagoon (Figure 18). The sediment in the deeper (>2m water depth) basins of the South Lagoon had high total nutrient, organic carbon and AVS concentrations (~5–7% TOC, 0.5–0.7% TN, 0.5–0.6% TP, >0.004% AVS). This is also where predominantly black ooze sediment was found with no aquatic plants (additionally, no bioturbating macroinvertebrates in the South Lagoon). The southern region of the North Lagoon (i.e. 7 Mile Basin) also has high total nutrient, TOC and AVS concentrations and is also dominated by a black ooze sediment type. Samples collected in the vicinity of the key source water inputs, Salt Creek and barrage outflows near the Murray Mouth, showed lower sediment nutrient and TOC concentrations.

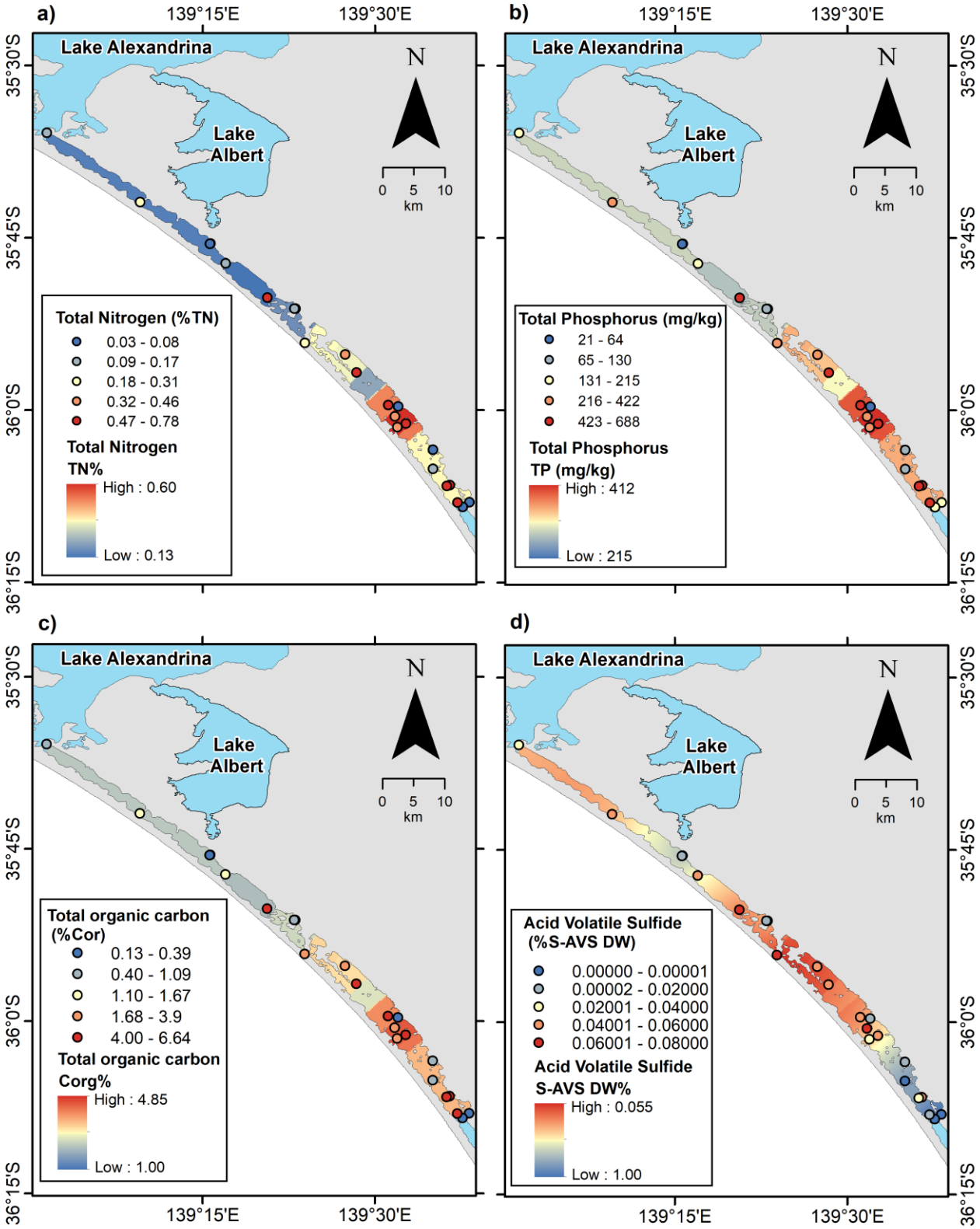

Figure 18. Map of sediment quality for total nitrogen (TN), total phosphorus (TP), total organic carbon (TOC) and acid volatile sulfide (AVS, dry weight basis). Interpolation between sampling points was performed via kriging. There is lower accuracy of interpolation where there is a lower sampling density.

The similar patterns present for TN, TP and TOC in the water column suggests strong organic matter-nutrient coupling between the water column and sediment, as supported by stable isotope measurements in the Coorong sediment and water column indicating algal derived organic matter sources (Priestley et al. 2022b). This is also similar to previous findings in some other shallow eutrophic estuaries (Heip 1995).

The sulfide parameters, AVS and S_{Cr} (chromium reducible sulfur-reduced inorganic sulfur), showed more variability but tended to increase with salinity (e.g. see Figure 18 for AVS). A total of 18 of 26 (69%) of the surface (0–5 cm) sediment core samples were classified as Monosulfidic Black Ooze (MBO) based on AVS concentrations greater than the national guideline value (Sullivan et al. 2018) of 0.01% (on a dry sediment weight basis). The average (± standard deviation) AVS concentration in Coorong sediment samples classified as MBO was 0.046 ± 0.020 % (n = 18), which is over four times greater than the national guideline level. The exception to this general MBO distribution was when sediment salinity was comparatively low (i.e. dominated by freshwater), such as near the Murray Mouth or Salt Creek (Figure 3), likely because both sulfate and OM contents are lower in freshwater and flushing is higher at these locations.

Only minor exceedances of the sediment quality guideline values (SQGV) for total and 1 mol/L HCl extractable arsenic were observed (Figure 19). The SQGVs are based on effects data from a United States database (Simpson et al. 2013) and Arsenic (As) and Nickel (Ni) concentrations of sediments in Australia frequently exceed the corresponding SQGV but are generally considered a low risk when exceedances are moderate (e.g. with a factor of two), which is the case here. There were no clear patterns in metal(loid) concentration with latitude.

It is likely the amount of reactive iron available in the system limits the formation of AVS as free sulfides can diffuse out of the sediment. Much of the sediment iron is tied up in the more stable form of FeS_2 (pyrite), with the average 0.179% S S_{Cr} being much greater than the average AVS concentration.

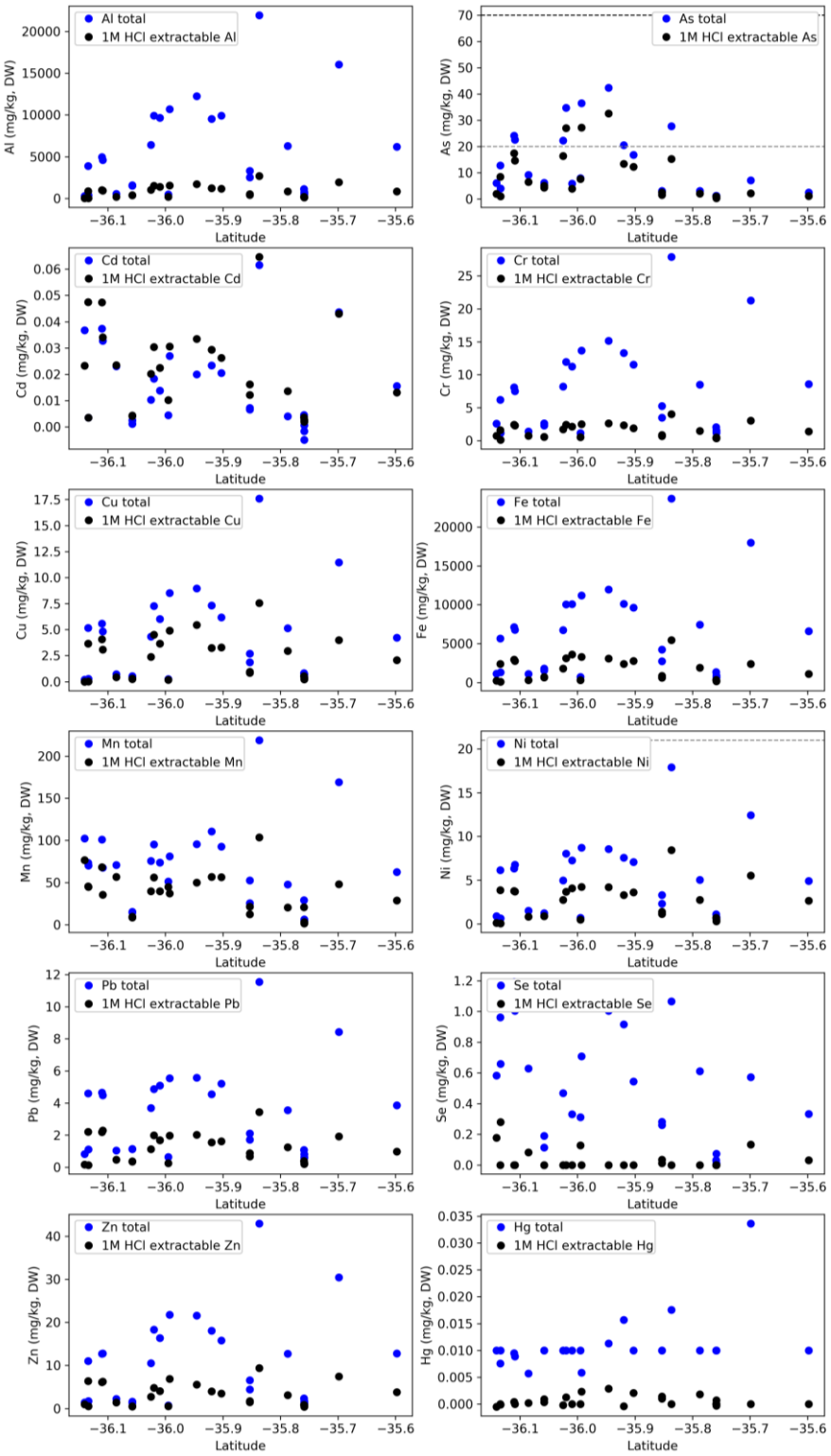

Figure 19. Total and potentially bioavailable (1M HCl extracted) metal(loid) concentrations in the Coorong (in milligrams per kilogram dry weight). Aluminium (Al), Arsenic (As), Cadmium (Cd), Chromium (Cr), Copper (Cu), Iron (Fe), Manganese (Mn), Nickel (Ni), Lead (Pb), Selenium (Se), Zinc (Zn), Mercury (Hg). The horizontal dashed line is the sediment quality guideline values (SQGV) for Arsenic (As), which when exceeded may lead to additional studies to confirm or deny the possibility of biological impacts of that contaminant. The upper dashed line is the upper sediment quality guideline value SQGV-high for Arsenic (As): equivalent to the median of the biological effects range.

3.2 Nutrient cycling and fluxes

3.2.1 Deep permanent dark site sediments

Sediment porewater depth profiles of inorganic nutrients, ferrous iron, and sulfide

Sediments collected from the two deep permanently dark sites – South of Salt Creek and Near Swan Island – in late February and early March 2021 consisted of black anoxic ooze sediment. The salinity at both sites was up to 110 PSU. Ammonium concentrations increased from surface water to the sediment 11 cm below SWI (Figure 20) and the concentrations varied significantly with depth ($p < 0.001$, GAM; Table 5-6a). The maximum porewater ammonium concentrations of 2800 and 1400 µmol/L were observed at 11 cm below SWI from the South of Salt Creek and Near Swan Island sites, respectively.

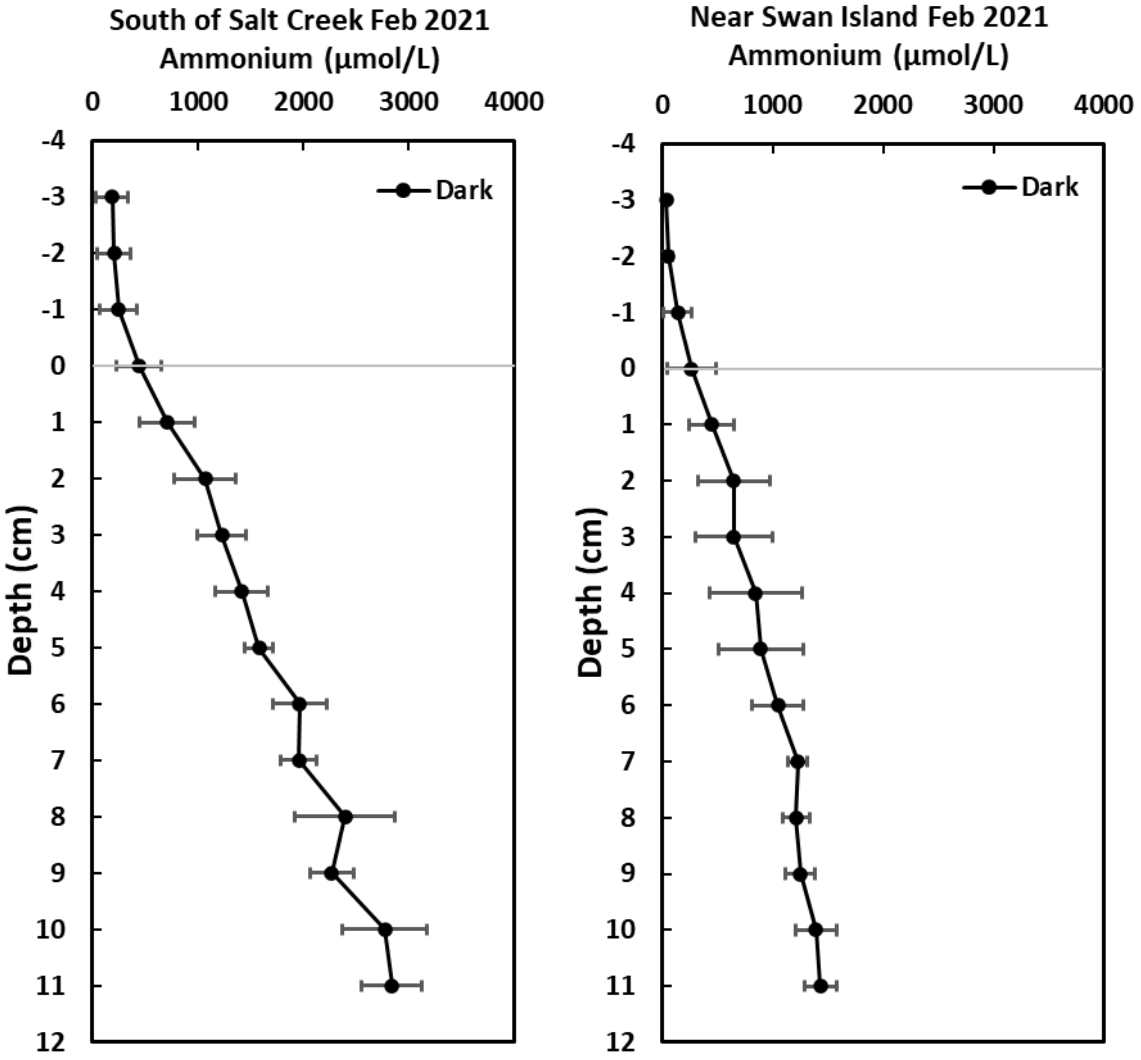

Figure 20. Depth profiles of ammonium in black anoxic ooze sediment from the South of Salt Creek and Near Swan Island during dark incubation. Data are mean values and error bars represent the standard deviation of the mean (n = 5). The grey solid line indicates the sediment-water interface (SWI).

Porewater phosphate concentrations also increased significantly from the surface water to the sediment 11 cm below SWI under dark incubation ($p < 0.001$, GAM; Figure 21 and Tables 5–6b). Porewater phosphate concentration profiles followed a similar pattern to those of ammonium. The highest porewater phosphate concentrations of 267 µmol/L and 112 µmol/L occurred 11 cm below SWI from the South of Salt Creek and Near Swan Island sites, respectively.

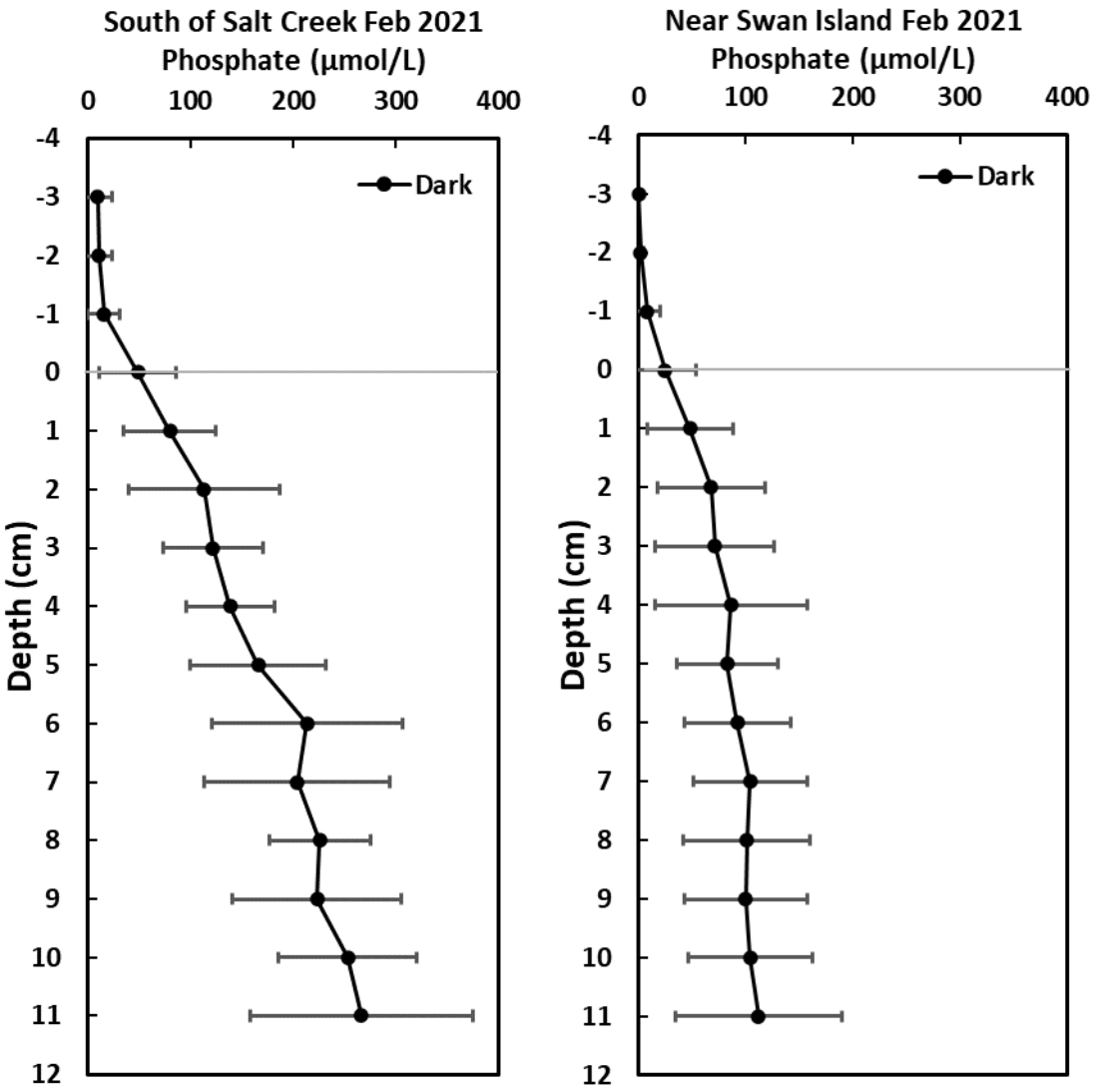

Figure 21. Depth profiles of phosphate in black anoxic ooze sediment from the South of Salt Creek and Near Swan Island during dark incubation. Data are mean values and error bars represent the standard deviation of the mean (n = 5). The grey solid line indicates the sediment-water interface (SWI).

Low dissolved ferrous (Fe^{2+}) iron concentrations were found in the two deep sites South of Salt Creek and near Swan Island. The profiles of dissolved ferrous iron from both two deep sites were significantly different across depth ($p < 0.001$, GAM; Tables 5–6c). The highest dissolved ferrous iron concentration in the surface water from the South of Salt Creek site was approximately 5 µmol/L. The dissolved ferrous iron profiles in the sediment fluctuated around 5 µmol/L throughout the depth. For the Near Swan Island site, the iron concentrations fluctuated between 4 to 10 µmol/L from the surface water to the sediment down to a depth of 11 cm (Figure 22).

Up to 50 µmol/L of sulfide was found in surface water at these deep sites. The sulfide concentrations increased from the surface water to the sediment and fluctuated in sediment over depth ($p < 0.001$, GAM; Figure 23 and Tables 5–6d). The maximum sulfide concentrations in sediment were 87 ± 16 µmol/L and 93 ± 58 µmol/L at the South of Salt Creek and Near Swan Island sites, respectively.

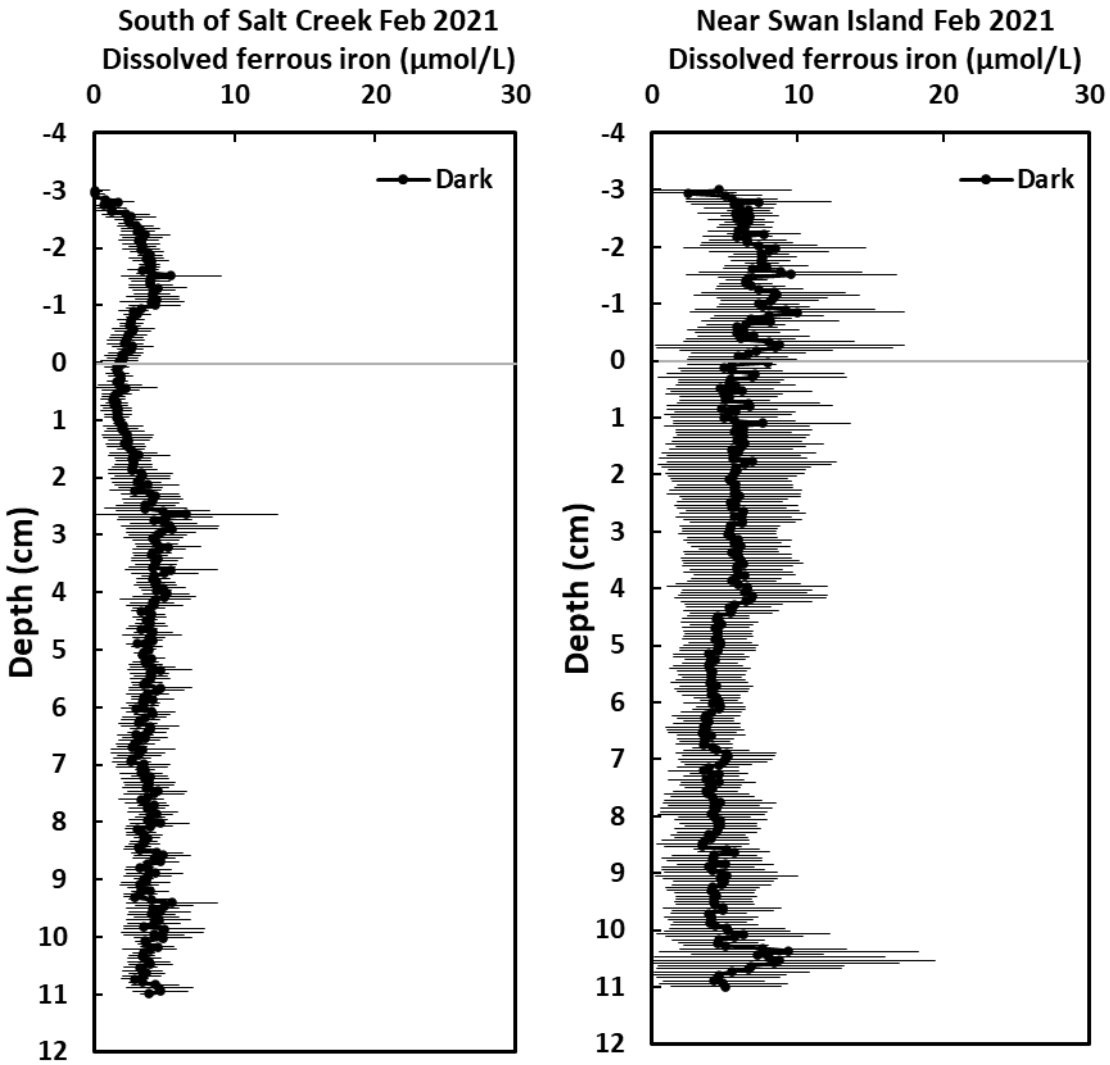

Figure 22. Depth profiles of dissolved ferrous iron in black anoxic ooze sediment from the South of Salt Creek and Near Swan Island during dark incubation. Data are mean values and error bars represent the standard deviation of the mean (n = 5). The grey solid line indicates the sediment-water interface (SWI).

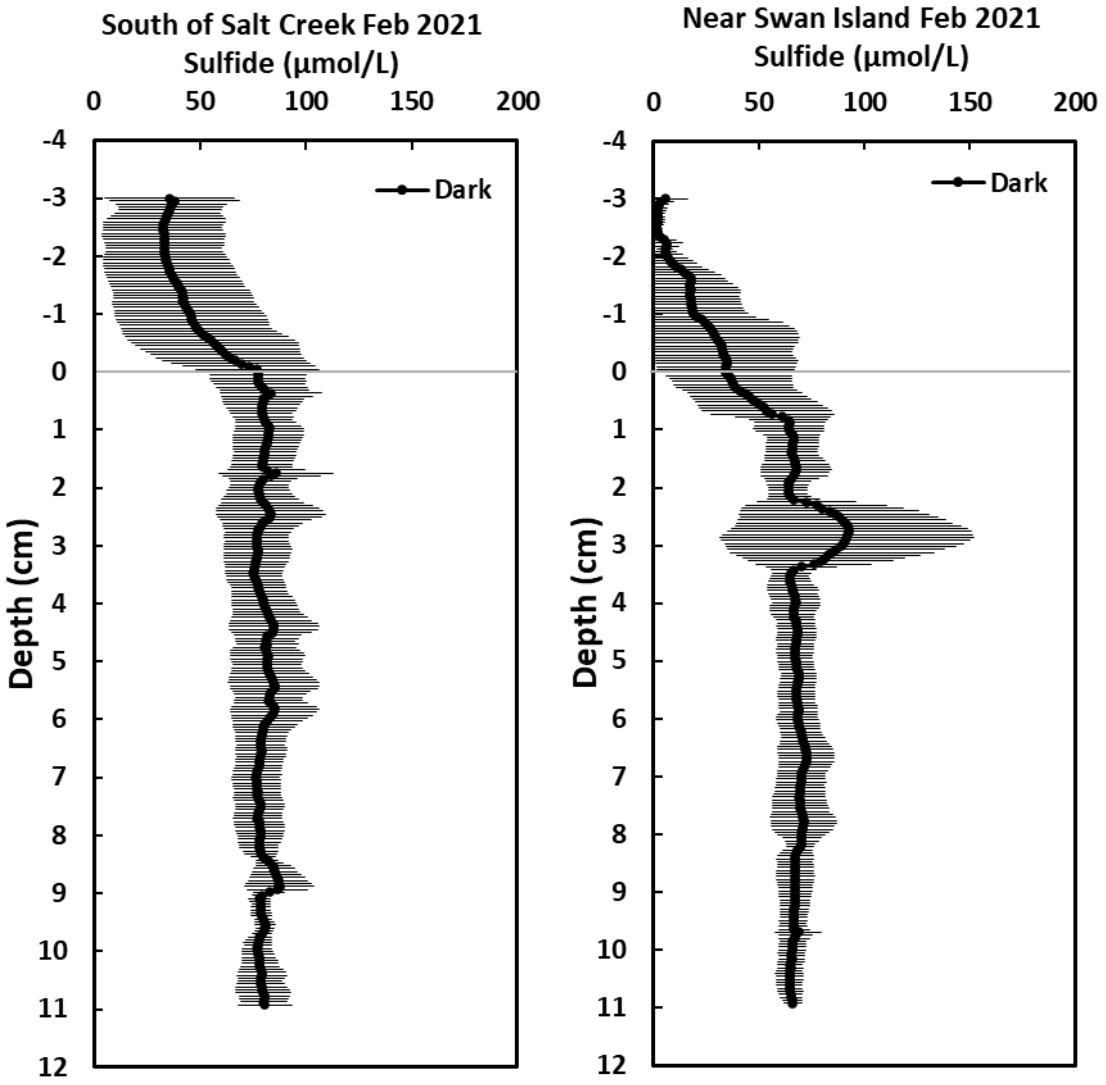

Figure 23. Depth profiles of sulfide in black anoxic ooze sediment from the South of Salt Creek and Near Swan Island during dark incubation. Data are mean values and error bars represent the standard deviation of the mean (n = 5). The grey solid line indicates the sediment-water interface (SWI).

Table 5. Summary table of the results from the Generalised Additive Models (GAM) for inorganic nutrients, dissolved ferrous iron, and sulfide at the South of Salt Creek site.

PARAMETRIC COEFFICIENTS	ESTIMATE	STD. ERROR	T VALUE	PR(>|T|)	DEVIANCE EXPLAINED	AIC
a) Ammonium						
Parametric coefficients						
Dark	1417.000	29.890	47.410	< 0.001	92.70%	1052.4
Smooth terms						
Depth	edf = 3.277	Ref.df = 9	F = 99	< 0.001		
b) Phosphate						
Parametric coefficients						
Dark	139.550	6.814	20.480	< 0.001	69.40%	829.6
Smooth terms						

Depth	edf = 2.18	Ref.df = 9	F = 17.84	< 0.001		
c) Ferrous iron						
Parametric coefficients						
Dark	4.096	0.409	100.100	< 0.001	27.30%	5036.4
Smooth terms						
Depth	edf = 8.789	Ref.df = 9	F = 55.87	< 0.001		
d) Sulfide						
Parametric coefficients						
Dark	72.142	0.484	149.100	< 0.001	44.45%	11805.2
Smooth terms						
Depth	edf = 8.3	Ref.df = 9	F = 120.5	< 0.001		

Table 6. Summary table of the results from the Generalised Additive Models (GAM) for inorganic nutrients, dissolved ferrous iron, and sulfide at the Near Swan Island site.

PARAMETRIC COEFFICIENTS	ESTIMATE	STD. ERROR	T VALUE	PR(>|T|)	DEVIANCE EXPLAINED	AIC
a) Ammonium						
Parametric coefficients						
Dark	768.380	25.180	30.510	< 0.001	83.20%	1026.0
Smooth terms						
Depth	edf = 2.611	Ref.df = 9	F = 39.02	< 0.001		
b) Phosphate						
Parametric coefficients						
Dark	66.932	5.283	12.670	< 0.001	41.90%	791.1
Smooth terms						
Depth	edf = 1.89	Ref.df = 9	F = 5.566	< 0.001		
c) Ferrous iron						
Parametric coefficients						
Dark	6.106	0.094	64.690	< 0.001	8.89%	7325.1
Smooth terms						
Depth	edf = 6.742	Ref.df = 9	F = 14.01	< 0.001		
d) Sulfide						
Parametric coefficients						
Dark	56.734	0.509	111.400	< 0.001	59.90%	11943.7
Smooth terms						
Depth	edf = 7.849	Ref.df = 9	F = 224.6	< 0.001		

Benthic metabolism and nutrient fluxes

Light did not penetrate to the sediments at deep sites so fluxes were only measured under dark conditions. Both deep sites were sinks for water column oxygen during dark incubations with oxygen consumption at 2308 ± 709 and 4007 ± 612 µmol O_2 /m^2/h (Figure 24) with a statistical difference between sites (p = 0.004, Student T-test). Additionally, both sites were sinks for water column DOC under dark incubation with the DOC influxes of -8225 ± 37490 and -29687 ± 14464 µmol/m^2/h at the South of Salt Creek and Near Swan Island sites, respectively (Figure 25). No significant difference was observed for the DOC between the sites (p = 0.267, Student T-test).

Ammonium and nitrate were released from the sediment to the water under dark conditions at both sites (Figure 42). The mean ammonium and nitrate efflux was 1074 ± 167 µmol/m^2/h and 52.9 ± 21.0 µmol/m^2/h at the South of Salt Creek site, respectively (Figure 42). Whereas, for the Near Swan Island site, the mean ammonium and nitrate effluxes were about half of those at the South of Salt Creek, measuring 503 ± 363 µmol/m^2/h and 26.9 ± 11.8 µmol/m^2/h, respectively. The sediment-water column fluxes of ammonium and nitrate were significantly different at the two sites (p = 0.013 for ammonium and p = 0.042, Student T-test). For phosphate, the sediment-water column fluxes were negligible at both sites (Figure 42). Both nitrate and phosphate fluxes were quantitatively small compared to those of ammonium at both deep sites.

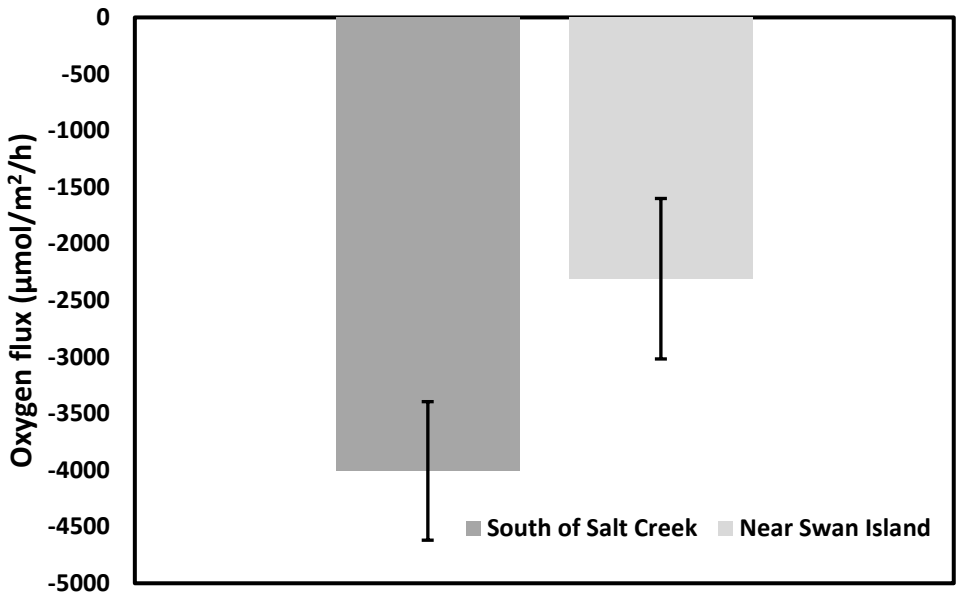

Figure 24. Sediment-water column fluxes of oxygen at sediment from the South of Salt Creek (dark grey bar) and Near Swan Island (light grey bar) sites during dark incubation. Data are mean values and error bars represent the standard deviation of the mean (n = 5).

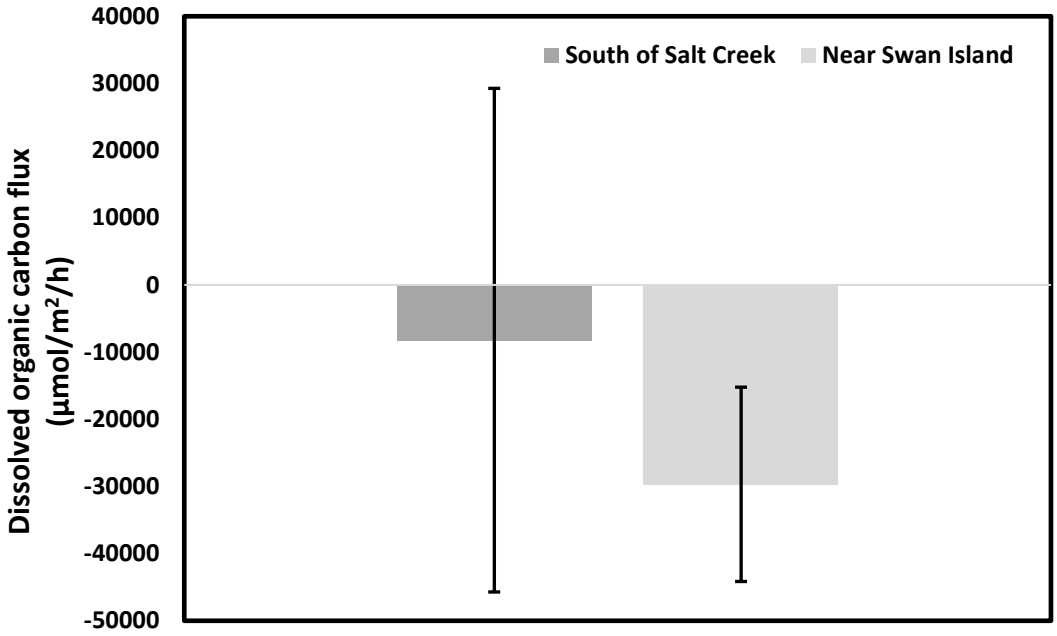

Figure 25. Sediment-water column fluxes of dissolved organic carbon (DOC) at sediment from the South of Salt Creek (dark grey bar) and Near Swan Island (light grey bar) sites during dark incubation. Data are mean values and error bars represent the standard deviation of the mean (n = 5).

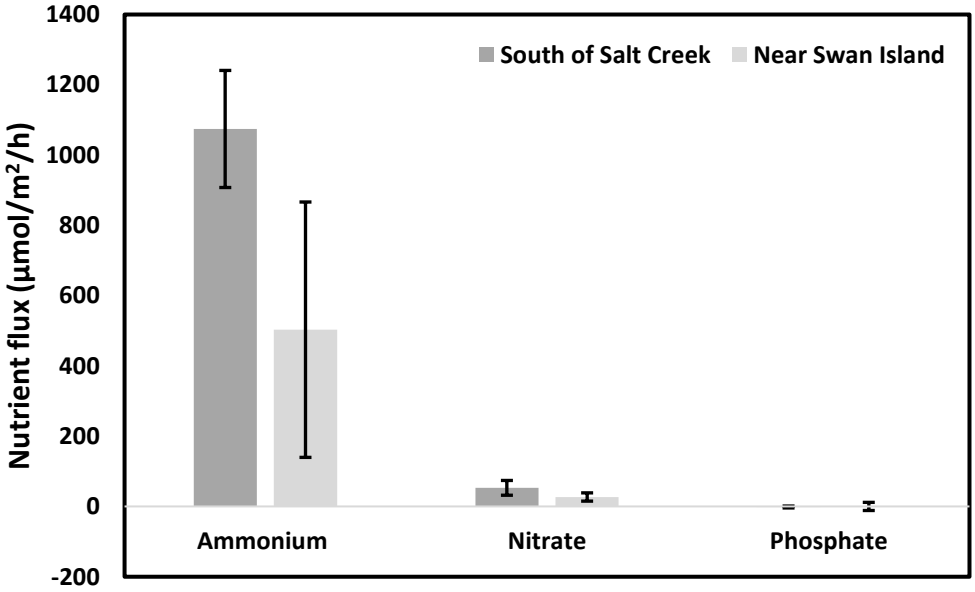

Figure 26. Sediment-water column fluxes of nutrients at sediment from the South of Salt Creek (dark grey bar) and Near Swan Island (light grey bar) sites during dark incubations. Data are mean values and error bars represent the standard deviation of the mean (n = 5).

3.2.2 Shallow water sediments

Sediment porewater depth profiles of inorganic nutrients, ferrous iron, and sulfide

Sediments that were collected from various shallow sediment sites had sufficient light to support the photosynthesis of microphytobenthos (microalgae and cyanobacteria), so fluxes were measured under both dark and light conditions. The shallow sediment sites showed differences in sediment porewater

concentration profiles of dissolved inorganic nutrients, ferrous iron, and sulfide among sites, over depth and between light and dark conditions.

Profiles of ammonium in the sediment from the Noonameena site in November 2020 were significantly different across depth ($p < 0.001$, GAM; Figure 28 and Table 7a) and between the light and dark incubation ($p < 0.001$, GAM; Figure 28 and Table 7a). Ammonium concentrations started low in surface water and increased with increased sediment profile depth up to 2 and 3 cm below the SWI under light and dark incubation, respectively (Figure 28). The ammonium concentrations were slightly higher under dark incubation than light incubation, fluctuating between 30 and 40 µmol/L, and between 40 and 50 µmol/L under light and dark incubation, respectively beyond the top 2–3 cm.

Most of the phosphate concentrations were lower than the method detection limit (MDL) of 5 µmol/L from the DET technique (Figure 27). The phosphate concentrations detected by the DET technique were at the sediment depth of 8.5 cm below SWI. No significant difference was observed for phosphate profiles across depth ($p = 0.677$, GAM; Table 8a) or between the light and dark incubation ($p = 0.827$, GAM; Table 8a).

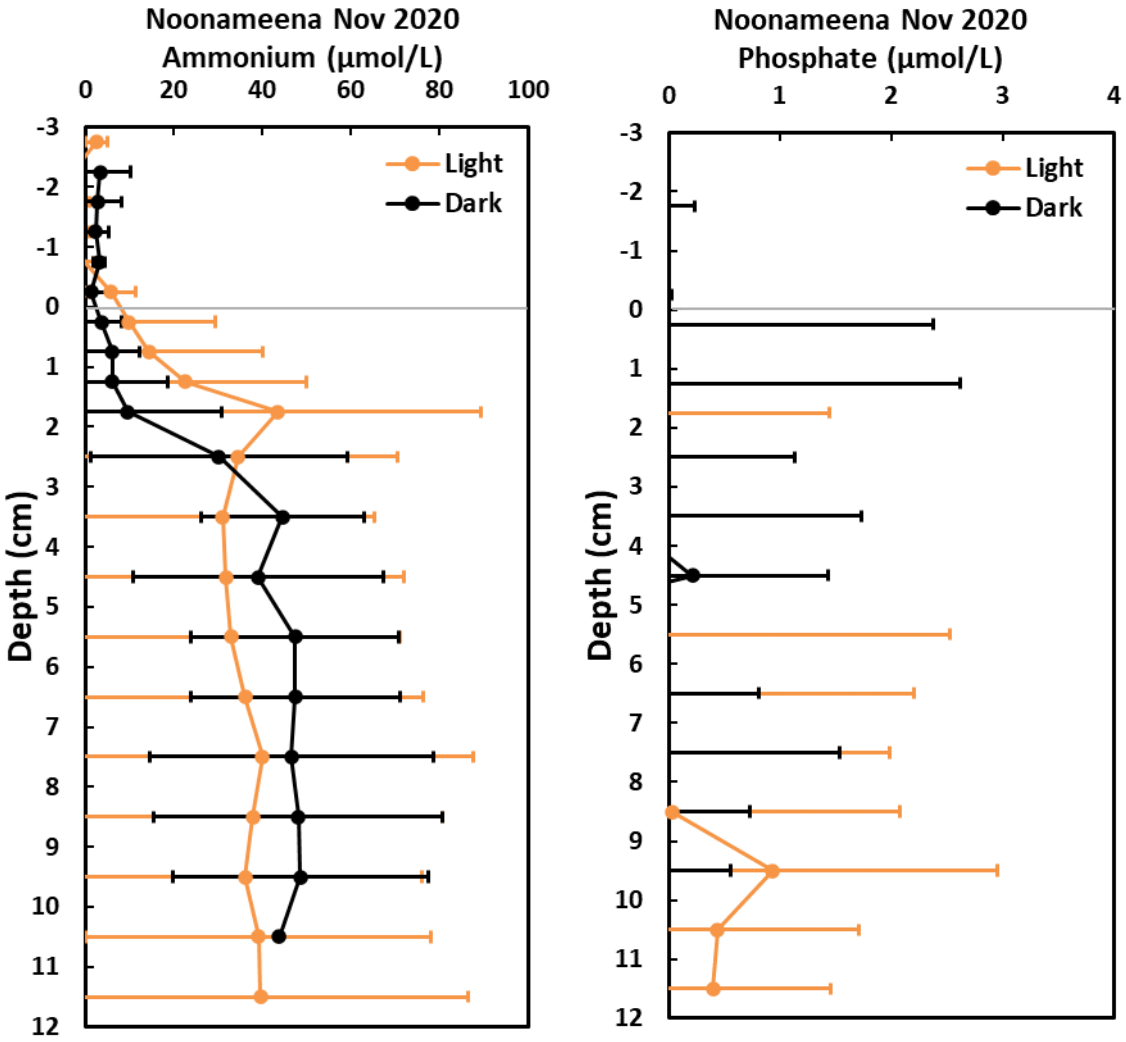

Figure 27. Depth profiles of ammonium and phosphate in sandy sediment at the Noonameena site with burrowing organisms present during light and dark incubations. Data are mean values and error bars represent the standard deviation of the mean (n = 5). The grey solid line indicates the sediment-water interface (SWI).

The ammonium concentrations from the Policeman's Point site in November 2020 increased significantly from surface water to the sediment ($p < 0.001$, GAM; Figure 28 and Table 7b). The ammonium profiles in the sediment were significantly different between the light and dark incubation ($p < 0.001$, GAM; Figure 28 and

Table 7b). Higher ammonium concentrations were measured under dark incubation. The maximum ammonium concentration was about 150 and 500 µmol/L during light and dark incubation, respectively.

The phosphate profiles in sediments were significantly different across depth ($p < 0.001$, GAM; Table 8b) and between the light and dark incubation ($p < 0.05$, GAM; Table 8b), although some of the phosphate concentrations were less than the MDL of 5 µmol/L from the DET technique (Figure 28). In addition, the phosphate concentrations in sediments were higher between 7 and 11.5 cm below the SWI under dark incubation than light incubation.

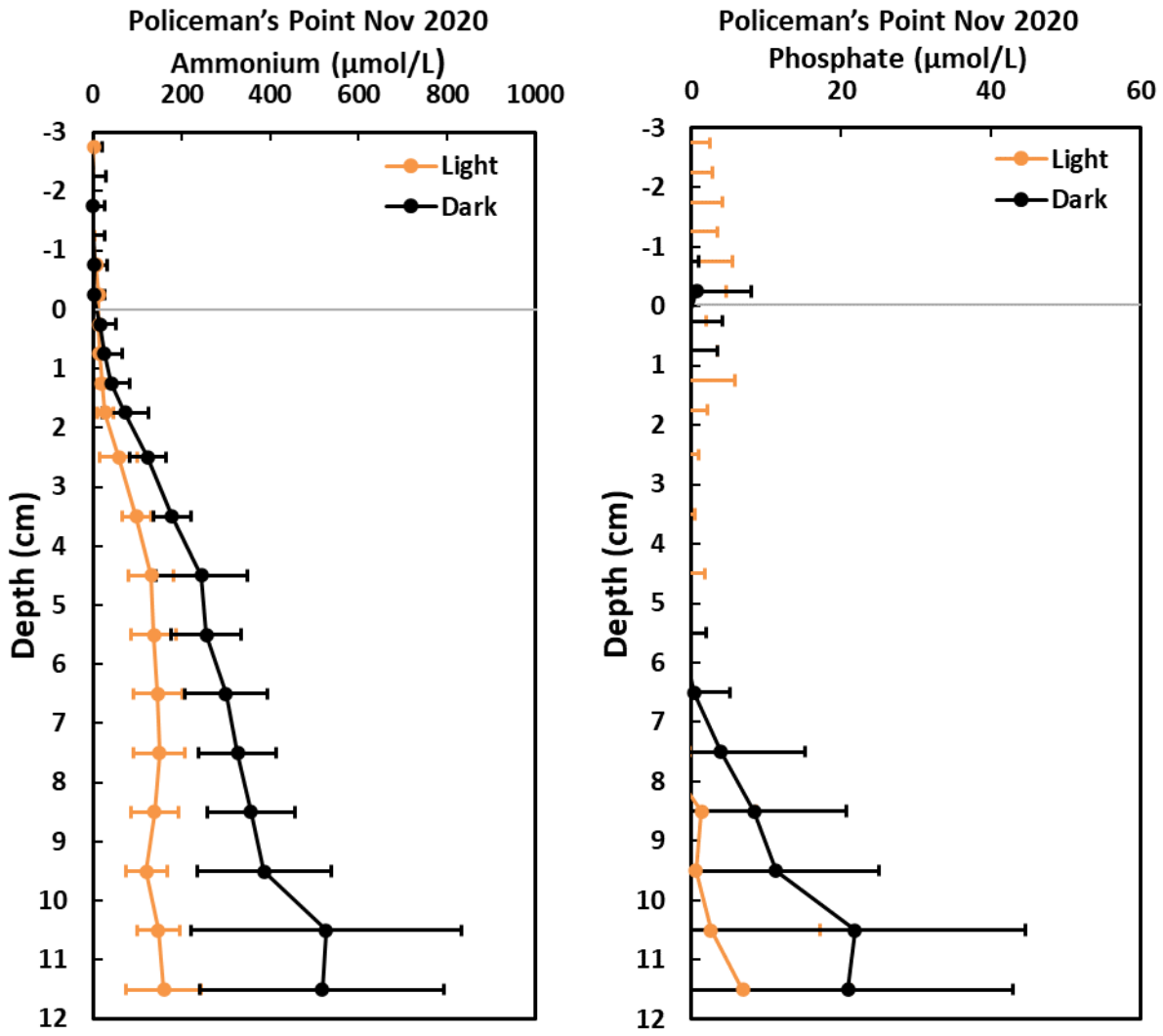

Figure 28. Depth profiles of ammonium and phosphate in muddy sediment at the Policeman's Point site colonised by *Ruppia* sp. during light and dark incubations. Data are mean values and error bars represent the standard deviation of the mean (n = 5). The grey solid line indicates the sediment-water interface (SWI).

Ammonium profiles in sediments from the Parnka Point site in February 2021 were significantly different across depth ($p < 0.001$, GAM; Figure 28 and Table 7c) and between light and dark incubations ($p < 0.05$, GAM; Figure 28 and Table 7c). The ammonium concentrations increased from surface water up to 3 and 4 cm below the SWI, followed by a gradual decrease up to 11 cm below the SWI under both light and dark incubation. The ammonium concentrations were higher under light incubation than in dark incubation. Under light incubation, the highest ammonium concentration was approximately 220 µmol/L at 3 cm below SWI. The maximum ammonium concentration of 170 µmol/L was observed at 4 cm below SWI under dark incubation.

Phosphate concentrations in sediments from the Parnka Point site were also significantly different across depth ($p < 0.001$, GAM; Figure 28 and Table 8c) but not significantly different between the light and dark

incubation ($p > 0.05$, GAM; Figure 28 and Table 8c). Phosphate concentrations increased slightly, followed by a decrease, then rose again under the light condition, while the phosphate concentrations increased slightly with the increased depth under the dark condition. Phosphate concentrations ranged from 2.5 to 11 µmol/L under light and dark conditions. The MDL of phosphate from the DET technique was 1.5 µmol/L for this field study.

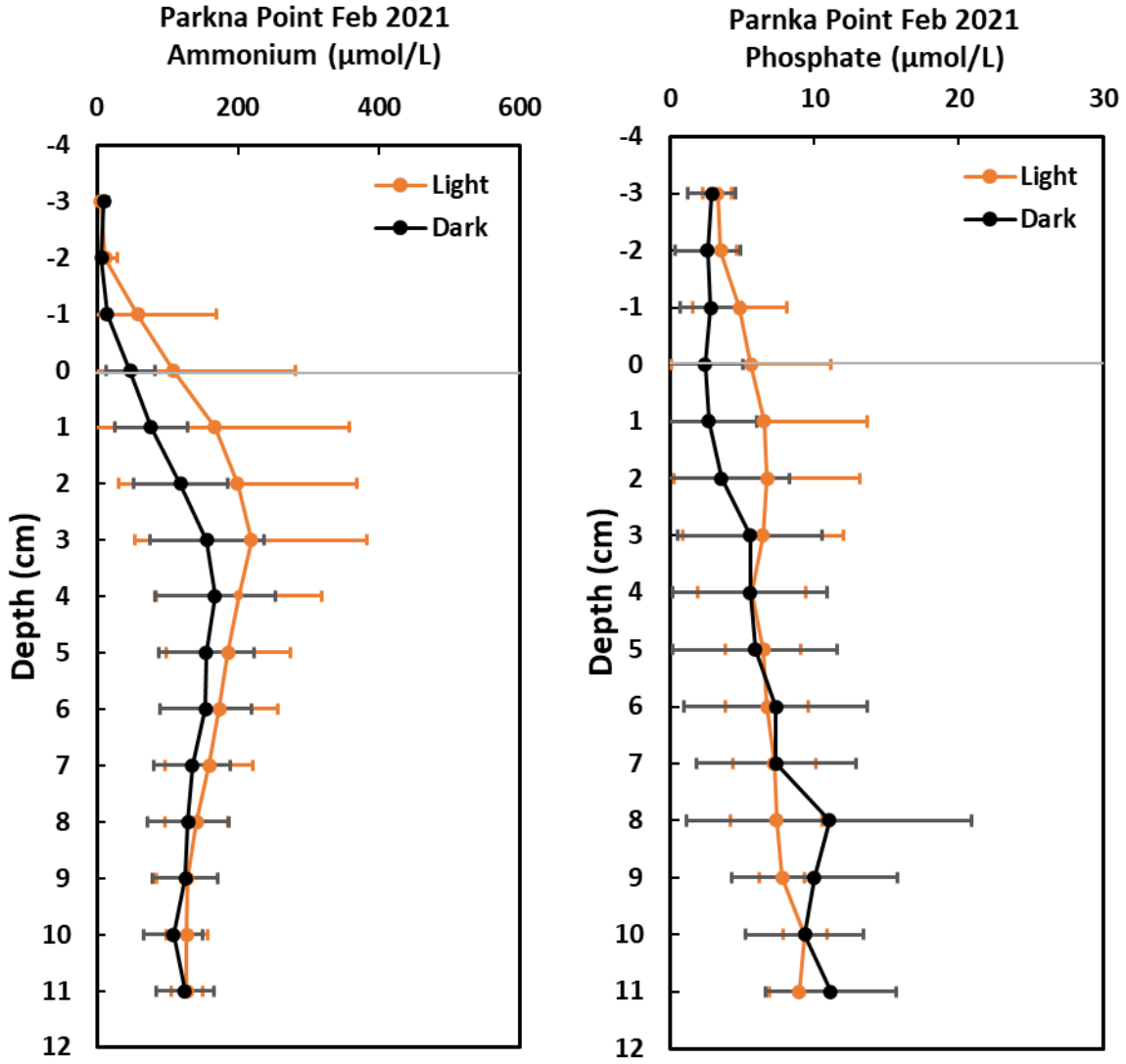

Figure 29. Depth profiles of ammonium and phosphate in muddy sediment at the Parnka Point site without *Ruppia* sp. during light and dark incubations. Data are mean values and error bars represent the standard deviation of the mean (n = 5). The grey solid line indicates the sediment-water interface (SWI).

For the sediment that was collected from the Policeman's Point site in February 2021, the ammonium concentrations increased significantly from surface water to the sediment ($p < 0.001$, GAM; Table 7d) and reached the highest concentration at 11 cm below SWI under light and dark incubation (Figure 28). Statistical analysis showed that the ammonium concentrations were significantly different between the light and dark incubation ($p < 0.01$, GAM; Table 7d). The ammonium concentrations were higher under light incubation than dark incubation. The maximum ammonium concentration was 310 ± 89 µmol/L and 280 ± 61 µmol/L under light and dark incubation.

The phosphate profiles in sediment from the Policeman's Point site showed significant difference across depth ($p < 0.001$, GAM; Table 8d) but no significant difference between light and dark incubations ($p > 0.05$, GAM; Table 8d). Phosphate concentrations ranged from 0 to 8 µmol/L in sediment, and the concentrations increased gradually from surface water to the sediment with some fluctuations (Figure 28).

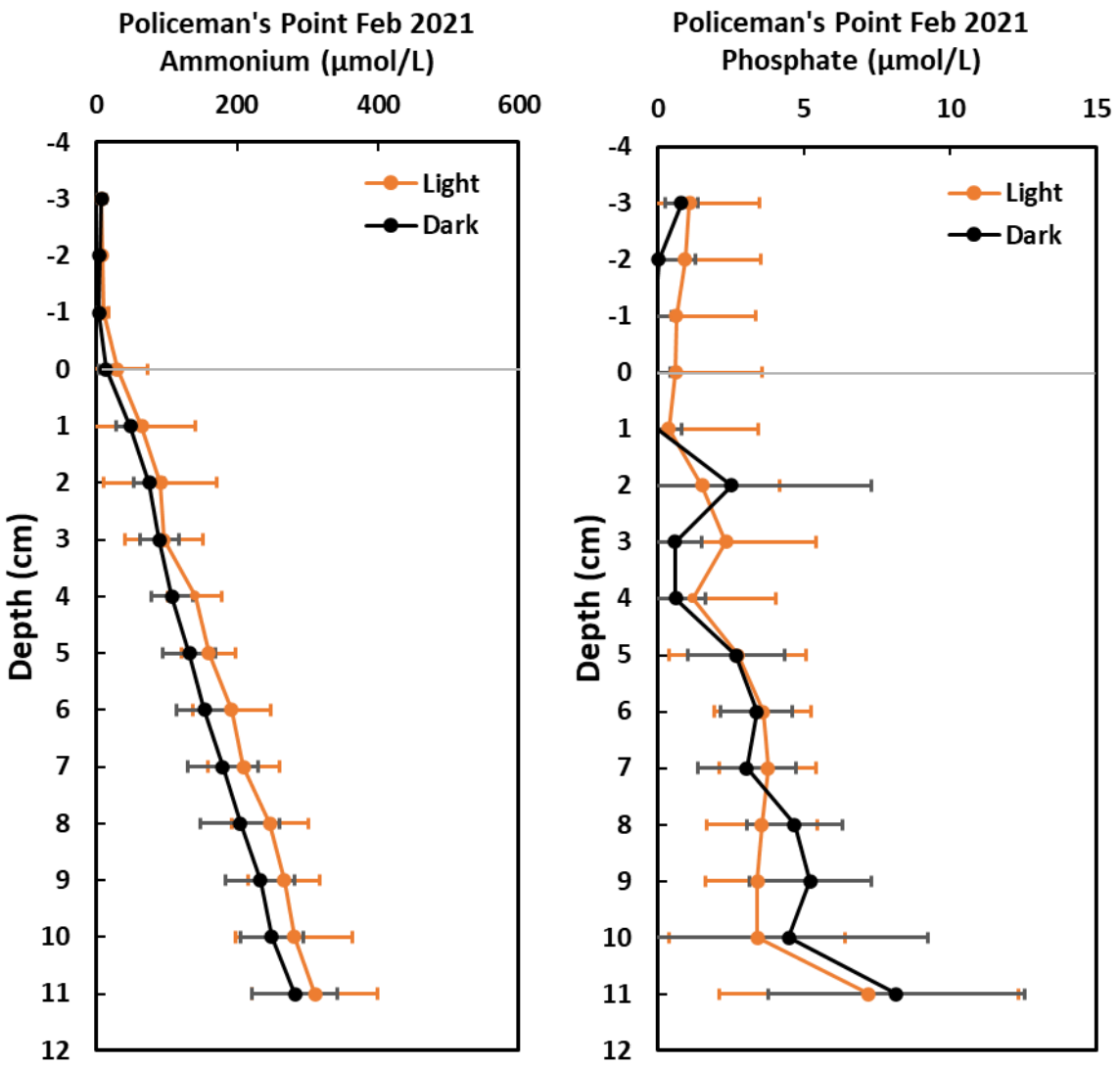

Figure 30. Depth profiles of ammonium and phosphate in sandy sediment at the Policeman's Point site without *Ruppia* sp. during light and dark incubations. Data are mean values and error bars represent the standard deviation of the mean (n = 5). The grey solid line indicates the sediment-water interface (SWI).

Table 7. Summary table of the results from the Generalised Additive Models (GAM) for porewater ammonium.

PARAMETRIC COEFFICIENTS	ESTIMATE	STD. ERROR	T VALUE	PR(>|T|)	DEVIANCE EXPLAINED	AIC
a) Noonameena November 2020						
Parametric coefficients						
Intercept (Light)	22.945	2.962	7.747	< 0.001		
Dark	-7.578	4.524	-1.675	0.090	24.50%	1320.7
Smooth terms						
Depth	edf = 2.005	Ref.df = 9	F = 4.373	< 0.001		
b) Policeman's Point November 2020						
Parametric coefficients						
Intercept (Light)	69.165	9.919	6.973	< 0.001		

Dark	98.327	13.957	7.045	< 0.001	63.90%	2385.2
Smooth terms						
Depth	edf = 3.013	Ref.df = 9	F = 31.97	< 0.001		
c) Parnka Point February 2021						
Parametric coefficients						
Intercept (Light)	134.347	9.134	14.708	< 0.001		
Dark	-32.357	12.918	-2.505	0.013	36.30%	1744.2
Smooth terms						
Depth	edf = 3.424	Ref.df = 9	F = 8.093	< 0.001		
d) Policeman's Point February 2021						
Parametric coefficients						
Intercept (Light)	140.638	5.115	27.493	< 0.001		
Dark	-21.912	7.673	-2.856	0.005	83.70%	1413.6
Smooth terms						
Depth	edf = 3.081	Ref.df = 9	F = 72.75	< 0.001		

Table 8. Summary table of the results from the Generalised Additive Models (GAM) for porewater phosphate.

PARAMETRIC COEFFICIENTS	ESTIMATE	STD. ERROR	T VALUE	PR(>|T|)	DEVIANCE EXPLAINED	AIC
a) Noonameena November 2020						
Parametric coefficients						
Intercept (Light)	0.336	1.537	0.219	0.827		
Dark	8.862	2.348	3.774	< 0.001	9.35%	1135.1
Smooth terms						
Depth	edf = 0.0003	Ref.df = 9	0.0	0.677		
b) Policeman's Point November 2020						
Parametric coefficients						
Intercept (Light)	1.852	0.676	2.742	0.006		
Dark	2.071	0.956	2.167	0.031	28.90%	1338.4
Smooth terms						
Depth	edf = 3.155	Ref.df = 9	F = 7.908	< 0.001		
c) Parnka Point February 2021						

Parametric coefficients						
Intercept (Light)	6.431	0.477	13.490	< 0.001		
Dark	-0.307	0.674	-0.456	0.649	22.40%	856.5
Smooth terms						
Depth	edf = 1.591	Ref.df = 9	F = 4.509	< 0.001		
d) Policeman's Point February 2021						
Parametric coefficients						
Intercept (Light)	2.624	0.273	9.622	< 0.001		
Dark	-0.091	0.409	-0.223	0.824	36.40%	621.3
Smooth terms						
Depth	edf = 2.245	Ref.df = 9	F = 8.057	< 0.001		

At the Noonameena site in the North Lagoon the dissolved ferrous iron concentrations in the sediment were significantly different across depth where macroinvertebrates were present ($p < 0.001$, GAM; Figure 31 and Table 9a) and under the light and dark incubation ($p < 0.01$, GAM; Figure 31 and Table 9a). The dissolved iron concentrations were less than 20 µmol/L through the sediment profile during light and dark incubation, except there was a dissolved ferrous iron peak of 20 µmol/L at 1 cm below the SWI during the light incubation and another iron peak of 30 µmol/L at 1 cm above the SWI during the dark incubation (Figure 31).

The sulfide profiles in Noonameena sediment varied significantly across depth ($p < 0.001$, GAM; Figure 31 and Table 10a) and under light and dark conditions ($p < 0.001$, GAM; Figure 31 and Table 10a). Sulfide concentration increased over depth and reached a peak around 20 µmol/L between 2–6 cm below SWI during the light incubation, and then the sulfide concentration decreased with the increasing depth (Figure 31). However, the sulfide concentration went up to 80 µmol/L at 2 cm below SWI, and then decreased during the dark incubation.

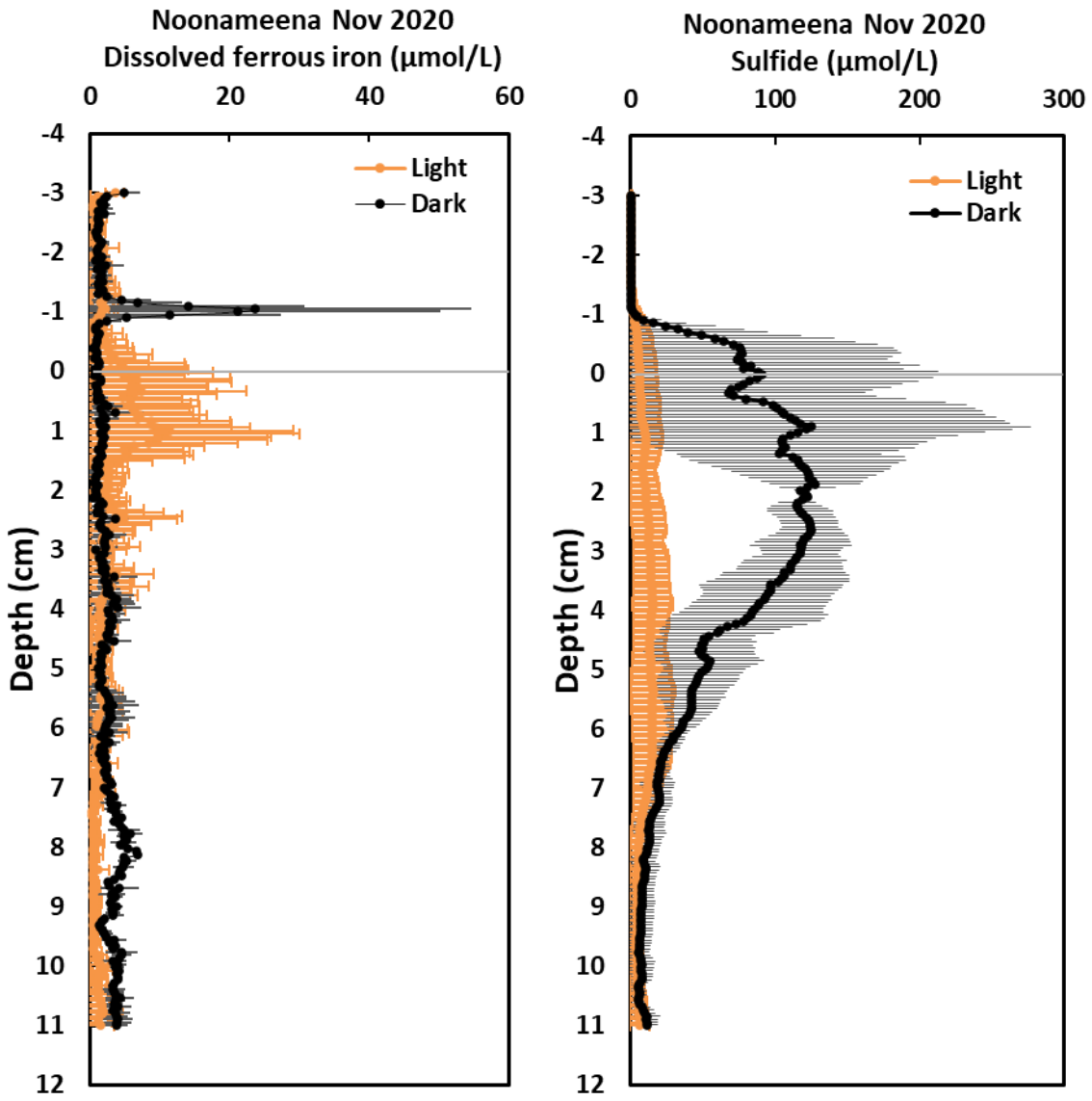

Figure 31. Depth profiles of ferrous iron (Fe) and sulfide (S) in sandy sediment at the Noonameena site with burrowing organisms present during light and dark incubations. Data are mean values and error bars represent the standard deviation of the mean (n = 5). The grey solid line indicates the sediment-water interface (SWI).

For sediment that was collected from the Policeman's Point site in November 2020 dissolved ferrous iron in sediment were significantly different across depth where *Ruppia* sp. was present ($p < 0.001$, GAM; Figure 32 and Table 9b) and under the light and dark incubation ($p < 0.001$, GAM; Figure 32 and Table 9b). The dissolved ferrous iron concentration was low in the surface water and the concentration increased with depth and reached the highest concentration of approximately 150 µmol/L at 3-4 cm below the SWI during the light and dark incubation before decreasing gradually (Figure 32). The profiles of sulfide varied significantly over depth ($p < 0.001$, GAM; Figure 32 and Table 10b), but no significant difference was observed for sulfide profiles under the light and dark incubation ($p > 0.05$, GAM; Figure 32 and Table 10b). The sulfide in Policeman Point sediment was low in the surface water and started to increase about 3 cm and 2 cm below the SWI during the light and dark incubation, respectively. The sulfide concentration increased gradually over depth and reached a peak concentration of approximately 150 µmol/L between 3–4 cm below SWI (Figure 32). The highest concentrations for dissolved ferrous iron and sulfide were similar during the light and dark incubation, but the dissolved iron and sulfide peaks were shifted toward the SWI under dark incubation compared to the light incubation. These changes were similar to what we observed in section 3.2.3.

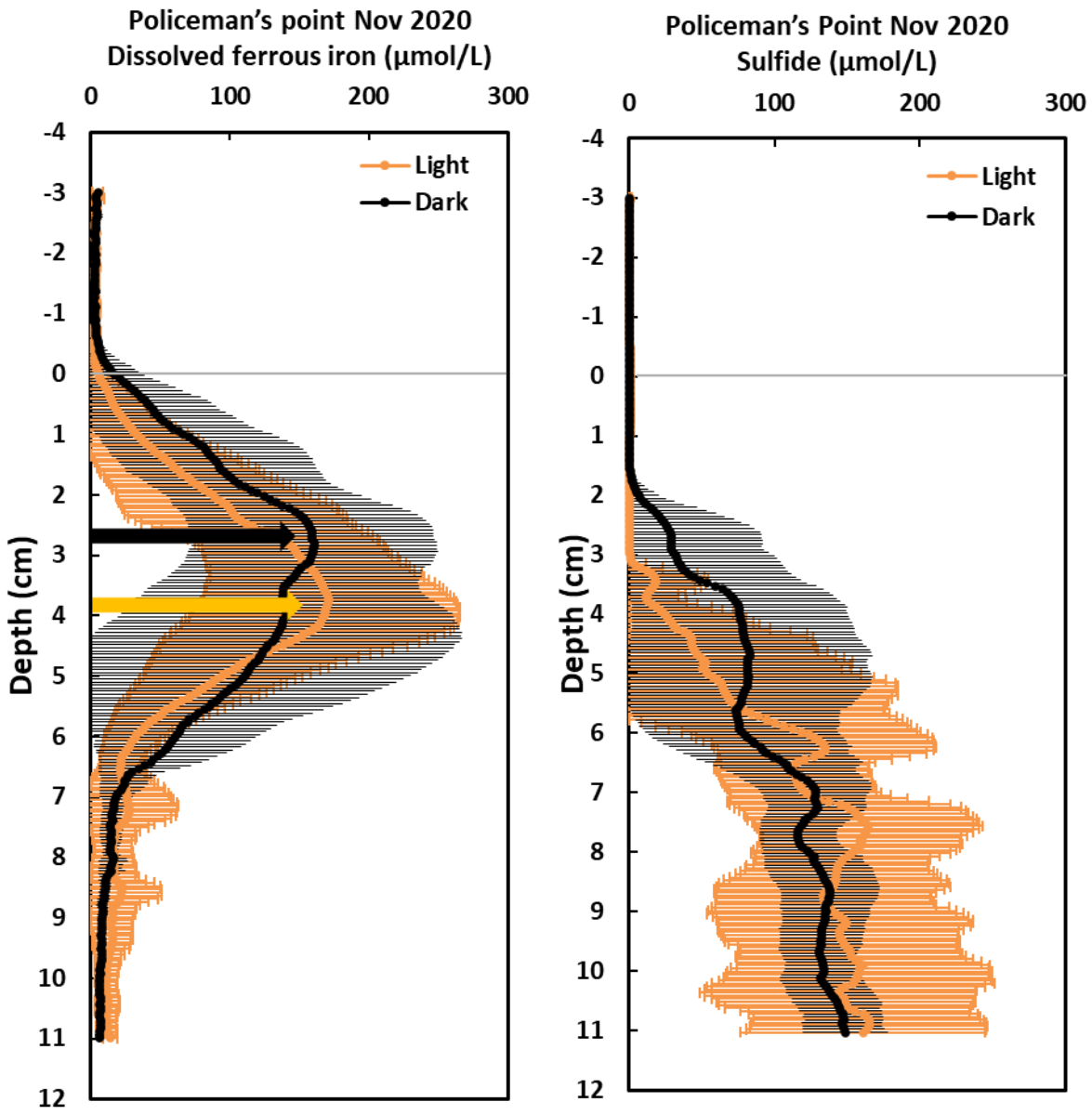

Figure 32. Depth profiles of ferrous iron (Fe) and sulphide (S) in muddy sediment at the Policeman's Point site colonised by *Ruppia* sp. during light and dark incubations. Data are mean values and error bars represent the standard deviation of the mean (n = 5). The grey solid line indicates the sediment-water interface (SWI). The orange and black arrows indicate the changes of the ferrous iron peak during light and dark incubations, respectively.

The profiles of dissolved ferrous iron from the Parnka Point site in February 2021 varied significantly across depth ($p < 0.001$, GAM; Figure 33 and Table 9c) and under the light and dark incubation ($p < 0.001$, GAM; Figure 33 and Table 9c). Under light incubation, the dissolved ferrous iron concentrations were stable between the surface water and approximately 1 cm below SWI, and then started to increase and reached the highest concentration of 20 µmol/L at 3.5 cm below SWI. Below that, the dissolved ferrous iron concentrations decreased gradually. Under dark incubation, the dissolved ferrous iron concentrations fluctuated from surface water to 1 cm below the sediment and then started to increase. The highest concentration of 14 µmol/L was at about 2 cm below SWI. After that the dissolved ferrous iron concentrations decreased gradually, similar to the light incubation.

For sulfide, the profiles also varied significantly across depth ($p < 0.001$, GAM; Figure 33 and Table 10c) and under the light and dark incubation ($p < 0.001$, GAM; Figure 33 and Table 10c). The sulfide concentrations were low in the surface water and started to increase at SWI and 2 cm below SWI during light and dark incubation, respectively (Figure 33). The sulfide concentrations were slightly higher under dark incubation than light incubation.

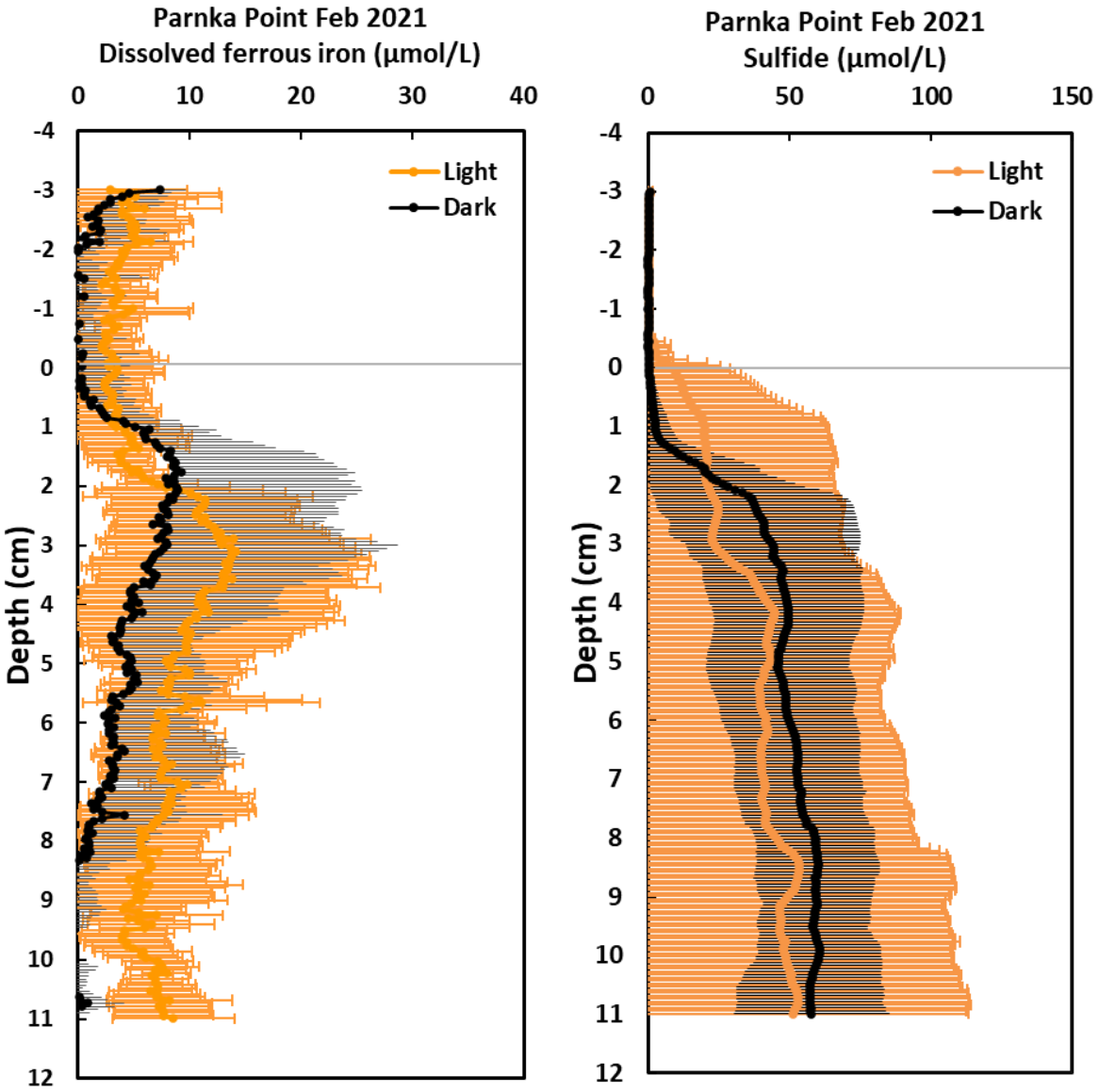

Figure 33. Depth profiles of ferrous iron (Fe) and sulphide (S) in muddy sediment at the Parnka Point site without *Ruppia* sp. during light and dark incubations. Data are mean values and error bars represent the standard deviation of the mean (n = 5). The grey solid line indicates the sediment-water interface (SWI).

For sediment that was collected from the Policeman's Point site in February 2021, the dissolved ferrous iron concentrations in the sediment were significantly different across depth ($p < 0.001$, GAM; Figure 34 and Table 9d) and under the light and dark incubation ($p < 0.001$, GAM; Figure 34 and Table 9d). The dissolved ferrous iron concentrations were below 1 µmol/L from surface water to 1 cm below SWI. Concentrations then increased up to 5 µmol/L 5 cm below SWI, then decreased until 11 cm below SWI under light incubation (Figure 34). For the dark incubation, the dissolved ferrous iron concentrations increased gradually from surface water to SWI and fluctuated between 5 and 10 µmol/L throughout the profile depth.

In addition, the sulfide profiles varied significantly across depth ($p < 0.001$, GAM; Figure 34 and Table 10d) and under the light and dark incubation ($p < 0.001$, GAM; Figure 34 and Table 10d). The sulfide concentration was low in the surface water and started to increase at 2 cm below the SWI, increasing over depth under both light and dark incubation (Figure 34). Higher sulfide concentrations were found in the sediment under the light incubation.

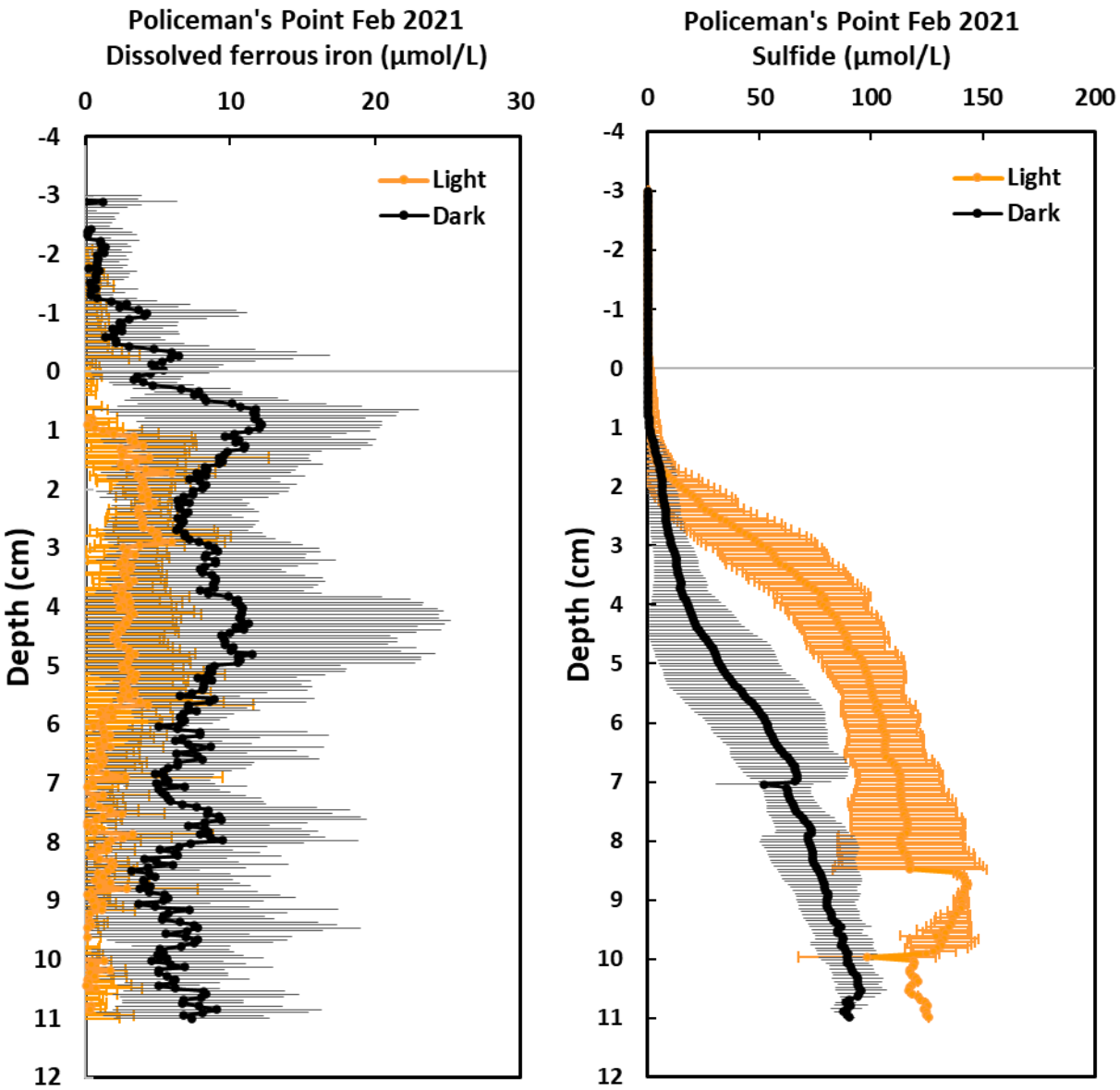

Figure 34. Depth profiles of ferrous iron (Fe) and sulfide (S) in sandy sediment at the Policeman's Point site without *Ruppia* sp. during light and dark incubations. Data are mean values and error bars represent the standard deviation of the mean (n = 5). The grey solid line indicates the sediment-water interface (SWI).

Table 9. Summary table of the results from the Generalised Additive Models (GAM) for porewater ferrous irons.

PARAMETRIC COEFFICIENTS	ESTIMATE	STD. ERROR	T VALUE	PR(>|T|)	DEVIANCE EXPLAINED	AIC
a) Noonameena November 2020						
Parametric coefficients						
Intercept (Light)	2.127	0.109	19.609	< 0.001		
Dark	0.516	0.203	2.541	0.011	6.47%	10785.6
Smooth terms						
Depth	edf = 6.788	Ref.df = 9	F = 13.2	< 0.001		
b) Policeman's Point November 2020						

Parametric coefficients						
Intercept (Light)	39.317	1.431	27.483	< 0.001		
Dark	6.160	1.919	3.209	0.001	54.30%	26037.4
Smooth terms						
Depth	edf = 8.61	Ref.df = 9	F = 322.2	< 0.001		
c) Parnka Point February 2021						
Parametric coefficients						
Intercept (Light)	11.194	0.189	59.150	< 0.001		
Dark	-4.225	0.268	-15.790	< 0.001	19.30%	18454.7
Smooth terms						
Depth	edf = 7.877	Ref.df = 9	F = 44.03	< 0.001		
d) Policeman's Point February 2021						
Parametric coefficients						
Intercept (Light)	5.502	0.145	37.950	< 0.001		
Dark	5.239	0.202	25.910	< 0.001	34.00%	14429.6
Smooth terms						
Depth	edf = 7.401	Ref.df = 9	F = 60.97	< 0.001		

Table 10. Summary table of the results from the Generalised Additive Models (GAM) for porewater sulfide.

PARAMETRIC COEFFICIENTS	ESTIMATE	STD. ERROR	T VALUE	PR(>|T|)	DEVIANCE EXPLAINED	AIC
a) Noonameena November 2020						
Parametric coefficients						
Intercept (Light)	7.963	0.744	10.700	< 0.001		
Dark	38.485	1.392	27.640	< 0.001	40.80%	18173.2
Smooth terms						
Depth	edf = 7.159	Ref.df = 9	F = 60.73	< 0.001		
b) Policeman's Point November 2020						
Parametric coefficients						
Intercept (Light)	65.870	1.365	48.260	< 0.001		
Dark	0.568	1.831	0.310	0.757	63.40%	27354.2
Smooth terms						
Depth	edf = 7.06	Ref.df = 9	F = 498.9	< 0.001		

c) Parnka Point February 2021						
Parametric coefficients						
Intercept (Light)	23.110	0.695	33.256	< 0.001		
Dark	6.214	0.983	6.323	<0.001	32.50%	25581.3
Smooth terms						
Depth	edf = 6.22	Ref.df = 9	F = 141.1	< 0.001		
d) Policeman's Point February 2021						
Parametric coefficients						
Intercept (Light)	53.399	0.549	97.270	< 0.001		
Dark	-27.489	0.757	-36.300	< 0.001	83.70%	20173.1
Smooth terms						
Depth	edf = 7.868	Ref.df = 9	F = 1226	< 0.001		

Benthic metabolism and nutrient fluxes

Sediments were collected from Parnka Point and Policeman's Point sites between February and March 2021 for core incubation to determine their benthic metabolism and nutrient fluxes. Both Parnka Point and Policeman's Point sediments were sinks for water column oxygen during dark incubations with a mean community respiration rate of 1060 ± 1335 and 2250 ± 3484 µmol O_2 /m^2/h, respectively (Figure 35). During light incubations, photosynthetic oxygen production by microphytobenthos reduced sediment oxygen demand at the Parnka Point site by approximately 60% and at the Policeman's Point site there was a small net oxygen production of ~400 µmol O_2 /m^2/h. However, light-dark shifts in oxygen fluxes at both sites were not significant (p = 0.387 for Parnka Point and p = 0.128 for Policeman's Point; Student T-test).

Based on the trophic oxygen status index (TOSI) of Viaroli and Christensen (2004), the Policeman's Point site would be classified as net heterotrophic (Score = 1), whereas the Parnka Point site would be in the lowest possible category of fully heterotrophic (Score = 0).

The Parnka Point site was also a sink for water column DOC during light and dark incubations, with mean DOC influxes of approximately -700 and -3700 µmol/m^2/h under light and dark incubation, respectively (Figure 36). But the light and dark incubations were not significantly different (p = 0.363; Student T-test). Conversely, there was a significant shift in DOC fluxes with light conditions (p = 0.018; Student T-test), with DOC effluxing to water column with the mean value of ~13200 µmol/m^2/h during the light incubation and being consumed by the sediment (mean influx of -10500 µmol/m^2/h) under dark conditions (Figure 36).

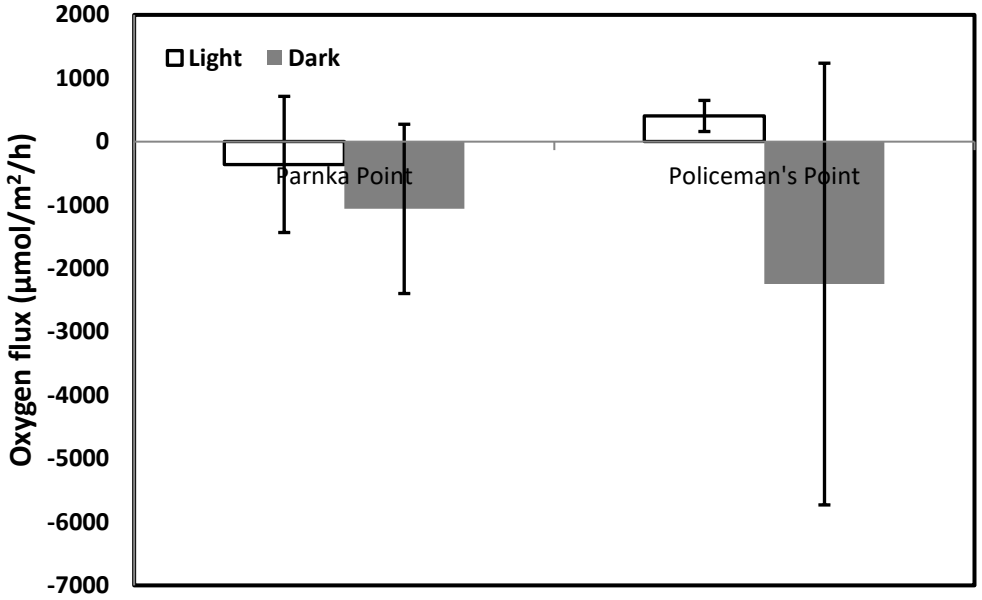

Figure 35. Sediment-water column fluxes of oxygen at the Parnka Point and Policeman's Point sites during light (white bar) and dark (grey bar) incubations. Data are mean values and error bars represent the standard deviation of the mean (n = 5).

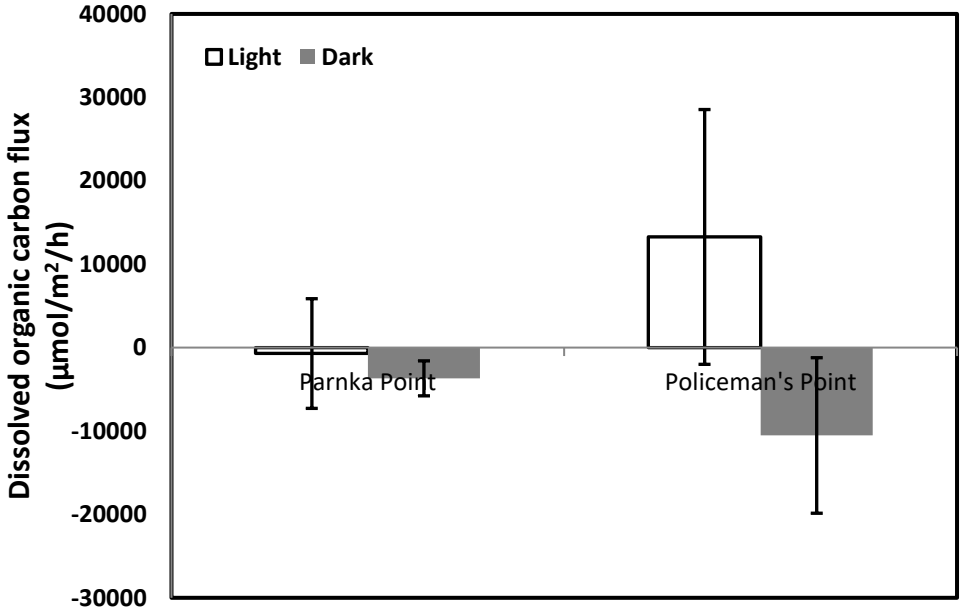

Figure 36. Sediment-water column fluxes of dissolved organic carbon (DOC) from the Parnka Point and Policeman's Point sites during light (white bar) and dark (grey bar) incubations. Data are mean values and error bars represent the standard deviation of the mean (n = 5).

The nutrient fluxes differed between locations and for different nutrient species (Figures 37 and 38). At the Parnka Point site, ammonium effluxed from the sediment to the water under the light condition with a mean efflux of 48.8 ± 97.6 µmol/m^2/h, while ammonium fluxed from the water to the sediment under the dark condition with a mean influx of -26.7 ± 11.1 µmol/m^2/h. However, the statistical analysis showed no significant difference for ammonium fluxes between light and dark conditions (p = 0.124; Student T-test). Nitrate effluxed from the sediment to the water under both light and dark conditions with the mean effluxes of 10.0 ± 4.6 µmol/m^2/h and 16.4 ± 8.5 µmol/m^2/h, respectively, but these differences were not significant (p = 0.179; Student T-test). Phosphate fluxes were negligible during light incubations (mean influx of -1.9 ±

0.8 µmol/m^2/h). However, during dark incubation a mean efflux of 42.9 ± 39.9 µmol/m^2/h was determined and this shift in fluxes under light and dark conditions was significant (p = 0.036; Student T-test).

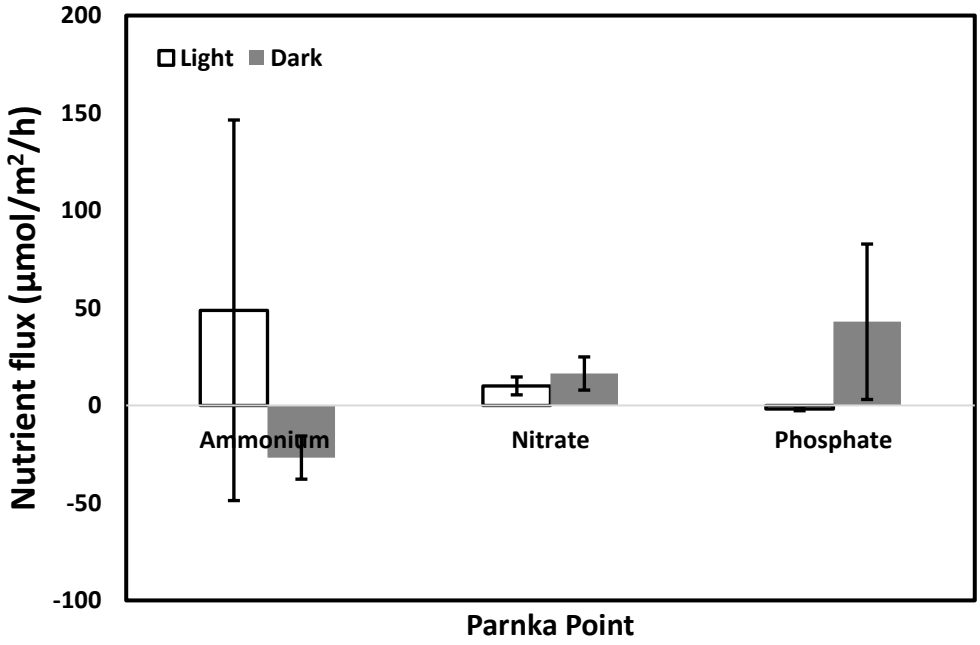

Figure 37. Sediment-water column fluxes of inorganic nutrients from the Parnka Point site during light (white bar) and dark (grey bar) incubations. Data are mean values and error bars represent the standard deviation of the mean (n = 5).

For the Policeman's Point site, the sediment was a sink for ammonium under both light and dark conditions, with influxes of -0.1 ± 11.3 µmol/m^2/h and -14.1 ± 14.4 µmol/m^2/h in the light and dark incubations respectively, but this change in flux was not significant (p = 0.126; Student T-test). Sediments were a source of both nitrate and phosphate under light and dark incubations. Mean nitrate efflux was significantly higher under the light (17.7 ± 9.2 µmol/m^2/h) than the dark (2.1 ± 2.1 µmol/m^2/h) conditions (p = 0.006; Student T-test). For Phosphate, the effluxes were 0.5 ± 1.4 µmol/m^2/h and 0.9 ± 2.1 µmol/m^2/h during light and dark conditions, respectively but this change was not significant (p = 0.733; Student T-test).

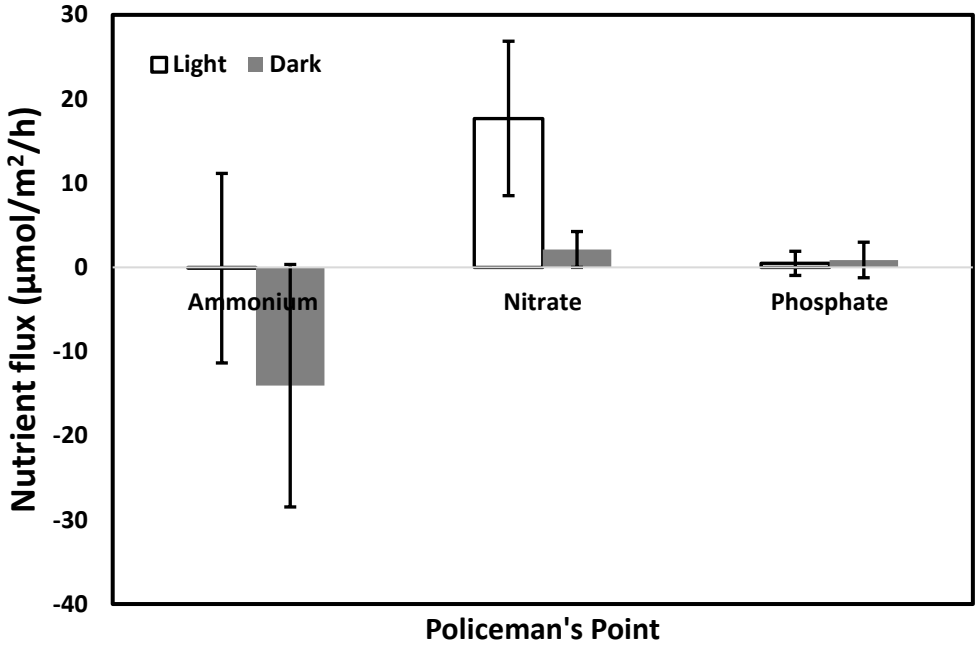

Figure 38. Sediment-water column fluxes of inorganic nutrients from the Policeman's Point site during light (white bar) and dark (grey bar) incubations. Data are mean values and error bars represent the standard deviation of the mean (n = 5).

3.2.3 *Ruppia tuberosa* colonised sediments

Ex situ core incubation

Sediment characteristics and *Ruppia tuberosa* biomass

Sediments at the Parnka Point site were composed of carbonate sands and muds with a mean density of 1.75 g/mL and a porosity of 0.61 (mL H_2O/mL sediment). The sediments showed a distinct redox discontinuity with a layer of black anoxic deep sediment overlain by a 1.5–2 cm thick yellowish oxidised layer, which approximately corresponded with the depth of the *R. tuberosa* rhizosphere. *R. tuberosa* had a mean biomass of 118.9 ± 28.1 g dry weight/m^2.

Sediment porewater depth profiles of inorganic nutrients, ferrous iron, and sulfide

Porewater profiles of ammonium and phosphate concentrations varied significantly with light conditions and depth ($p < 0.05$; PERMANOVA) and a significant interaction existed between these factors and the solute concentrations ($p < 0.05$, GAM; Table 11a and b). Higher ammonium concentrations were measured in the 0–6 cm depth horizon in the light, whereas phosphate concentrations were higher throughout the depth profile in the dark incubations (Figure 39).

Porewater nitrate concentrations were below the MDL of 20 µmol/L of the DET technique at all depths in all probes deployed in both light and dark incubations, with the exception of some depths in a single light deployed probe (data not shown).

Profiles of porewater dissolved ferrous iron and sulfide concentrations varied significantly with light conditions and depth ($p < 0.05$; PERMANOVA) and a significant interaction existed between these factors and the solute concentrations ($p < 0.05$, GAM; Table 11c and d). Porewater dissolved ferrous iron concentrations were consistently higher throughout the depth profile during dark compared to light incubations. Concentrations in the upper 5 cm of sediment in the dark were approximately double those measured at the same depth in the light, although the peak concentrations of ~70 (light) and ~145 (dark) µmol/L occurred at a similar depth of ~1 cm (Figure 40). Similarly, although less consistently, dissolved sulfide concentrations tended to be higher in the dark compared to the light as the profile moved towards the sediment surface

with the peak concentrations of 120–140 µmol/L occurring at ~10 and ~8 cm depth under light and dark conditions, respectively (Figure 40).

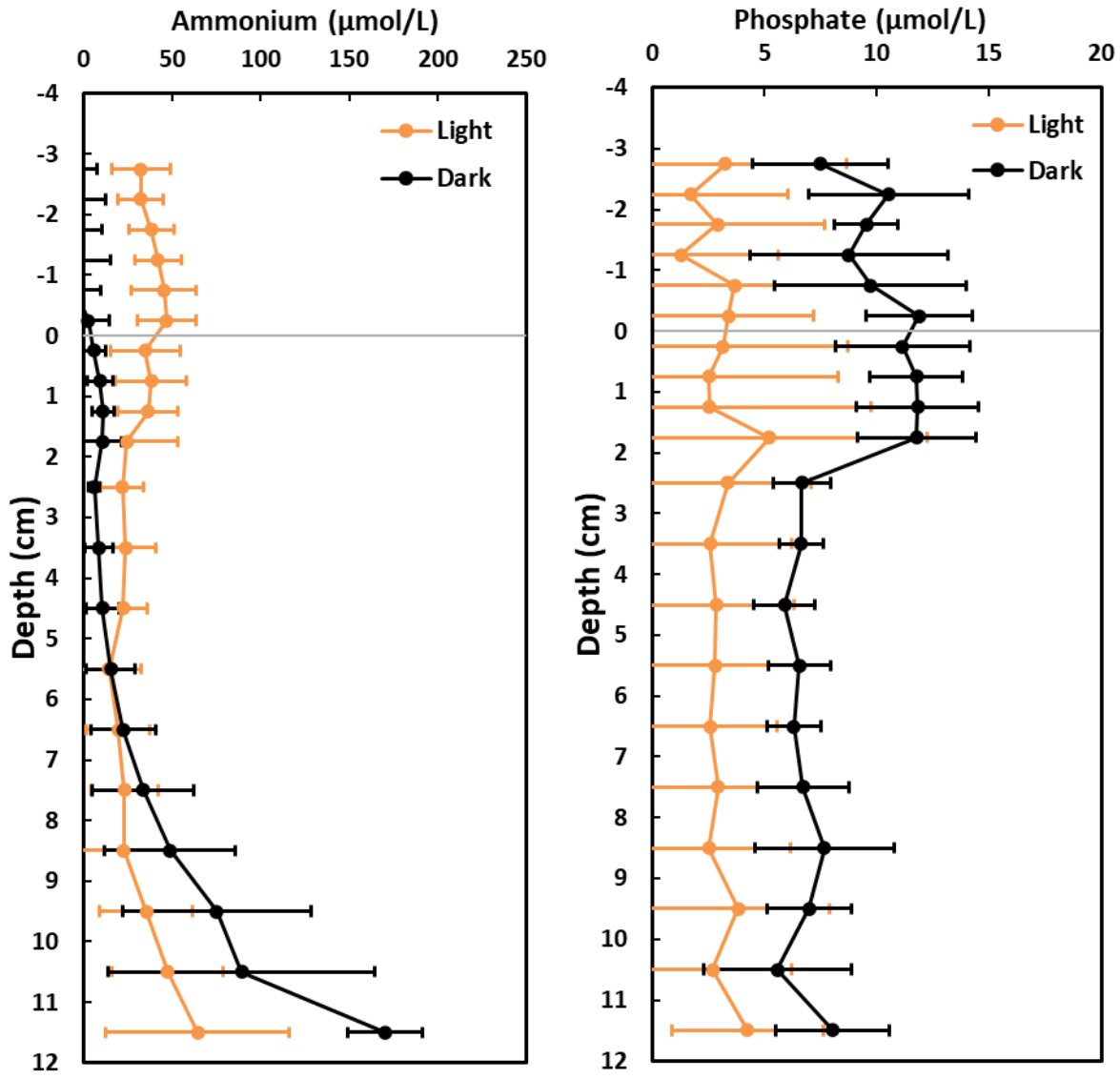

Figure 39. Depth profiles of ammonium and phosphate in *Ruppia tuberosa* colonised sediment at the Parnka Point site during light and dark incubations. Data are mean values and error bars represent the standard deviation of the mean (n = 5). The grey solid line indicates the sediment-water interface (SWI).

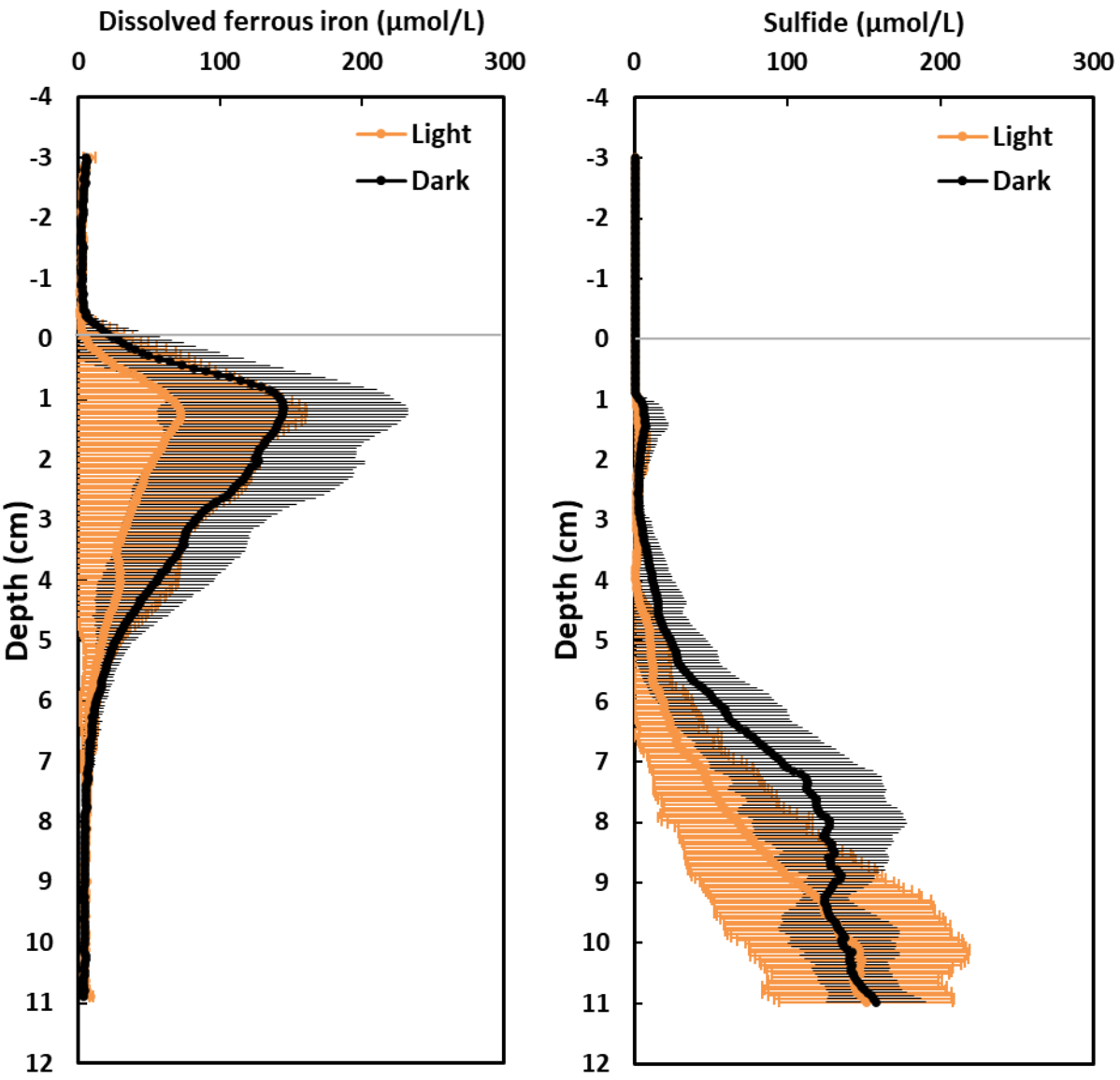

Figure 40. Depth profiles of ferrous iron (Fe) and sulfide (S) in *Ruppia tuberosa* colonised sediment at the Parnka Point site during light and dark incubations. Data are mean values and error bars represent the standard deviation of the mean (n = 5). The grey solid line indicates the sediment-water interface (SWI).

Table 11. Summary table of the results from the Generalised Additive Models (GAM) for inorganic nutrients, dissolved ferrous iron, and sulfide at the Parnka Point site.

PARAMETRIC COEFFICIENTS	ESTIMATE	STD. ERROR	T VALUE	PR(>|T|)	DEVIANCE EXPLAINED	AIC
a) Ammonium						
Parametric coefficients						
Intercept (Light)	32.586	2.824	11.539	< 0.001		
Dark	-10.075	4.004	-2.516	0.012	37.00%	1881.0
Smooth terms						
Depth	edf = 3.879	Ref.df = 9	F = 11.22	< 0.001		
b) Phosphate						
Parametric coefficients						

Intercept (Light)	3.524	0.322	10.960	< 0.001		
Dark	4.883	0.454	10.730	< 0.001		
					42.20%	1042.0
Smooth terms						
Depth	edf = 3.282	Ref.df = 9	F = 2.654	< 0.001		
c) Ferrous iron						
Parametric coefficients						
Intercept (Light)	12.385	0.768	16.130	< 0.001		
Dark	16.947	1.152	14.720	< 0.001	51.80%	23581.3
Smooth terms						
Depth	edf = 8.863	Ref.df = 9	F = 268	< 0.001		
d) Sulfide						
Parametric coefficients						
Intercept (Light)	36.912	1.024	36.040	< 0.001		
Dark	16.617	1.536	10.820	< 0.001	72.30%	24938.0
Smooth terms						
Depth	edf = 7.236	Ref.df = 9	F = 697.7	< 0.001		

Benthic metabolism and sediment water column nutrient fluxes

Sediment-water column oxygen fluxes in cores from the Parnka Point site differed significantly between light and dark incubation conditions ($p < 0.01$; Student T-test). The benthos (sediment and seagrass) was a strong sink for water column DO during dark incubations with O_2 fluxes ranging from -5705 to -4421 µmol/m^2/h, which equated to a mean community respiration rate of 4925 ± 541 µmol O_2 /m^2/h (Figure 41). Photosynthetic oxygen production off-set sediment oxygen demand during light incubations, greatly reducing oxygen consumption. The net oxygen production by the benthos with fluxes in the individual incubation cores ranged from -2260 to 4744 µmol O_2 /m^2/h, which equated to an average net primary production rate of 1546 ± 2857 µmol O_2 /m^2/h. The GPP of the seagrass was estimated from the light-dark shift in oxygen fluxes (CR + NPP) and averaged 6471 ± 2486 µmol O_2 /m^2/h. However, as dark oxygen consumption greatly exceeded oxygen production in the light the benthos would still be classified as net heterotrophic (Viaroli and Christensen, 2004), i.e. net oxygen consuming.

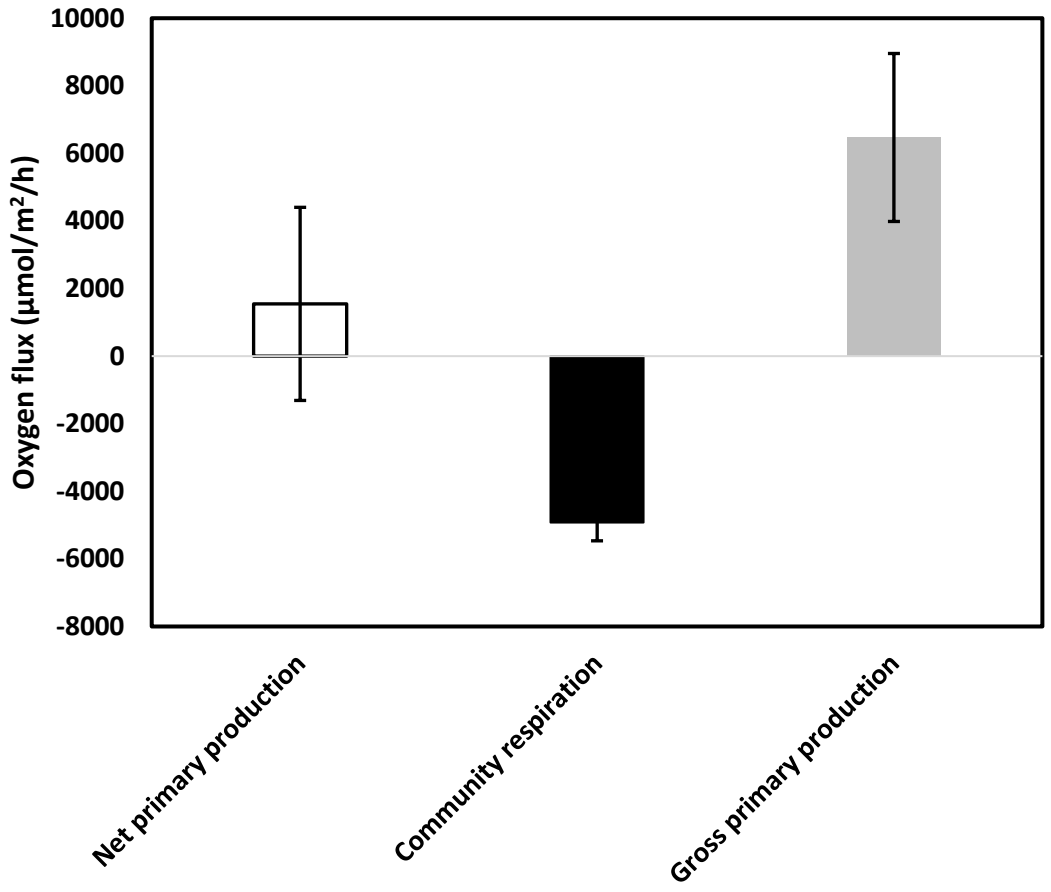

Figure 41. Rates of benthic net primary production, community respiration and gross primary production in the sediment-water column of the *Ruppia tuberosa* colonised sediment. Data are mean values and error bars represent the standard deviation of the mean (n = 5).

Ammonium fluxed from the sediment to the water under both light and dark conditions (Figure 42), but the flux difference in ammonium between light and dark was not statistically significant ($p = 0.27$; Student T-test). In contrast, nitrate fluxes differed between light and dark conditions ($p < 0.05$; Student T-test). Under dark conditions, the nitrate flux was close to zero (Figure 42), whereas under light conditions there was a mean nitrate efflux of 267 ± 286 µmol/m^2/h.

In the light incubation, the phosphate concentrations in the overlying water were below the MDL of 0.5 µmol/L of the nutrient analyser in the water samples collected at both the start and end of the incubation and therefore the phosphate flux could not be calculated. Similarly, in the dark incubation the phosphate concentration in the initial samples were below the MDL. Therefore, the dark flux was conservatively calculated by assuming that the initial concentration was equal to the MDL. Consequently, the dark phosphate efflux of 28.3 ± 16.9 µmol/m^2/h, represents a minimum possible value, as it is likely that the true initial concentration was lower than the one used for the flux rate calculations.

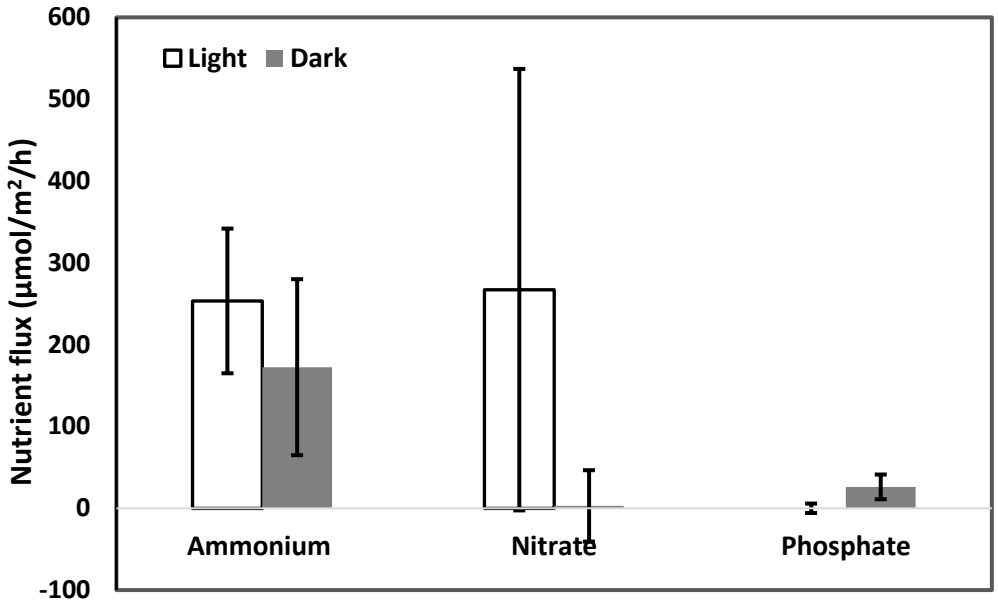

Figure 42. Sediment-water column fluxes of ammonium, nitrate, and phosphate in *Ruppia tuberosa* colonised sediment during light (white bars) and dark (grey bars) incubations. Data are mean values and error bars represent the standard deviation of the mean (n = 5).

In situ benthic chamber determinations of sediment-water column nutrient fluxes over a diel light cycle

Water and sediment characteristics and *Ruppia tuberosa* biomass

Various physicochemical parameters were measured in water 30 cm below the surface at the Woods Well site between 8 to 11 November 2021. The mean salinity was 73.8 ± 11.0 PSU. The mean values of turbidity and pH were 3.85 ± 0.59 Formazin Nephelometric Unit (FNU) and 8.07 ± 0.12, respectively. The mean temperature value was 18.0 ± 1.6 °C. The light intensity increased from 6 am to 12 pm and there were some fluctuations between 10 am to 2 pm on 10 November. A significant increase of the light intensity to a peak value of approximately 2800 µmol/s/m^2 occurred at approximately 12 pm, followed by a significant drop and then slight increase to around 2200 µmol/s/m^2. The light intensity decreased again from 1 pm and reduced to 0 µmol/s/m^2 at approximately 7 pm and remained as 0 µmol/s/m^2 until 6 am on 11 November (Figure 43). The DO saturation was 78.5% (equal to 4.79 mg/L) at 6 am on 10 November and increased gradually during the daytime and reached the highest value of 123% (equal to 7.48 mg/L) at 6:30 pm on the same day. The DO saturation decreased gradually returning to a value of 75.4% (equal to 4.73 mg/L) at 6 am on 11 November (Figure 44).

Sediment from the site was sandy with a mean density of 1.95 g/mL and a porosity of 0.43. The sediment had a 2–4 cm thick yellowish oxidised layer, which approximately corresponded with the depth of the *R. tuberosa* rhizosphere, overlying darker more reduced sediments. The *R. tuberosa* biomass collected near the benthic chamber site (102.8 ± 52.7 g dry weight/m^2) was 1.6 times higher than that collected near the DET deployment site at Woods Well (64.7 ± 20.7 g dry weight/m^2), although no significant difference was found ($p < 0.05$; Student T-test).

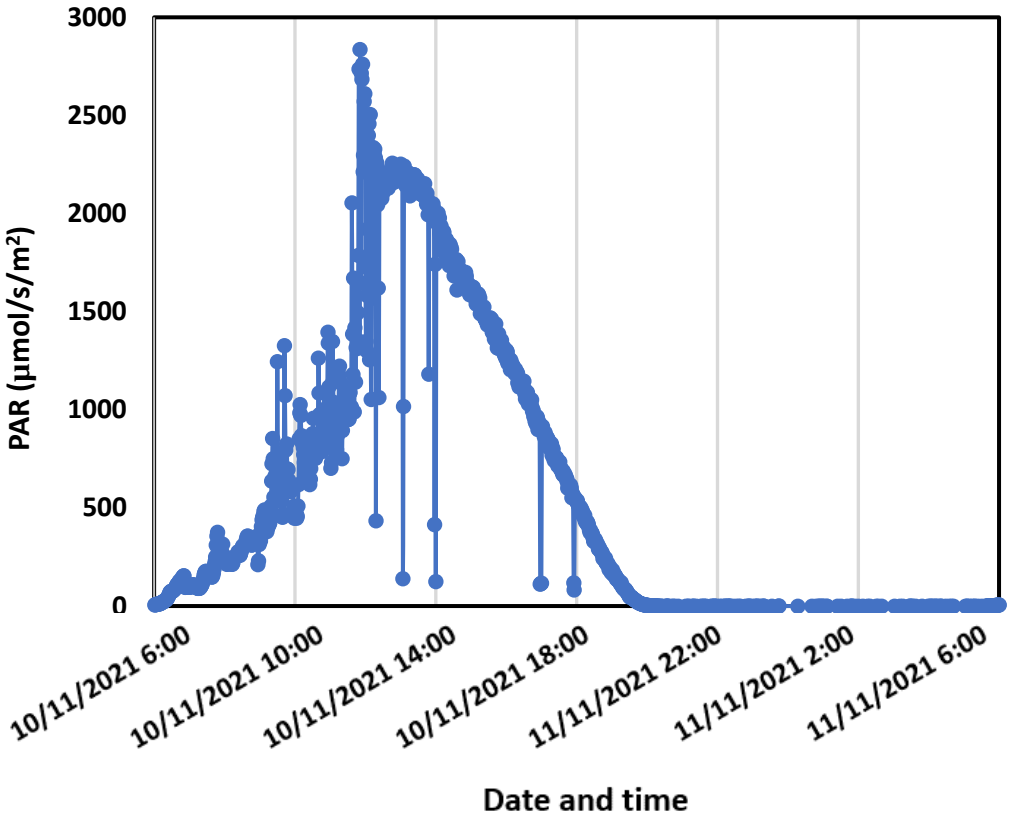

Figure 43. The changes of light intensity in water at the Woods Well site from 6 am on 10 November to 6 am on 11 November 2021. Light intensity is shown as photosynthetically active radiation (PAR). The grey lines indicate the sampling time for the diffusive equilibrium in thin films (DET) probes.

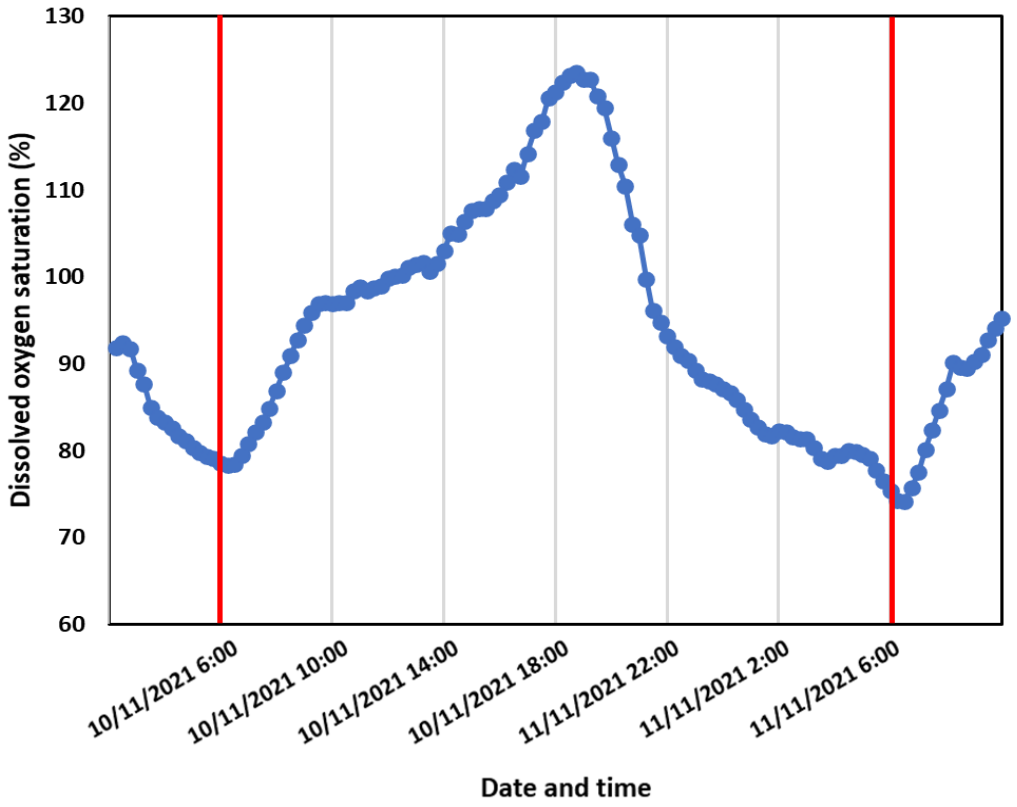

Figure 44. The dissolved oxygen saturation (blue dotted line) in water at the Woods Well site. The grey lines indicate the sampling time for the diffusive equilibrium in thin films (DET) probes. The red lines indicate the 24 h experimental period.

Sediment porewater depth profiles of inorganic nutrients, ferrous iron, and sulfide

Ammonium concentrations increased from the surface water to the sediment up to 6 and 8 cm below SWI and then decreased until 11 cm below SWI (Figure 45). Ammonium concentration profiles differed significantly over depth and the diel cycle ($p < 0.001$, GAM; Figure 45 and Table 12) with lowest and highest peak ammonium concentrations measured at 10 am on 10 November and 2 am on 11 November, respectively. Depth integrated average porewater ammonium concentration was approximately 13.5 µmol/L at 6 am on 10 November 2021. It then decreased and reached the lowest average concentration of 9 µmol/L at 10 am on the same day (Figure 46). Thereafter, the concentrations increased throughout the day and reached the highest average concentration of 40.7 µmol/L at 10 pm on 10 November, followed by a decrease until 6 am (17.0 µmol/L) on 11 November 2021. The general pattern of ammonium profiles for all times with depth is similar where all peaks were around 6-8 cm below SWI.

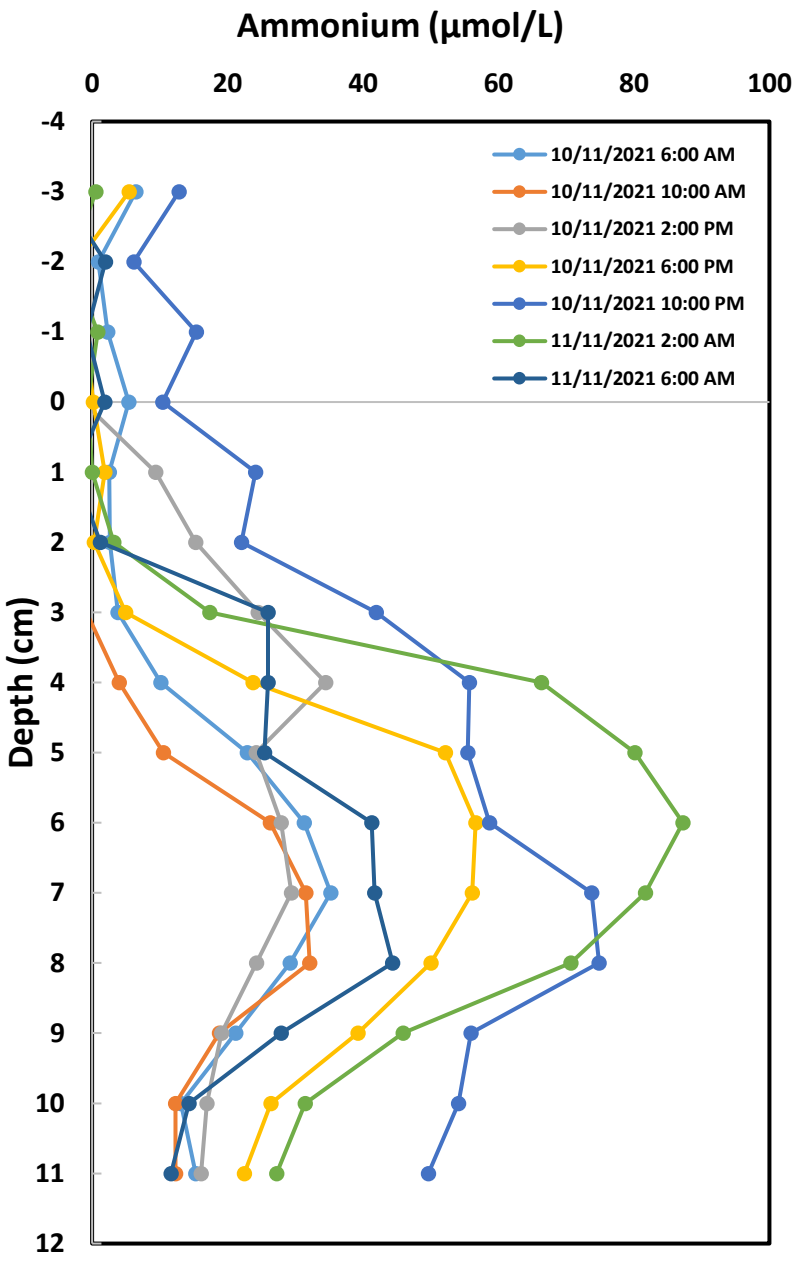

Figure 45. Depth profiles of ammonium in *Ruppia tuberosa* colonised sandy sediment at the Woods Well site during light and dark incubations. Data are mean values (n = 5). The grey solid line indicates the sediment-water interface (SWI).

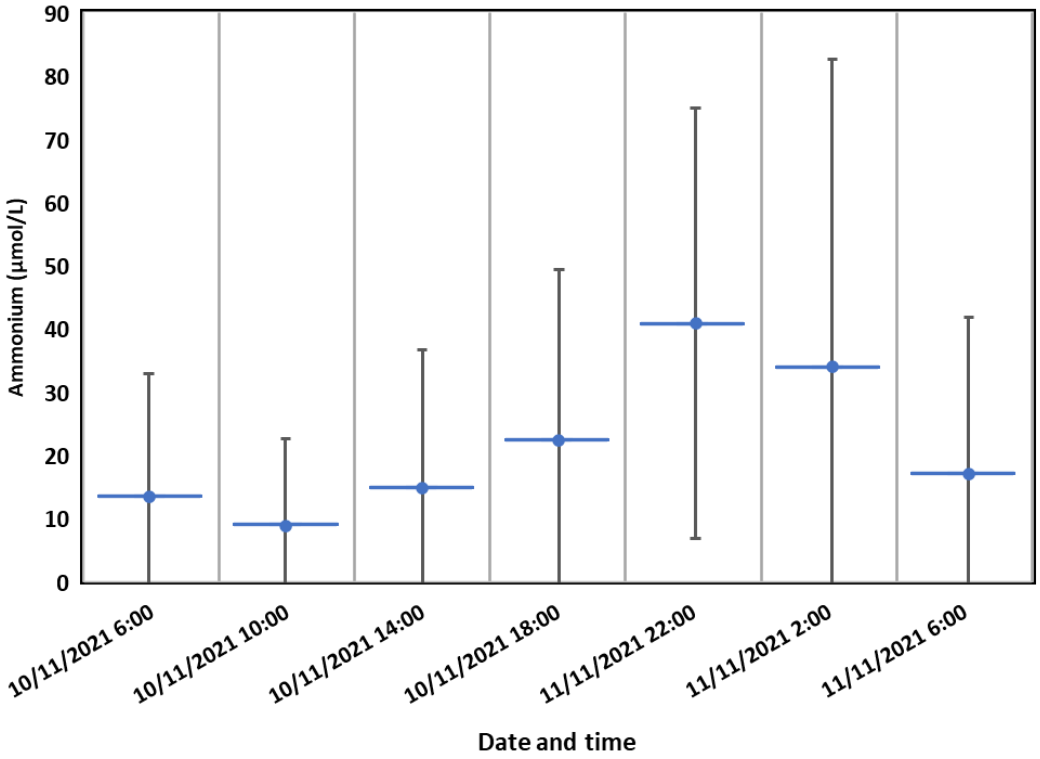

Figure 46. The average ammonium concentrations in *Ruppia tuberosa* colonised sandy sediment at the Woods Well site at different sampling time within 24 h. Data are mean values and error bars represent the standard deviation of the mean (n = 5). The grey solid lines indicate the different sampling time.

Table 12. Summary table of the results from the Generalised Additive Models (GAM) for porewater ammonium.

PARAMETRIC COEFFICIENTS	ESTIMATE	STD. ERROR	T VALUE	PR(>|T|)	DEVIANCE EXPLAINED	AIC
Parametric coefficients						
Intercept **(6 am 10 November)**	13.497	2.546	5.302	< 0.001		
10 am 10 November	-4.542	3.600	-1.261	0.207		
2 pm 10 November	1.281	3.600	0.356	0.722		
6 pm 10 November	8.929	3.600	2.480	0.013		
10 pm 10 November	27.232	3.819	7.131	< 0.001	46.40%	4345.9
2 am 11 November	20.422	3.819	5.348	< 0.001		
6 am 11 November	3.546	3.819	0.929	0.356		
Smooth terms						
Depth	edf = 5.48	Ref.df = 9	F = 32.34	< 0.001		

The MDL of the DET technique for phosphate is 1.1 µmol/L. Phosphate concentrations varied significantly with both depth ($p < 0.001$, GAM; Figure 47 and Table 13) and over the diel cycle ($p < 0.001$, GAM; Figure 47 and Table 13). The depth integrated average phosphate concentration was 2.6 µmol/L at 6 am on 10 November. It then increased with time over the day, reaching the highest concentration of 5.7 µmol/L at 10 pm on 10 November and then declined to 1.6 µmol/L at 2 am on 11 November 2021 (Figure 48). The average phosphate concentration then increased to 3.1 µmol/L at 6 am on 11 November 2021. The general pattern of phosphate profiles was more variable than ammonium for all times with depth.

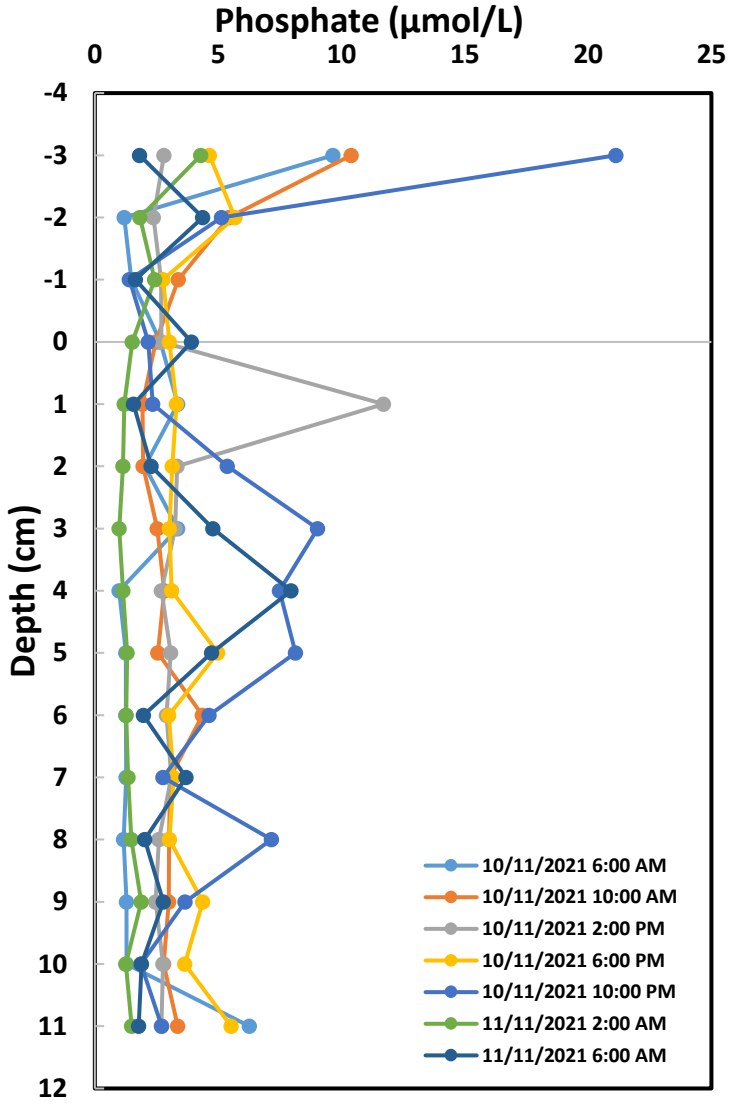

Figure 47. Depth profiles of phosphate in *Ruppia tuberosa* colonised sandy sediment at the Woods Well site during light and dark incubations. Data are mean values (n = 5). The grey solid line indicates the sediment-water interface (SWI).

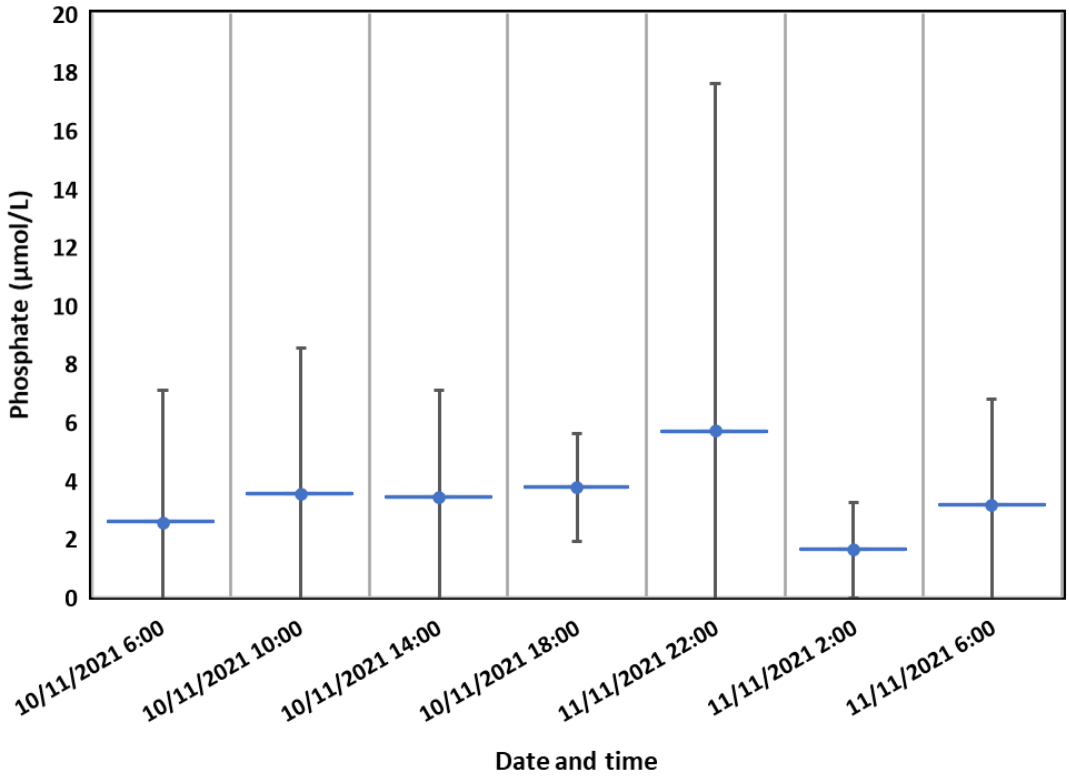

Figure 48. The average phosphate concentrations in *Ruppia tuberosa* colonised sandy sediment at the Woods Well site at different sampling time within 24 h. Data are mean values and error bars represent the standard deviation of the mean (n = 5). The grey solid lines indicate the different sampling time.

Table 13. Summary table of the results from the Generalised Additive Models (GAM) for porewater phosphate.

PARAMETRIC COEFFICIENTS	ESTIMATE	STD. ERROR	T VALUE	PR(>|T|)	DEVIANCE EXPLAINED	AIC
Parametric coefficients						
Intercept **(6 am 10 November)**	2.589	0.615	4.212	< 0.001		
10 am 10 November	0.954	0.869	1.097	0.273		
2 pm 10 November	0.831	0.869	0.956	0.339		
6 pm 10 November	1.175	0.869	1.352	0.177		
10 pm 10 November	3.087	0.922	3.348	< 0.001	5.63%	2977.7
2 am 11 November	-0.950	0.922	-1.030	0.303		
6 am 11 November	0.573	0.922	0.622	0.534		
Smooth terms						
Depth	edf = 1.363	Ref.df = 9	F = 0.775	< 0.001		

Porewater nitrate concentrations were typically below the MDL limit of 1.8 µmol/L in the majority of samples in all depth profiles and are therefore not shown.

The dissolved ferrous iron concentrations varied significantly with depth ($p < 0.001$, GAM; Figure 49 and Table 14) and over the diel cycle ($p < 0.001$, GAM; Figure 49 and Table 14). The dissolved ferrous iron concentrations were low in the surface water and started to increase at 1–2 cm below SWI. The dissolved ferrous iron peak occurred at 6 cm below SWI at 6 am on 10 November 2021. As the sun rose, the dissolved iron peak shifted

down to 7 cm below SWI from 10 am to 6 pm on the same day. After sunset, the dissolved iron peak moved towards to approximately 5 cm below SWI between 10 pm on 10 November and 2 am on 11 November 2021. The dissolved iron peak was at 5.5 cm below SWI at 6 am on 11 November 2021.

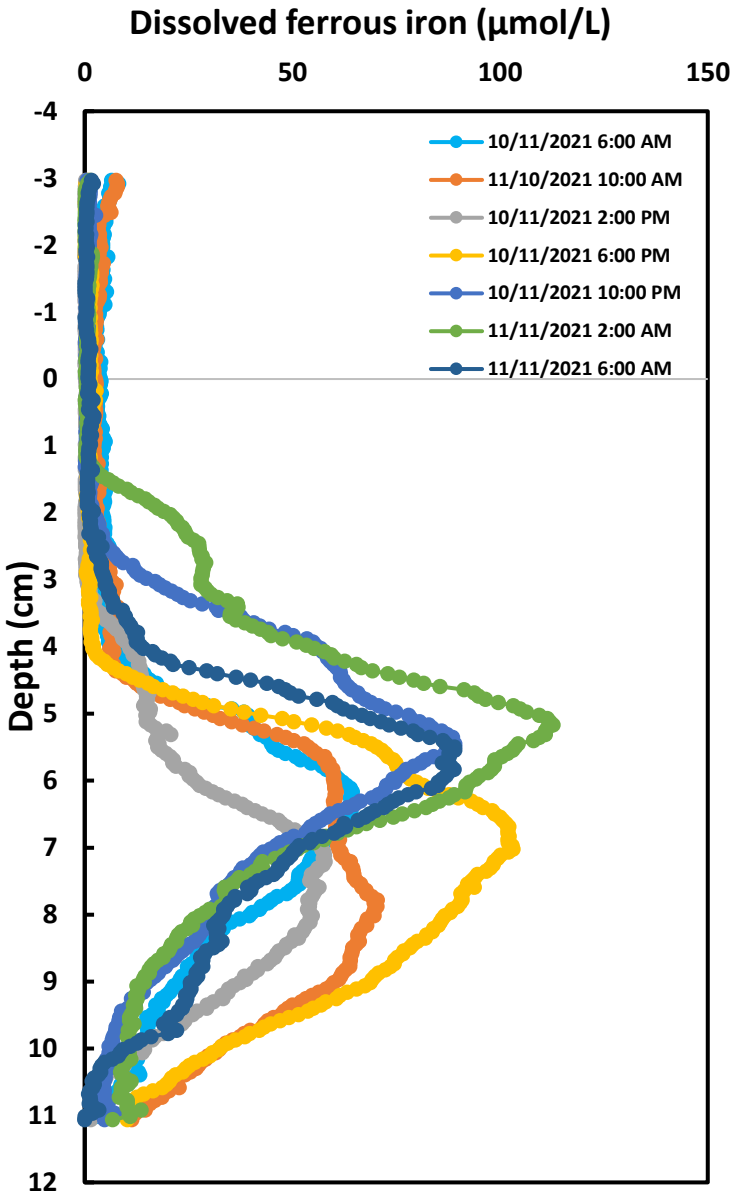

Figure 49. Depth profiles of ferrous iron (Fe) in *Ruppia tuberosa* colonised sandy sediment at the Woods Well site during light and dark incubations. Data are mean values (n = 5). The grey solid line indicates the sediment-water interface (SWI).

Table 14. Summary table of the results from the Generalised Additive Models (GAM) for porewater dissolved ferrous iron.

PARAMETRIC COEFFICIENTS	ESTIMATE	STD. ERROR	T VALUE	PR(>|T|)	DEVIANCE EXPLAINED	AIC
Parametric coefficients						
Intercept **(6 am 10 November)**	18.790	0.708	26.533	< 0.001		
10 am 10 November	6.289	1.002	6.274	< 0.001		
2 pm 10 November	-3.350	1.002	-3.344	< 0.001		

6 pm 10 November	15.995	1.063	15.044	< 0.001		
10 pm 10 November	4.564	1.065	4.287	< 0.001	45.10%	83513.7
2 am 11 November	10.671	1.065	10.020	< 0.001		
6 am 11 November	2.793	1.161	2.407	0.016		
Smooth terms						
Depth	edf = 8.708	Ref.df = 9	F = 742.12	< 0.001		

The sulfide concentrations were generally low (less than 4 µmol/L) with a few spikes in the sediment throughout the depth profile. Profiles of porewater sulfide concentrations varied significantly with depth ($p < 0.001$, GAM; Figure 50 and Table 15) and over the diel cycle ($p < 0.001$, GAM; Figure 50 and Table 15).

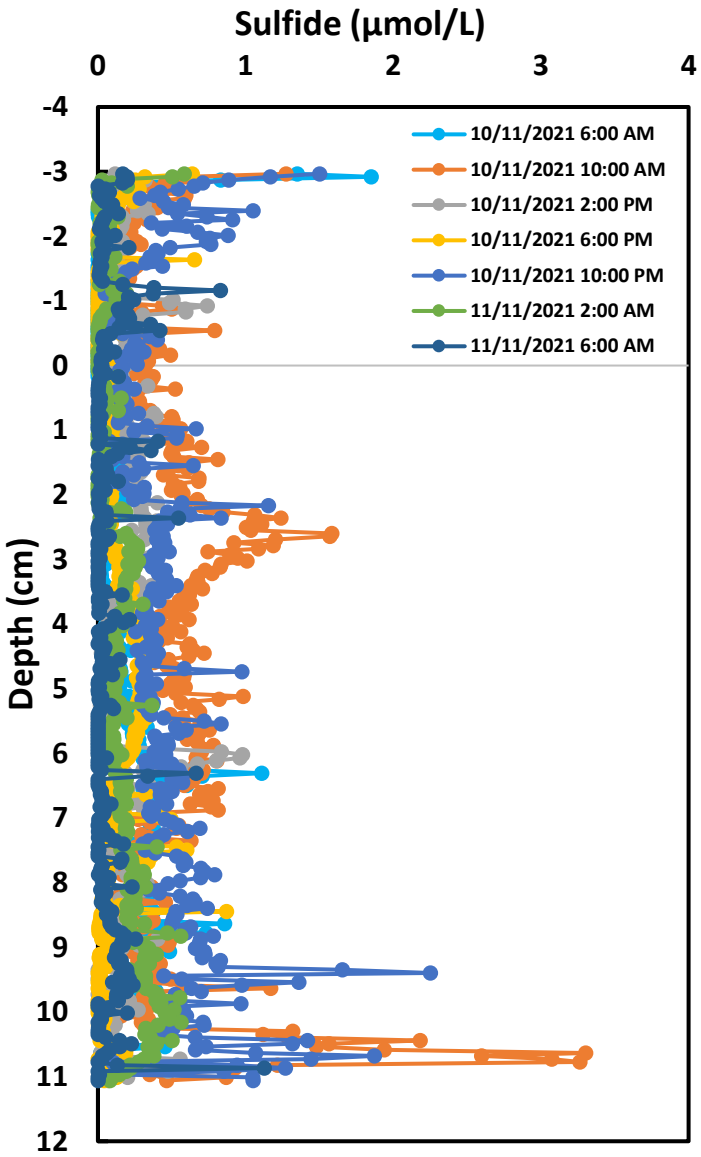

Figure 50. Depth profiles of sulfide (S) in *Ruppia tuberosa* colonised sandy sediment at the Woods Well site during light and dark incubations. Data are mean values (n = 5). The grey solid line indicates the sediment-water interface (SWI).

Table 15. Summary table of the results from the Generalised Additive Models (GAM) for porewater sulfide.

PARAMETRIC COEFFICIENTS	ESTIMATE	STD. ERROR	T VALUE	PR(>|T|)	DEVIANCE EXPLAINED	AIC
Parametric coefficients						
Intercept **(6 am 10 November)**	0.177603	0.014572	12.188	< 0.001		
10 am 10 November	0.364004	0.019535	18.633	< 0.001		
2 pm 10 November	-0.00074	0.019529	-0.038	0.965		
6 pm 10 November	-0.05141	0.019617	-2.621	0.008	12.50%	13157.1
10 pm 10 November	0.286177	0.020613	13.884	< 0.001		
2 am 11 November	-0.02765	0.020553	-1.345	0.178		
6 am 11 November	-0.1067	0.020574	-5.186	< 0.001		
Smooth terms						
Depth	edf = 7.943	Ref.df = 9	F = 25.07	< 0.001		

Benthic metabolism

The differences of DO concentrations at the beginning and the end of the incubation inside and outside the chamber are presented in Figure 51 and Table 16. The changing pattern of DO inside the chamber was similar to the changes outside the chamber. The DO levels were higher at the end of the incubation compared to the beginning of the incubation for the 6–9 am, 10 am–1 pm and 2–5 pm time periods on 10 November 2021. Conversely, the DO levels had decreased at the end of the incubation compared to the beginning of the incubation for the 6–9 pm time period on 10 November, and over the 10 pm on 10 November – 1 am on 11 November and 2–5 pm on 11 November 2021 time periods. The DO concentrations inside the chamber were similar to the outside at 6 am and 10 am on 10 November, and 5 am on 11 November when the experiment finished. For the rest of the incubation time, the DO levels inside the chamber were 6–24% higher than outside the chamber except 9 am on 10 November where the DO levels inside the chamber were 6% lower than the DO level outside the chamber. The oxygen flux results inside the chamber showed that there were average net primary production rates of 3188 and 3500 µmol O_2 /m^2/h between 6 am and 9 am, and between 10 am and 1 pm on 10 November, respectively. From 2 pm to 5 pm, the average net primary production rate decreased to 1190 µmol O_2 /m^2/h. From 6 pm to 9 pm, the oxygen flux turned negative with a mean community respiration rate of -2165 µmol O_2 /m^2/h. The mean community respiration rates were -4200 and -2244 µmol/m^2/h between 10 pm on 10 November and 1 am on 11 November, and between 2 am and 5 am on 11 November, respectively.

Table 16. The differences of dissolved oxygen concentrations (% and mg/L) at the beginning and the end of the incubation inside and outside the chamber.

TIME	DO	6 AM – 9 AM 10 NOVEMBER 2021		10 AM – 1 PM 10 NOVEMBER 2021		2 PM – 5 PM 10 NOVEMBER 2021		6 PM – 9 PM 10 NOVEMBER 2021		10 PM 10 NOVEMBER – 1 AM 11 NOVEMBER 2021		2 AM – 5 AM 11 NOVEMBER 2021	
Inside chamber	%	77.7	89.8	98.2	120.6	128.8	134.1	136.3	121.8	114.3	93.9	88.4	78.9
	mg/L	4.60	5.35	5.81	6.82	7.24	7.55	7.72	7.19	6.77	5.69	5.37	4.83
Outside chamber	%	78.5	95.8	97.7	102.5	105.1	117.1	123.0	102.7	92.7	83.2	82.5	79.4
	mg/L	4.70	5.69	5.79	5.96	6.08	6.82	7.27	6.14	5.55	5.07	5.05	4.86

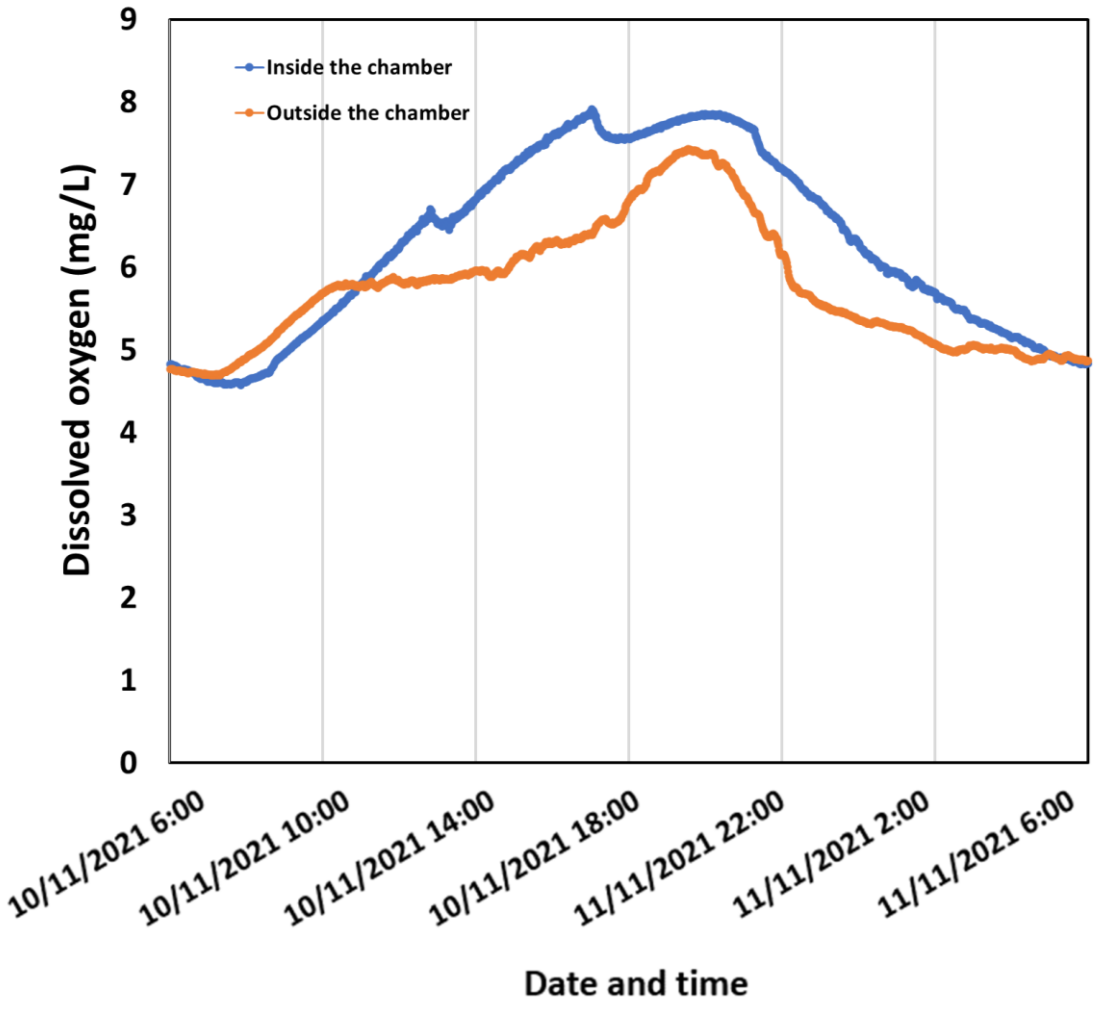

Figure 51. The changes of dissolved oxygen saturation % in water inside the chamber at the Woods Well site from 6 am on 10 November to 6 am on 11 November 2021.

3.3 Microbial ecology

3.3.1 Denitrifier community dynamics and activity

In sediment cores spanning the salinity gradient of the Coorong Lagoon, salinity was found to be the most important variable in shaping overall prokaryotic microbial community structure (*adonis,* R^2 = 0.29, p =

0.001). DO (*adonis*, $R^2 = 0.25$, $p = 0.02$), TN (*adonis*, $R^2 = 0.26$, $p = 0.002$) and TP (*adonis*, $R^2 = 0.20$, $p = 0.008$) were also important to community structure. Salt-tolerant Euryarchaeaota and bacterial taxa were more dominant in South Lagoon sediments, which are subject to higher salinity (Figure 52).

The calculated *nirK* activity ratio was elevated in South Lagoon sediments, suggesting a potential increase in denitrification efficiency in these salt-adapted microbial communities.

Abundance of the assayed denitrification gene (*nirK*) had a strong inverse relationship with salinity (*Spearman's* $\rho = -0.81$, $p < 0.001$) (Figure 53), as did its RNA transcript abundance (*Spearman's* $\rho = -0.72$, $p < 0.01$). This suggests that salinity has a strong negative influence on regular inorganic nitrogen removal processes in the South Lagoon.

Metagenome inference suggested an increase in biochemical pathways related to metabolic plasticity in North Lagoon benthic communities, consistent with a previous metagenomic study in the region (Newton *et al.* 2018). A shift towards osmoadaptation and cell growth-related pathways was observed in South Lagoon sediment communities (Figure 54). This analysis is based on algorithmic matching of 16S sequence-identified bacteria to taxa with full genomes available in publicly-available databases, therefore it is not empirical, but aims to suggest functional roles for further research and validation in ongoing work.

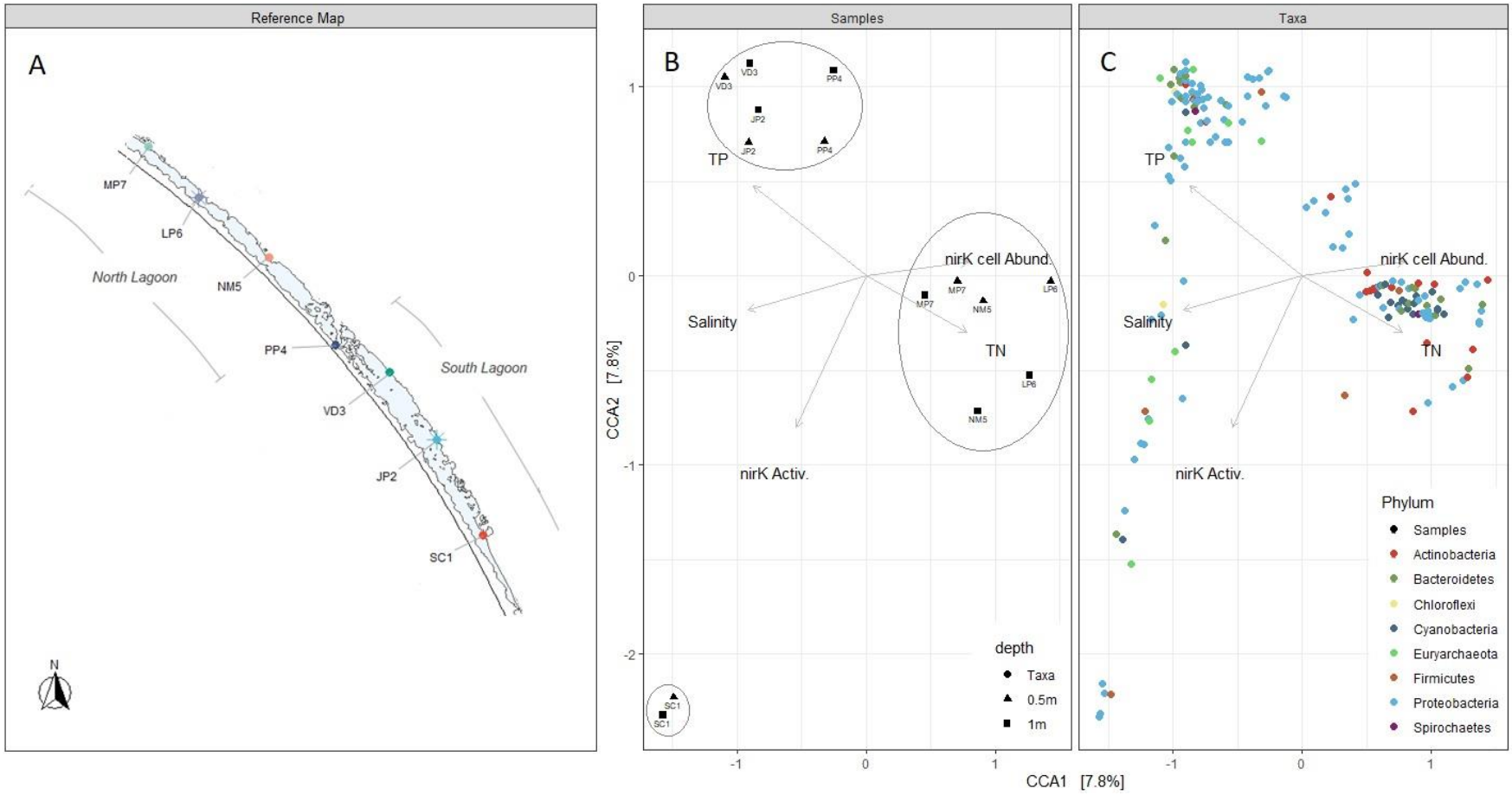

Figure 52. Constrained correspondence analysis (CCA) of benthic Coorong prokaryotic microbial communities sampled in 2019. A) Reference map of the study site. B) CCA of samples. Circled are Salt Creek samples (lower left), remaining Southern Lagoon sites, with Parnka Point (upper left) and Northern Lagoon sites (right), to indicate clear sample groupings relevant to the site, explained by continuous variables. C) Parallel CCA of major phyla (>1%) present, generated alongside B with the plot_ordination(…type = "split"… function in R "phyloseq". (*anova* (CCA): F = 1.01, p = 0.001).

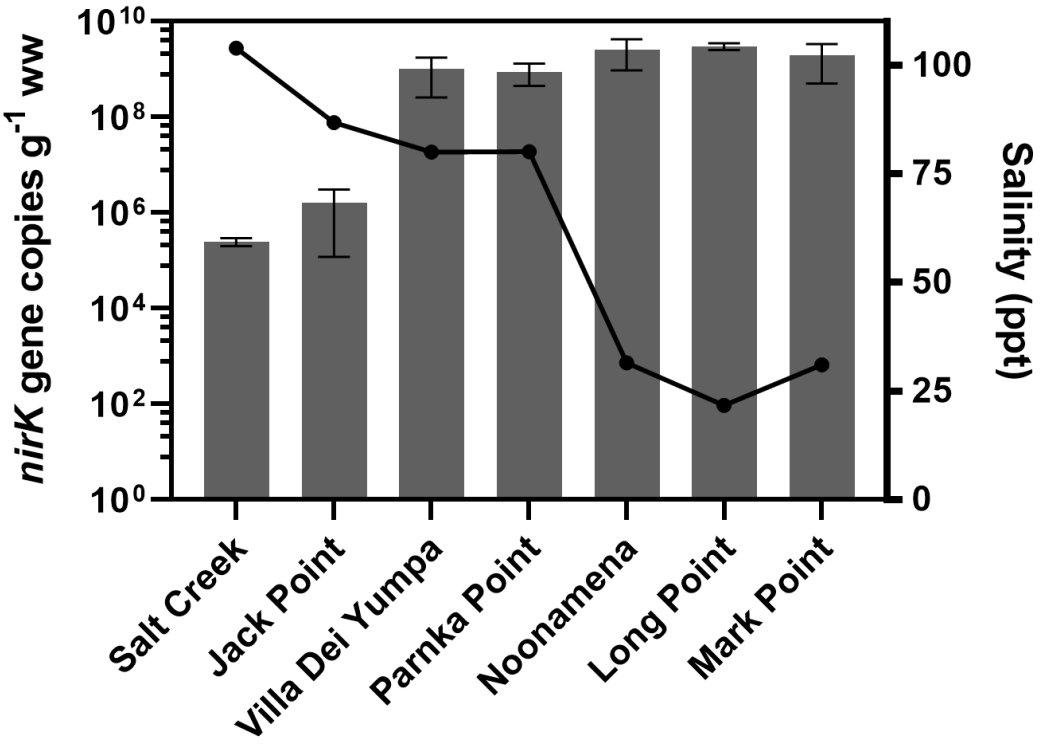

Figure 53. Salinity (parts per thousand, 2nd Y-axis) plotted against gene abundance of *nirK* in log copies per gram of sediment (wet weight (ww), 1st Y-axis), a community-shared gene encoding a rate–limiting enzyme in denitrification. Sites are listed in order of sampling, southern-most to northern-most, as listed in Table 3.

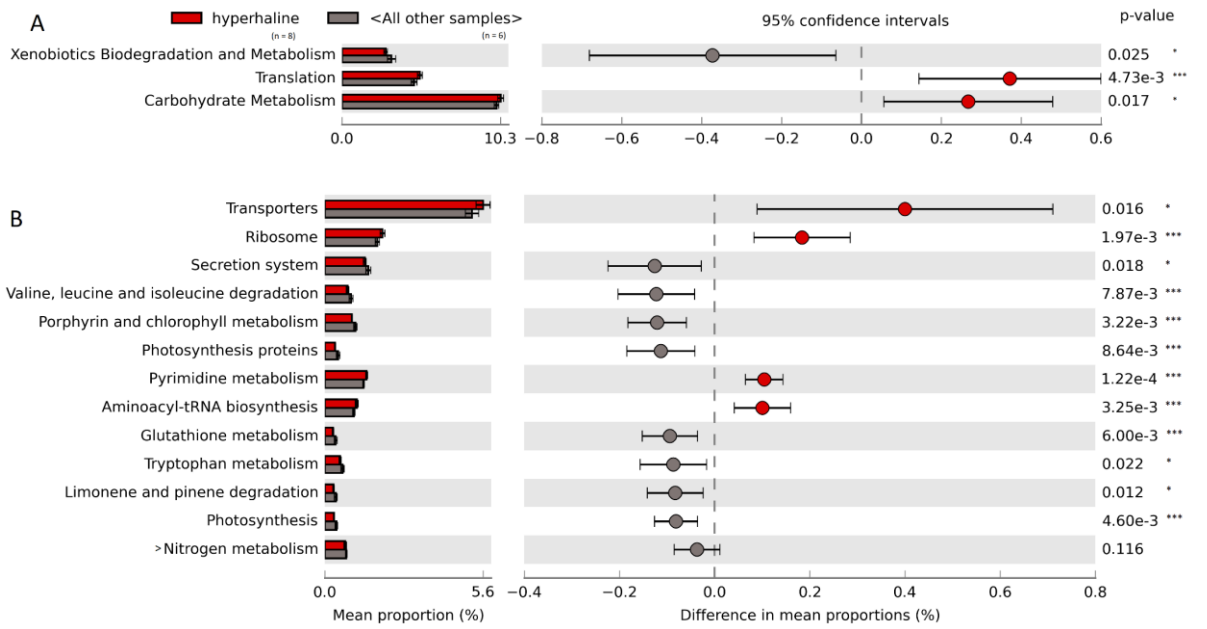

Figure 54. Differential (relative) abundance of inferred metagenome pathways at A) KEGG level 2 and B) KEGG level 3, generated from preliminary sampling 16S data with PICRUSt ancestral state reconstruction and analysed with Welch's Two-sample T-Test. Mean proportion (left) explains the pathway's proportion of the total sample. Difference in mean proportion (right) shows the difference of this relative to the opposite group. The hypersaline group, groups samples > 40 g/L TDS, and the second group includes all samples below this threshold.

3.4 Macroinvertebrate influences on nutrient dynamics

3.4.1 Evaluation 1: Salinity gradient survey

Macroinvertebrate composition

In total, 17 taxa were recorded across seven sites across the North and South lagoons of the Coorong. Annelida showed the highest number of taxa (29.4%, 5 taxa), followed by Insecta (23.5%, 4 taxa), Bivalvia (17.7%, 3 taxa), Crustacea (17.7%, 3 taxa), and Gastropoda (11.8%, 2 taxa). The macrobenthic richness across the seven sites ranged from 1 to 9 taxa, with greater numbers at the Murray Mouth (Hunters Creek (HC), Pelican Point (PP)) and North Lagoon (Long Point (LP), Noonameena (NM)) sites than the South Lagoon (Hells Gate, Jack Point, Salt Creek) sites. The macrobenthic species richness recorded between sites were significantly different ($p = 0.0001$, PERMANOVA; Table 17). In pairwise comparisons between North and south Lagoon sites, significant differences in richness were found for HC, PP, LP and NM compared to the other three sites in the South Lagoon which contained almost no macroinvertebrates ($p < 0.01$).

Table 17. Test results from univariate one-way fixed factor PERMANOVA to compare number of taxa (richness), abundance, and community structure of macroinvertebrates in the Coorong. Significant p values are in bold. DF= degrees of freedom, SS= sum of squares, MS= mean of sum of squares. Reprinted from Lam-Gordillo et al. 2022, with permission from Elsevier.

SOURCE	DF	SS	MS	PSEUDO-F	P(PERM)
Richness					
Site	6	197.09	32.848	52.258	**0.0001**
Residual	28	17.6	0.62857		
Total	34	214.69			
Abundance (ind.m2)					
Site	6	2.19E+11	3.65E+10	42.178	**0.0001**
Residual	28	2.42E+10	8.66E+08		
Total	34	2.43E+11			
Community					
Site	6	69634	11606	29.589	**0.0001**
Residual	28	10982	392.23		
Total	34	80617			

In terms of macrobenthic abundance, Crustacea was the taxon with the greatest abundance overall (62.5%), followed by Bivalvia (21.1%) and Annelida (9.3%) (Figure 55a). The total abundance of macrobenthic individuals was significantly different across sites ($p = 0.0001$, PERMANOVA; Table 17). Individual densities at HC, PP and LP in the North Lagoon were significantly higher compared to the other four sites in the South Lagoon ($p < 0.01$; Figure 55b).

Macroinvertebrate communities

The macrobenthic communities displayed a clear separation based on the non-metric Multidimensional Scaling (nMDS) (Figure 56). Differences in communities were significant ($p = 0.0001$, PERMANOVA, Table 17) and revealed distinct communities across sites ($p < 0.01$). Community separation based on the region was also identified. For example, HC, PP, (Murray Mouth), LP and NM (North Lagoon) were very different to Hells Gate (HG), Jack Point (JP), and Salt Creek (SC) sites (South Lagoon). Although less evident, there was also a separation between HC, PP and LP, NM (Figure 56).

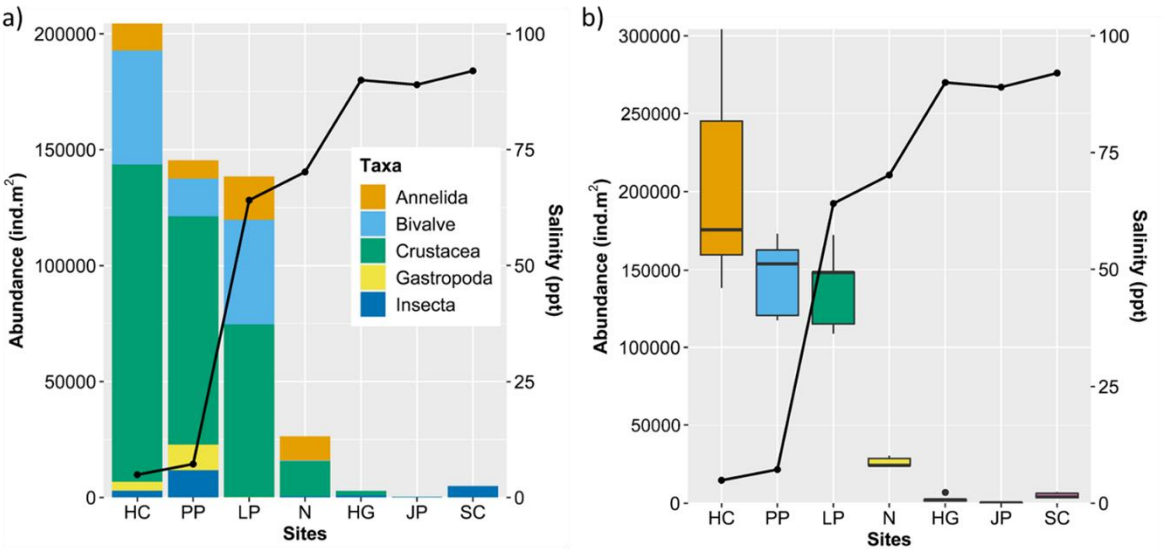

Figure 55. Mean total abundance of macroinvertebrates (a) stacked bar graph by taxa and (b) box plot of all taxa pooled across each of the seven sampling sites in the Coorong. Black line shows the salinity at each sampling site. Reprinted from Lam-Gordillo et al. 2022, with permission from Elsevier.

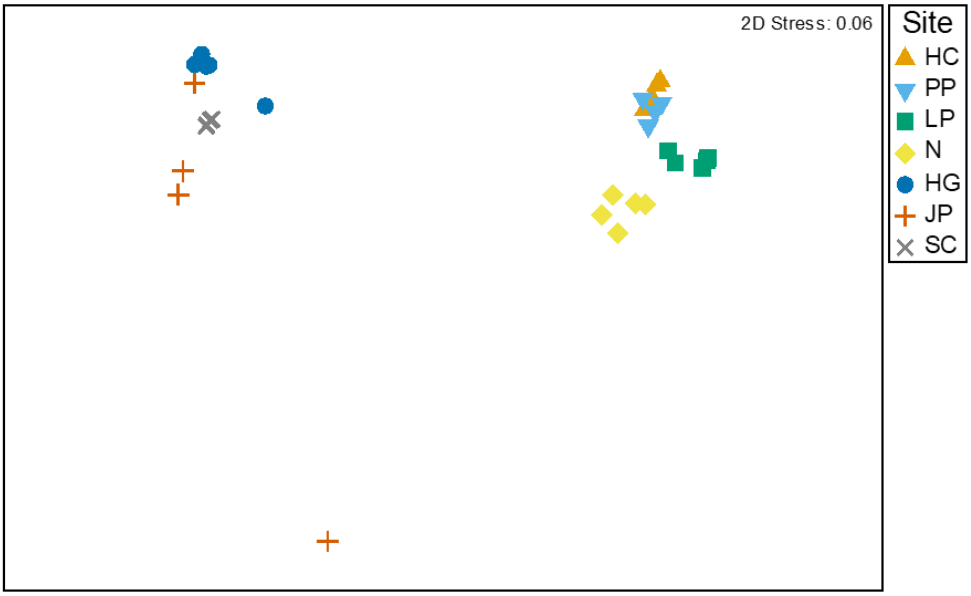

Figure 56. nMDS (non-Metric Multidimensional Scaling) plots for macrobenthic communities across sites. HC: Hunters Creek; PP: Pelican Point; LP: Long Point; N: Noonameena; HG: Hells Gate; JP: Jack Point; SC: Salt Creek.

Environmental conditions

pH was similar across sites with the exception of NM that was more alkaline (Figure 57a). Salinity increased from sites in the Murray Mouth towards sites in the South Lagoon (Figure 57b). Sediment OM was highest at sites in the South Lagoon and the lowest at the North Lagoon (Figure 57c). For sediment Chlorophyll *a* (a proxy for microphytobenthic biomass), two sites (HC, LP) showed higher concentrations, while the other five sites were in the same range (Figure 57d). Sediment grain size, as D_{50}, varied across sites, while the sorting was more homogeneous at all sites (Figure 57e-f).

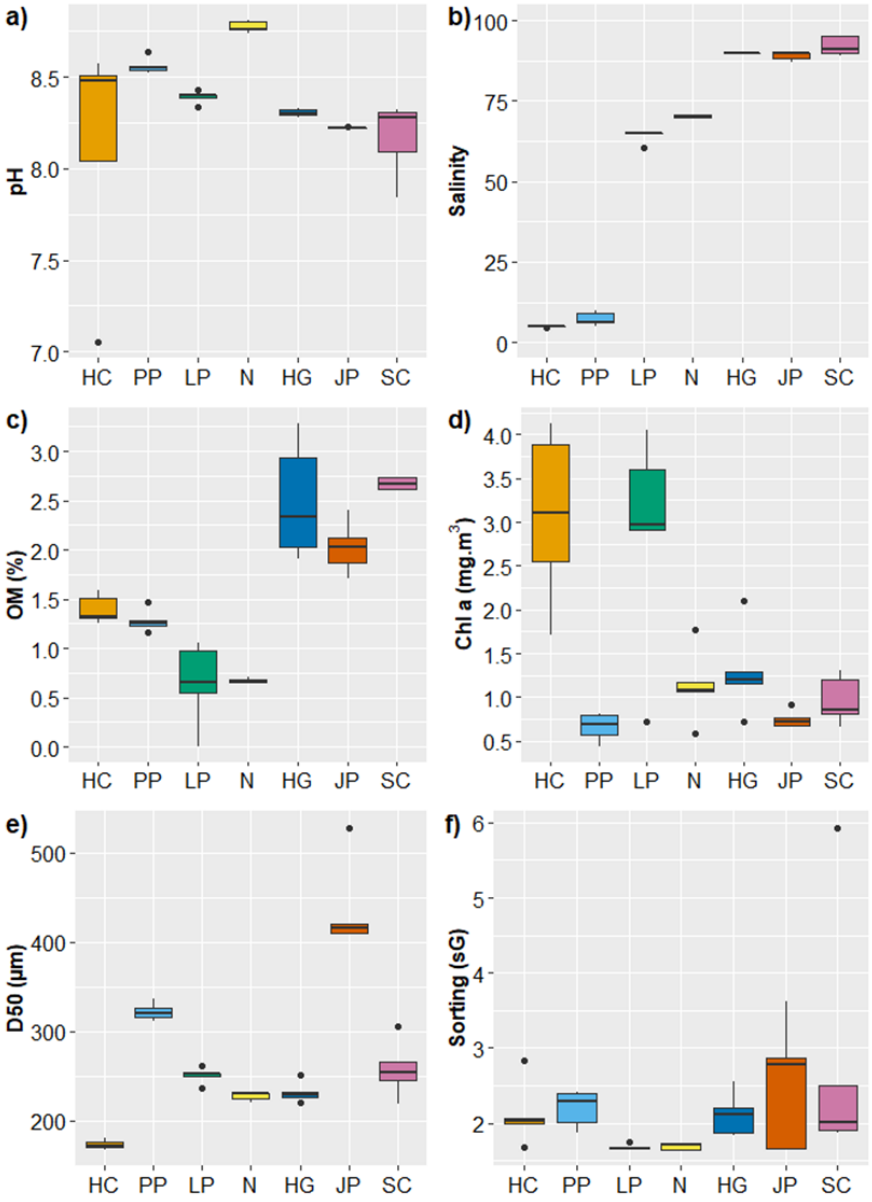

Figure 57. Boxplots of the environmental conditions (pH, salinity, organic matter (OM), chlorophyll a (Chl a) and sediment grain size (D_{50}, Sorting) recorded from water (a,b,c,) and sediment (d,e,f) in the Coorong across sampling sites. HC: Hunters Creek; PP: Pelican Point; LP: Long Point; N: Noonameena; HG: Hells Gate; JP: Jack Point; SC: Salt Creek.

Concentration of nutrients in porewater changed across sites (Figure 58). Nitrate concentrations were greater at the Murray Mouth sites, decreasing towards the South Lagoon (Figure 58a). Although concentrations of nitrite followed a similar pattern as nitrate, nitrite concentrations were lower (Figure 58b). Ammonium concentration was highest at JP (South Lagoon), followed by LP (North Lagoon) and SC (South Lagoon) (Figure 58c). Phosphate concentrations were more similar across sites (mean range 0.55–0.75 mg/L) with a higher concentration value recorded at HC (Figure 58).

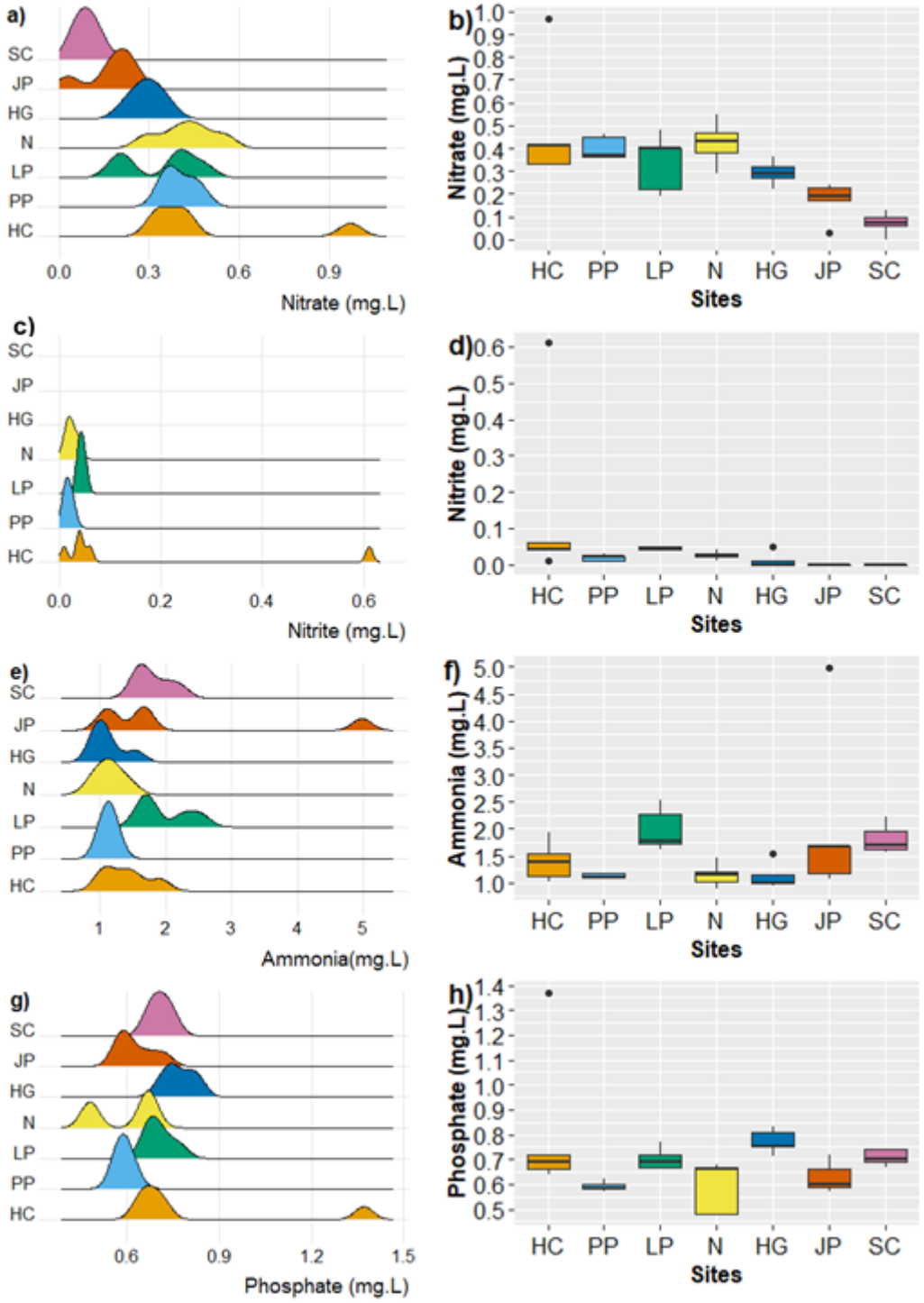

Figure 58. Ridgeline plots and boxplots showing the concentration of nutrients recorded in the Coorong across sampling sites. a-b) Nitrate, c-d) Nitrite, e-f) Ammonium, g-h) Phosphate. HC: Hunters Creek; PP: Pelican Point; LP: Long Point; N: Noonameena; HG: Hells Gate; JP: Jack Point; SC: Salt Creek.

Influence of macroinvertebrates on nutrient concentrations and organic matter degradation

Macroinvertebrate abundance was greater at sites at the Murray Mouth and decreased towards sites in the South Lagoon. Concentrations of nitrate in pore water were influenced by the abundance of macroinvertebrates ($p < 0.01$; Table 18), showing a correlation of low nitrate concentration and low macroinvertebrate abundance (Figure 59a-b). Concentrations of nitrite in porewater followed a

similar pattern to nitrate, decreasing towards the South Lagoon (Figure 59c-d), suggesting that the concentrations of nitrite were also influenced by the macroinvertebrate abundance ($p < 0.01$; Table 18). Ammonium showed an opposite pattern to nitrate and nitrite. Concentrations of ammonium increased from sites in the Murray Mouth towards sites in the South Lagoon (Figure 59e-f). However, concentrations of ammonium and phosphate were not significantly influenced by the macroinvertebrate abundance ($p > 0.01$; Table 18; Figure 59g-h).

Table 18. Test results from the Generalised Additive Model (GAM) assessing the interaction between each of the porewater nutrients and macroinvertebrates recorded in the Coorong. Results are based on Experiment 1 in Spring 2020. Significant *p* values are in bold.

PARAMETRIC COEFFICIENTS	ESTIMATE	STD. ERROR	T VALUE	PR(>|T|)	DEVIANCE EXPLAINED	AIC
(Intercept)	73.04	218.47	0.334	0.74024		
Nitrate	1755.39	606.97	2.892	**0.00673**	20.20%	555.46
(Intercept)	233.1	144.9	1.609	0.117544		
Nitrite	19845.3	5387.9	3.683	**0.000845**	29.80%	535.83
(Intercept)	750.5	283.7	2.645	0.0124		
Ammonium	-83.9	168	-0.499	0.6209	0.75%	563.10
(Intercept)	473.5	600.5	0.789	0.436		
Phosphate	216.4	856.1	0.253	0.802	0.19%	563.30

The organic matter (ROMA plate) degradation rate was different across sites and depths ($p < 0.01$; Table 19). Degradation rates at HC and PP were similar across depths with differences at 16–20 cm depth. HC and PP showed higher OM degradation rates compared to the LP and NM sites (Figure 60). LP and NM degradation rates were similar across most of the depths; the only differences identified were at 4–8 cm depth (Figure 60).

Table 19. Test results from univariate one-way fixed factor PERMANOVA comparing organic matter degradation from ROMA plates across four sites (Hunters Creek, Pelican Point, Long Point, Noonameena) in the Coorong. Significant p values are in bold. DF= degrees of freedom, SS= sum of squares, MS= mean of sum of squares. Reprinted from Lam-Gordillo et al. 2022, with permission from Elsevier.

SOURCE	DF	SS	MS	PSEUDO-F	P(PERM)
Site	3	0.032807	0.010936	14.878	**0.0001**
Depth	4	0.055369	0.013842	18.832	**0.0001**
Site × Depth	12	0.042752	0.0035626	4.8469	**0.0001**
Residual	80	0.058803	0.00073503		
Total	99	0.18973			

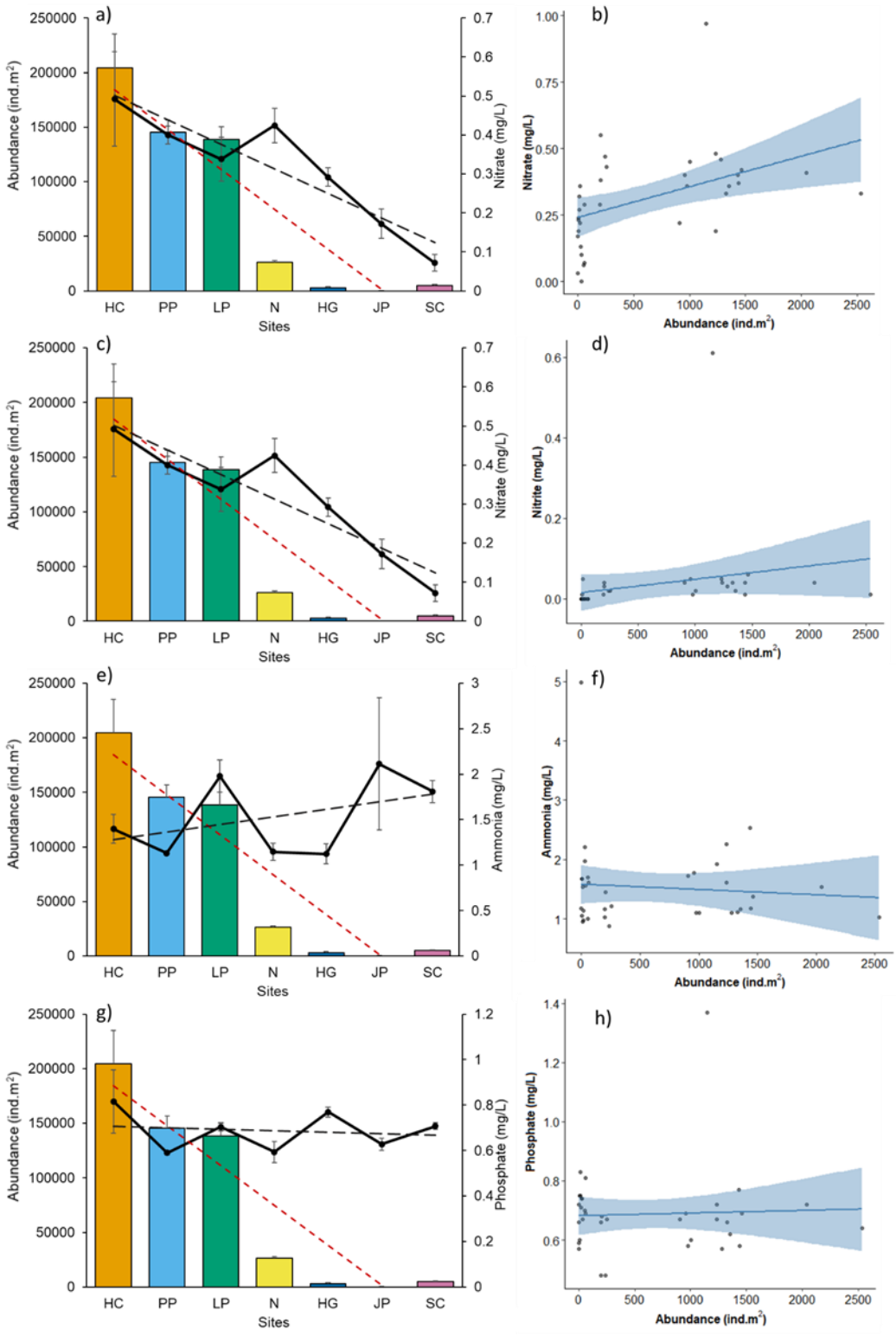

Figure 59. Bar graphs of the mean total abundance of macroinvertebrates in relation to the porewater nutrient concentrations (black line) at each sampling site (a, c, e and g). Red dotted lines show the macroinvertebrates abundace trend line. Black dotted line shows the porewater nutrient concentrations trend line. Generalised additive model plots (b, d, f, and h) show the interaction between porewater nutrient concentrations and macroinvertebrates abundance. Blue shading represents the confidence interval (95%).

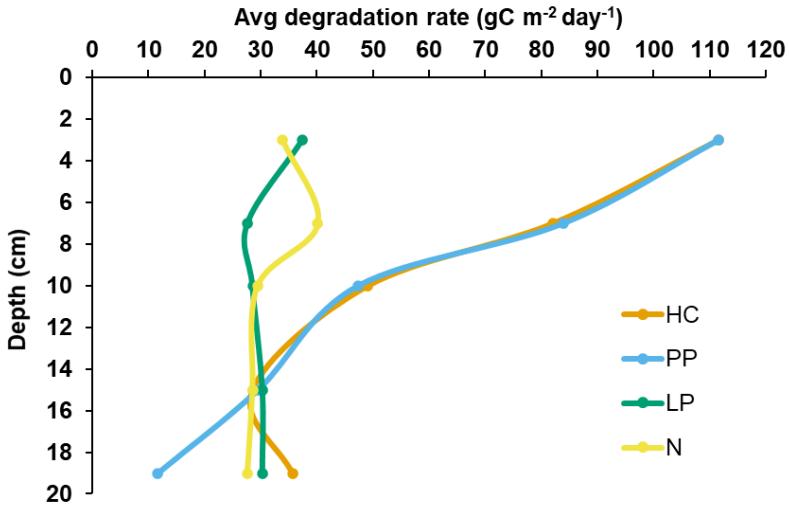

Figure 60. Organic matter degradation rate between sites, based on Rapid Organic Matter Assessment (ROMA) plates. Data points indicate mean values (n = 5) and error bars show the standard error (SE). HC: Hunters Creek; PP: Pelican Point; LP: Long Point; N: Noonameena. Hells Gate, Jack Point, and Salt Creek are not shown as the ROMA plates did not perform properly due to the hypersalinity at those sites. Reprinted from Lam-Gordillo et al. 2022, with permission from Elsevier.

3.4.2 Evaluation 2: Sediments and macroinvertebrates translocation

Macroinvertebrates recovered after translocation

Macrobenthic fauna colonised the sediment within one week after the hostile (i.e. hypersaline, sulfide-rich) sediment in the experimental units from PP were translocated into the lower salinity site at LP. Significant differences were found in the abundance of *S. aequisetis* (organisms recovered) across the treatments 0×, 0.5×, 1×, and 2× ($p < 0.05$). The recovery rate of *S. aequisetis*, which had been added to the experimental units, ranged from 48% to > 100%. In some experimental units, the density of *S. aequisetis* exceeded the number of polychaetes added to the treatment due to colonisation by local *S. aequisetis* (Table 20). Other taxa also found to have colonised experimental units were *Arthritica semen*, Amphipoda, *Capitella sp.*, and small-sized *S. aequisetis* (hereafter referred as 'S. aequisetis (s)'; length < 2 cm) (Table 20), yet the macrobenthic abundance (all taxa included) was significantly different across the treatments ($p < 0.05$). The macrobenthic community found in the control units (undisturbed sediment from LP) were characterised by the same four macrobenthic taxa, with significantly higher abundance compared to the experimental units from PP ($p < 0.05$).

Salinity characterisation

After an initial period of sediment settlement (five days), porewater salinity in PP experimental units at the LP site decreased from > 160 PSU to an average of 25 PSU, which enabled the colonisation of macrobenthic fauna. Porewater salinity in the experimental units (both LP and PP) during the experiment ranged from 17–34 PSU. Porewater salinity was not significantly different between LP and PP experiment units, and control units at both sites ($p > 0.05$; Table 21). Significant differences in porewater salinity were found between measurement events ($p < 0.05$; Table 21), where porewater salinity was lower at the start of the experiment and gradually increased towards the end of the experiment (week 4). Significant differences were also found across depth horizons ($p < 0.05$; Table 21), with lower porewater salinity recorded in the upper depth horizon (0–2 cm) and higher concentrations in the deepest 10–20 cm depth horizon in all experimental units.

Table 20. Number of *Simplisetia aequisetis* added to sediments from either LP or PP translocated to LP, and recovery of *S. aequisetis* and other macrobenthic fauna during each weekly sampling following additions of different densities of *S. aequisetis* (s) denotes juvenile *S. aequisetis*; smaller individuals than those added to the experimental units. Recovery was calculated using the mean + standard error values (n = 3) (Lam-Gordillo et al. 2022b).

	LONG POINT				POLICEMAN'S POINT				CONTROL
	0×	0.5×	1×	2×	0×	0.5×			
***Simpisetia aequisetis* added (ind.core)**	0	3	5	10	0	3	5	10	Undisturbed sediment
Week 1									
***Simpisetia aequisetis* recovered (ind.core)**	0.78 + 0.63	1.67 + 0.76	1.56 + 0.82	2.78 + 1.97	1.22 + 0.99	1.11 + 0.84	3.56 + 1.96	3.33 + 2.14	12.44 + 9.40
Recovery (%)	+1	81%	48%	48%	+2	65%	110%	55%	NA
Abundance of other taxa found (ind.core)									
Arthritica semen	8.67 + 7.70	11.56 + 9.03	15.33 + 13.57	13.56 + 14.38	7.00 + 6.24	20.89 + 17.18	27.78 + 25.99	24.00 + 19.62	56.11 + 75.08
Amphipoda									
Capitella sp.	0.56 + 0.96	1.89 + 1.99	0.78 + 1.56	1.22 + 2.86	1.11 + 0.84	0.67 + 0.96	0.44 + 1.59	0.33 + 2.41	73.89 + 43.30
Simplisetia aequisetis (s)	24.78 + 21.61	14.33 + 10.14	14.67 + 12.74	3.89 + 3.30	35.78 + 32.00	20.56 + 22.22	20.67 + 20.38	12.89 + 12.93	15.00 + 12.00
Week 2									
***Simpisetia aequisetis* recovered (ind.core)**	6.11 + 4.41	4.89 + 3.97	2.33 + 1.73	2.78 + 2.34	8.11 + 5.97	3.11 + 1.97	4.44 + 2.86	4.56 + 3.91	7.00 + 5.40
Recovery (%)	+11	295%	81%	51%	+14	169%	146%	85%	NA
Abundance of new taxa found (ind.core)									
Arthritica semen	9.67 + 5.24	15.33 + 11.33	7.78 + 6.07	7.44 + 5.54	10.78 + 12.46	10.00 + 10.63	9.33 + 6.41	3.44 + 3.71	53.89 + 67.03
Amphipoda									
Capitella sp.	2.89 + 6.86	2.00 + 4.15	3.67 + 2.29	1.33 + 2.63	2.78 + 5.25	0.67 + 1.58	0.89 + 2.79	4.67 + 3.42	49.11 + 38.76

Simplisetia aequisetis (s)	64.78 + 58.36	38.33 + 36.49	52.22 + 44.24	15.33 + 12.88	65.00 + 57.67	59.56 + 56.52	50.78 + 45.77	57.56 + 54.44	28.67 + 24.26
Week 3									
***Simpisetia aequisetis* recovered (ind.core)**	6.78 + 4.96	3.11 + 2.28	3.33 + 3.39	5.67 + 4.44	6.44 + 3.92	6.11 + 4.16	7.22 + 4.37	6.56 + 4.64	6.78 + 5.50
Recovery (%)	+12	180%	134%	101%	+10	342%	232%	112%	NA
Abundance of new taxa found (ind.core)									
Arthritica semen	13.22 + 14.00	4.00 + 2.25	5.33 + 4.13	4.00 + 4.04	13.67 + 12.91	18.00 + 18.11	11.89 + 12.18	18.78 + 26.30	69.89 + 62.57
Capitella sp.	7.11 + 6.98	4.89 + 3.43	3.56 + 3.06	2.89 + 5.32	4.33 + 3.75	2.00 + 4.84	1.89 + 4.06	7.56 + 4.87	44.67 + 36.15
Simplisetia aequisetis (s)	66.78 + 65.83	47.67 + 46.14	31.22 + 34.07	54.00 + 51.68	49.22 + 52.58	74.11 + 63.30	61.00 + 57.35	78.00 + 81.12	30.56 + 25.15
Week 4									
***Simpisetia aequisetis* recovered (ind.core)**	3.44 + 2.60	1.89 + 1.24	3.89 + 1.51	5.11 + 2.91	7.00 + 4.00	4.22 + 1.97	3.89 + 1.81	4.67 + 2.20	5.22 + 4.00
Recovery (%)	+6	104%	108%	80%	+11	206%	114%	69%	NA
Abundance of new taxa found (ind.core)									
Arthritica semen	3.33 + 3.42	8.11 + 8.57	5.78 + 7.12	7.33 + 5.97	14.56 + 13.81	13.44 + 14.66	16.56 + 15.50	3.33 + 2.89	43.44 + 86.50
Amphipoda									
Capitella sp.	2.22 + 3.50	2.44 + 1.85	4.11 + 3.05	4.11 + 5.85	5.33 + 4.73	4.67 + 1.89	7.00 + 1.91	3.56 + 2.22	66.11 + 49.93
Simplisetia aequisetis (s)	34.89 + 37.70	32.78 + 27.16	28.56 + 23.37	47.00 + 39.55	51.44 + 38.26	24.44 + 21.57	48.78 + 39.65	30.56 + 27.67	29.33 + 25.23

Table 21. Test results from univariate one-way fixed factor PERMANOVA to compare salinity between treatment densities, weeks, depths, and sediment sources. Only significant results are shown. Den = density, We = weeks, Dep = depth, Si = sediment source (modified from Lam-Gordillo et al. 2022b). DF= degrees of freedom, SS= sum of squares, MS= mean sum of squares.

SOURCE	DF	SS	MS	PSEUDO-F	P(PERM)	PERMS
Salinity						
Density	3	137.54	45.85	3.137	**0.0156**	9960
Week	3	1568.00	522.65	35.760	**0.0001**	9958
Deph	2	1191.30	595.63	40.752	**0.0001**	9958
DensityxWeek	9	245.31	27.26	1.865	**0.0461**	9943
WeekxDeph	6	490.03	81.67	5.588	**0.0001**	9943
WeekxSediment	3	332.70	110.90	7.588	**0.0001**	9947
DensityxWeekxSediment	9	272.59	30.29	2.072	**0.0239**	9941

Influence of macroinvertebrates on sediment biogeochemistry

Changes of total organic carbon concentrations in sediments were influenced by the presence of *S. aequisetis*, amphipods, *S. aequisetis* (s), *Capitella sp.* and *A. semen* ($p < 0.05$; Table 22). TOC concentrations in sediment ranged from 0.06 to 0.30%. Sediment TOC concentration in the experimental units was higher than the initial concentration recorded in control units (mean values: LP = 0.19% TOC, PP = 0.17% TOC, and C = 0.14% TOC). TOC concentrations in sediment were significantly higher in Week 1 (~0.13–0.28% TOC) compared to week 4, by which time the TOC concentrations were significantly lower (~0.06–0.24% TOC) in both sediment sources ($p < 0.05$). TN concentrations in sediment were also influenced by the presence of amphipods and *A. semen* ($p < 0.05$; Table 22). Sediment TN was low (range 0.006–0.040% TN), but higher in the experimental units than control units (mean values: LP = 0.022% TN, PP = 0.018% TN and C = 0.016% TN). TN concentration decreased significantly over time (Week 1: ~0.011–0.039% TN, Week 4: ~0.006–0.025% TN) in both LP and PP sediments ($p < 0.05$).

Changes of ammonium concentrations in porewater were influenced by the presence of *S. aequisetis*, amphipods, *S. aequisetis* (s), *Capitella sp.* and *A. semen* ($p < 0.05$; Table 22). Porewater ammonium concentrations in the experimental units were higher than in the control units (mean values: LP = 390 µmol/L, PP = 249 µmol/L and C = 67.6 µmol/L). Concentrations of ammonium in porewater decreased significantly over time (Week 1: ~150–400 µmol/L, Week 4: ~0–160 µmol/L) in both LP and PP experimental units ($p < 0.05$; Figure 5a; Table S8). *Capitella sp*. influenced the porewater phosphate concentrations ($p < 0.05$; Table 22). Concentrations of porewater phosphate were significantly higher in LP (~4-20 µmol/L) compared to PP (~0-9 µmol/L) experimental units ($p < 0.05$). Significant differences were also identified across weeks and depth ($p < 0.05$). Concentrations of porewater phosphate were also higher in LP experimental units than the control units (mean = 9.48 and 2.43 µmol/L respectively), but similar in PP experimental and control units (2.32 µmol/L; Figure 5b).

Initial concentrations of porewater nitrate in both experimental unit sediment sources ranged from 0–10.5 µmol/L and were similar to concentrations recorded in the control units. Significant differences, however, were found between weeks, depths, and sediment sources ($p < 0.05$), mainly due to the significantly higher concentrations of porewater nitrate found in the LP experimental units 1× and 2× in Week 2. Porewater nitrate concentrations were only influenced by *Capitella sp.* ($p < 0.05$; Table 22). Concentrations of porewater nitrite in experimental units ranged from 0–17.4 µmol/L and were similar to those in the control units. Significant differences were not found between any factor ($p > 0.05$), and direct effects of macrofauna on concentrations of nitrite in porewater were not detected (Table 22).

Table 22. Result of DistLM forward analysis for *Simplisetia aequisetis* and other macrofauna as predictor of the individual variables: total organic carbon and total nitrogen content, and porewater ammonium, phosphate, nitrate, and nitrite concentrations over time. Significant P values are in bold. *S. aequisetis* (s) = Juvenile *S. aequisetis*, smaller than those added in the experimental units. Proportion = variability (taken from Lam-Gordillo et al. 2022b).

SELECTED PREDICTOR	RESPONSE VARIABLE	AIC	R^2	SS (TRACE)	PSEUDO-F	P-VALUE	PROPORTION
Simplisetia aequisetis	Total organic Carbon	-826.1	0.0974	0.049	15.336	**0.0001**	0.0975
Amphipoda		-848.6	0.2594	0.117	43.294	**0.0001**	0.2337
S. aequisetis (s)				0.062	19.902	**0.0001**	0.1229
Capitella sp.				0.015	4.2654	**0.0369**	0.0292
Arthritica semen				0.072	23.979	**0.0001**	0.1445
Simplisetia aequisetis	Total nitrogen	-1181.9	0.0215	0.001	3.132	0.0685	0.0216
Amphipoda		-1187.4	0.0961	0.002	7.345	**0.0109**	0.0492
S. aequisetis (s)				0.000	1.844	0.1556	0.0128
Capitella sp.				0.000	0.678	0.2967	0.0048
Arthritica semen				0.003	11.965	**0.0080**	0.0777
Simplisetia aequisetis	Ammonium	1199.8	0.0922	1318.000	32.690	**0.0001**	0.0922
Amphipoda		1206.0	0.0915	22.944	0.000	0.0665	0.0888
S. aequisetis (s)				1018.800	24.701	**0.0001**	0.0712
Capitella sp.				430.100	9.985	**0.0247**	0.0301
Arthritica semen				573.870	13.462	**0.0068**	0.0401
Simplisetia aequisetis	Phosphate	-334.9	0.0040	0.457	1.291	0.2555	0.0040
Amphipoda		-331.7	0.0126	0.365	1.032	0.3031	0.0032
S. aequisetis (s)				0.168	0.473	0.4862	0.0015
Capitella sp.				1.259	3.586	**0.0479**	0.0110
Arthritica semen				0.376	1.062	0.3010	0.0033
Simplisetia aequisetis	Nitrate	-1183.0	0.0001	0.001	0.037	0.8526	0.0001
Amphipoda		-1190.1	0.03947	0.032	1.247	0.2616	0.0039
S. aequisetis (s)				0.081	3.170	0.0750	0.0097
Capitella sp.				0.132	5.185	**0.0274**	0.0158
Arthritica semen				0.074	2.902	0.0762	0.0089
Simplisetia aequisetis	Nitrite	-539.4	0.00316	0.192	1.021	0.2749	0.0032

Amphipoda		-532.8	0.0013	0.020	0.105	0.7570	0.0003
S. aequisetis (s)				0.020	0.106	0.7706	0.0003
Capitella sp.				0.037	0.195	0.5982	0.0006
Arthritica semen				0.002	0.013	0.9105	0.0000

Sulfide concentrations in sediment porewater changed significantly across time and depth horizons ($p < 0.001$; Table 23) and the influence of *S. aequisetis* and other macrofauna was evident (Figure 61a). Concentrations of sulfide at LP (~10–150 µmol/L) and PP (~10–200 µmol/L) experimental units were higher than in the control units, where porewater sulfide concentrations were close to zero (Figure 61a). Sulfide concentrations at LP and PP experimental units decreased over time, from ~10–200 µmol/L in week 0 to ~0–150 µmol/L in week 1 and 0–100 µmol/L in week 4 (Figure 61a). Significant differences in porewater sulfide concentrations were found across depths; sulfide concentrations decreased over shallower depth horizons (0–6 cm) but increased with depth, peaking between 8–12 cm ($p < 0.001$, GAM; Figure 61a). Shifts in sulfide concentrations across time and sediment depth were also identified; from ~150–200 µmol/L between 0–6 cm depth in week 0 to ~0-25 µmol/L in the same horizon depth in week 4 and between 6–12 cm depth sulfide decreased from ~100–150 µmol/L in week 1 to ~50–100 µmol/L in week 4 ($p < 0.001$, GAM; Figure 61a). Iron(II) concentrations in sediment porewater were low at LP and PP experimental units (~0–3 µmol/L) and differed from the control units (~0 µmol/L). Peaks of iron(II) concentrations were evident between 0–4 cm depth at LP in weeks 1 and 2. High variation in iron(II) concentrations were recorded across time and sediment depths in both LP and PP sediments. Although significant differences in concentrations of iron were found across weeks and depth ($p < 0.001$; Table 23), the model explained only 5% of the variation, as iron(II) concentrations in Week 0 and Week 4 in LP experimental units were significantly higher compared to any other experimental unit, due to the occurrence of "hotspots" of high iron(II) in some distributions of the experimental unit.

The influence of *S. aequisetis* and other macrofauna on porewater profiles of ammonium concentrations was identified ($p < 0.001$, GAM; Table 23). Ammonium concentrations in sediment porewater varied significantly with time and sediment depth ($p < 0.001$; Table 4). Concentrations of ammonium in LP (~10–1000 µmol/L) and PP (~10–250 µmol/L) experimental units were higher than in respective control units (Figure 61b). Porewater profiles of ammonium at LP showed peaks of high concentrations near the sediment surface in W0, decreasing at shallower depth horizons (0–6 cm), before increasing again in the deeper sediments (8–12 cm depth) (Figure 61b). Whereas, at PP and C units sediments porewater ammonium concentrations showed more typical profiles with concentrations gradually increasing with depth. Concentrations of porewater phosphate remained low across time and sediment depth in LP (~0–140 µmol/L) and PP (~0–20 µmol/L) experimental units, and were similar to the control units in weeks 1 and 4. Despite low concentrations of phosphate, there was significantly different across weeks and depth ($p < 0.001$; Table 23), but the model only explained 8.61% of the variability. Phosphate concentration profiles showed similar trends to those of ammonium, with LP sediments exhibiting sub-surface peaks in week 0, whereas in weeks 1 and 4 and in all three weeks in the PP and C treatments profiles were almost flat or showed gradual increase with sediment depth.

Nitrate concentrations in porewater were barely detected and similar between sediment sources (LP and PP experimental units) and control units. Significant differences were not detected with time or sediment depth ($p > 0.001$; Table 23), likely due to the low nitrate concentrations recorded.

Table 23. Summary table of the results from the Generalized Additive Model (GAM) assessing porewater concentrations of a) sulfide, b) iron, c) ammonium, d) phosphate, and e) nitrate. W0 = Week 0, W1 = Week 1, W4 = Week 4 (taken from Lam-Gordillo et al. 2022b).

PARAMETRIC COEFFICIENTS	ESTIMATE	STD. ERROR	T VALUE	PR(>|T|)	DEVIANCE EXPLAINED	AIC
a) Sulfide						
Parametric coefficients						
Intercept (W0)	79.716	0.330	241.370	< 0.001		
W1	-26.985	0.469	-57.530	< 0.001	48.80%	442260.0
W4	-56.904	0.467	-121.770	< 0.001		
Smooth terms						
Depth	edf = 8.711	Ref.df = 9	F = 2947.00	< 0.001		
b) Iron						
Parametric coefficients						
Intercept (W0)	1.313	0.028	46.686	< 0.001		
W1	-0.922	0.040	-23.004	< 0.001	5.00%	232187.4
W4	-0.206	0.040	-5.171	< 0.001		
Smooth terms						
Depth	edf = 8.793	Ref.df = 9	F = 190.90	< 0.001		
c) Ammonium						
Parametric coefficients						
Intercept (W0)	225.210	9.058	24.864	< 0.001		
W1	-102.357	12.202	-8.389	< 0.001	18.50%	1468413.0
W4	-118.873	12.307	-9.659	< 0.001		
Smooth terms						
Depth	edf = 4.467	Ref.df = 9	F = 15.76	< 0.001		
d) Phosphate						
Parametric coefficients						
Intercept (W0)	14.487	0.944	15.35	< 0.001		
W1	-10.355	1.322	-7.831	< 0.001	8.61%	10304.5
W4	-7.126	1.335	-5.339	< 0.001		
Smooth terms						
Depth	edf = 3.911	Ref.df = 9	F = 4.79	< 0.001		

e) Nitrate						
Parametric coefficients						
Intercept (W0)	0.829	0.294	3.32	< 0.001		
W1	-0.386	0.349	-1.10	0.268	0.15%	7148.52
W4	-0.424	0.353	-1.202	0.229		
Smooth terms						
Depth	edf = 0.003	Ref.df = 9	F = 0	0.784		

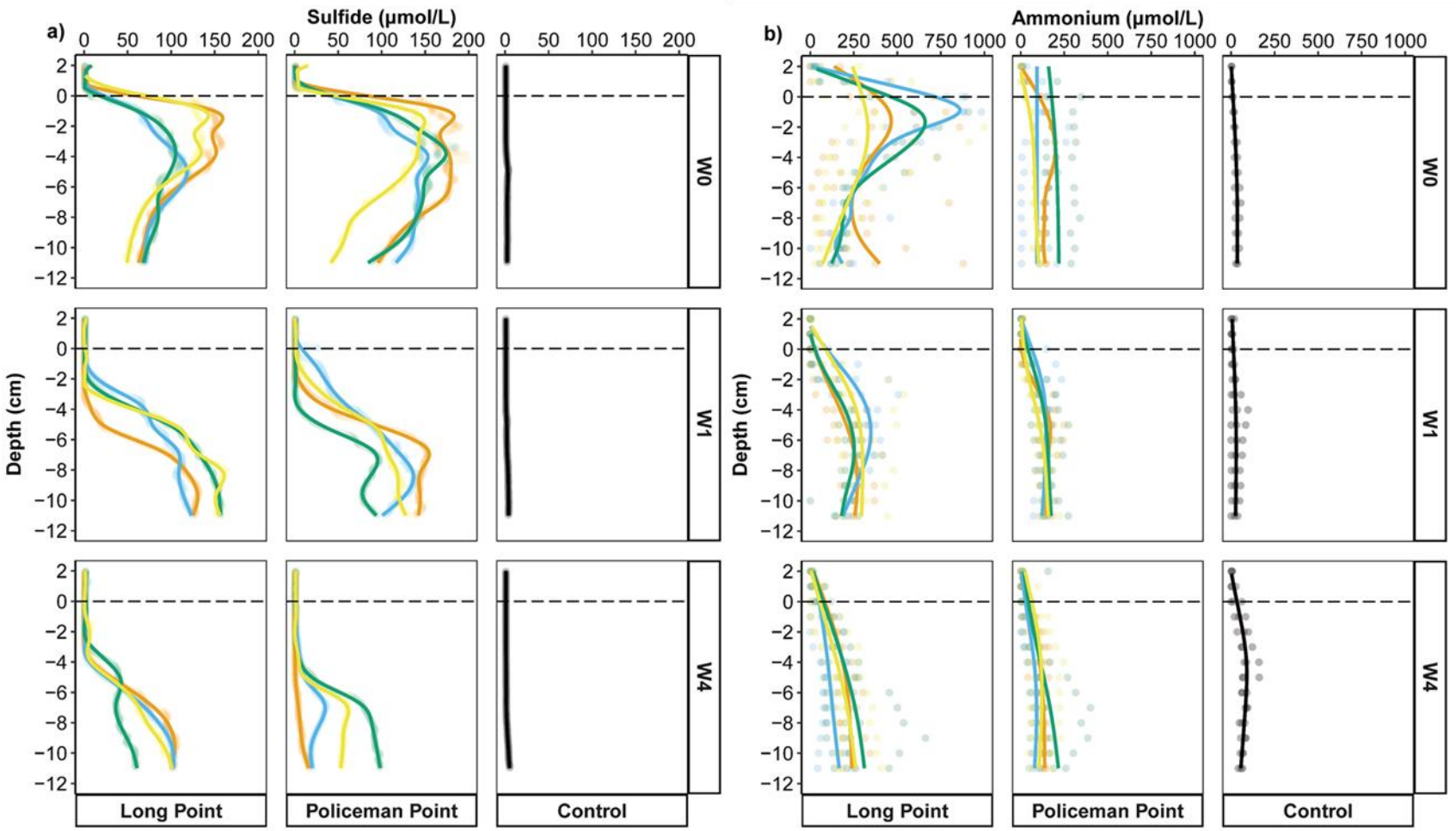

Figure 61. Generalised Additive Model (GAM) plots of sediment porewater concentrations profiles for experimental and control units of a) sulfide and b) ammonium. Plots show significant differences in sulfide and ammonium concentrations, and the influence of *S. aequisetis* and other macrofauna densities across weeks and depths. Colour shading represents the data values. W0 = Week 0, W1 = Week 1, W4 = Week 4. 0x = no S. aequisetis added, 0.5× = 3 *S. aequisetis*, 1× = 5 *S. aequisetis*, and 2× = 10 *S. aequisetis added*, C= Control. n=3 (modified from Lam-Gordillo et al. 2022b).

3.5 Sediment resuspension effects on water column nutrients

3.5.1 Sediment characteristics

The Villa dei Yumpa site was characterised by two major sediment types: predominantly sandy sediments in the shallow water depth (≤ 0.6 m water depth) locations closer to each shoreline and predominantly muddy sediments in the deeper (> 0.6 m water depth) water locations (Figure 62). The physical characteristics of these two sediment types varied (Figure 63) with the predominantly muddy sediments characterised by greater mean water content (66.82 ± 6.63%) and mean OM content (17.17 ± 3.26%) than the predominantly sandy sediments (WC 39.34 ± 6.08%; OM 6.20 ± 1.66%). The predominantly sandy sediments had a greater mean grain size (88.11 ± 32.44 µm) and mean bulk density (1.57 ± 0.09 g cm^3) than the predominantly muddy sediments (MGS 21.74 ± 4.04 µm, mean ρ 1.23 ± 0.07 g cm^3). Results of Kruskal-Wallis rank sum tests found significance differences between shallow and deeper water sediments in sand content, mud content, mean grain size, water content, organic matter content and bulk density (Table 24).

Table 24. Results of Kruskal-Wallis rank sum tests between shallow and deeper water sediments for sand content, mud content, mean grain size, water content, organic matter content and bulk density.

VARIABLE TESTED	STATISTIC			
	KRUSKAL-WALLIS CHI-SQUARED	*P*-VALUE	SHALLOW WATER SEDIMENTS MEDIAN (MAX, MIN)	DEEP WATER SEDIMENTS MEDIAN (MAX, MIN)
Sand content (%)	6.56	0.01	42.2 (92.1, 31)	16.9 (35.1, 0.1)
Mud content (%)	6.56	0.01	57.8 (69, 7.9)	83.1 (99.9, 64.9)
Mean grain size (µm)	6.56	0.01	41.22 (194, 32.1)	20.47 (37.1, 8.3)
Water content (%)	5.03	0.02	33.93 (64.8, 25.1)	75.52 (80.5, 45.2)
Organic matter content (%)	5.03	0.02	4.29 (13.9, 3.2)	21.74 (23.1, 6.8)
Bulk density (g cm^3)	5.03	0.02	1.64 (1.8, 1.2)	1.13 (1.46, 1.1)

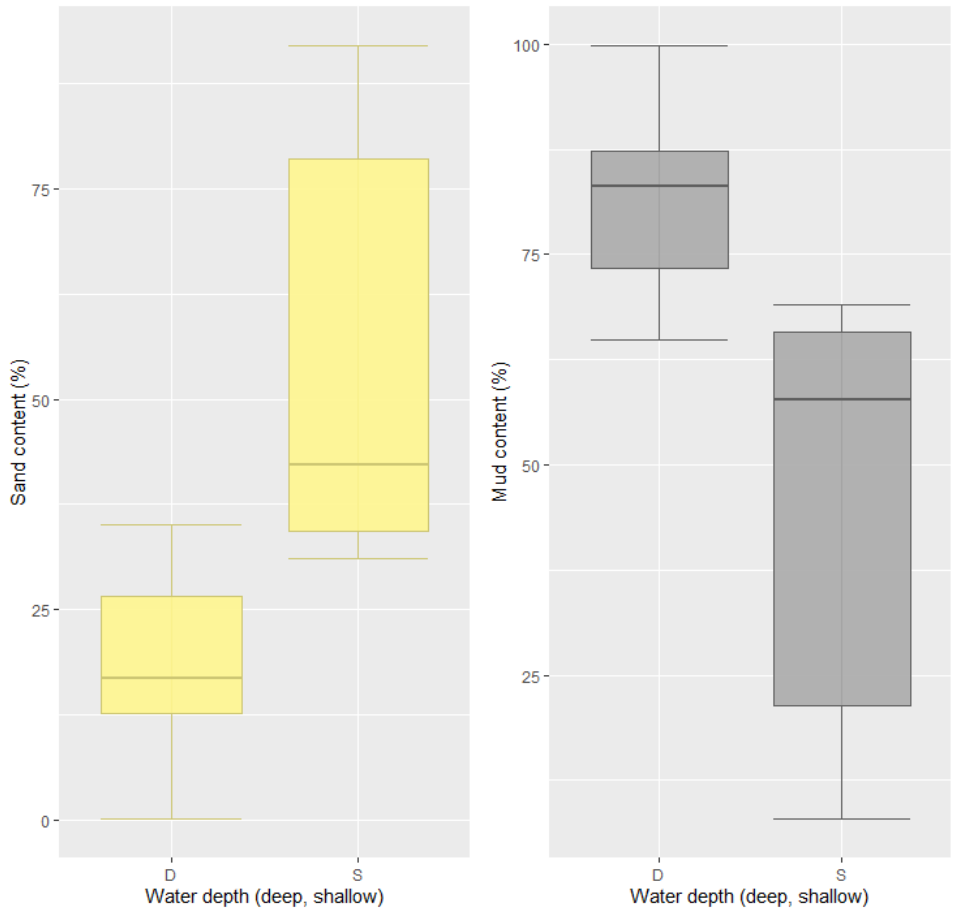

Figure 62. Characterisation of the two main sediment types at Villa dei Yumpa from March to June 2021 based on sand and mud content from sediments in shallow (S; ≤0.6 m) and deep (D; > 0.6 m) water depths. Error bars show the range of all measurements, the top and bottom of the box show the 75th and 25th percentiles, respectively. The centre line within each box indicates the median.

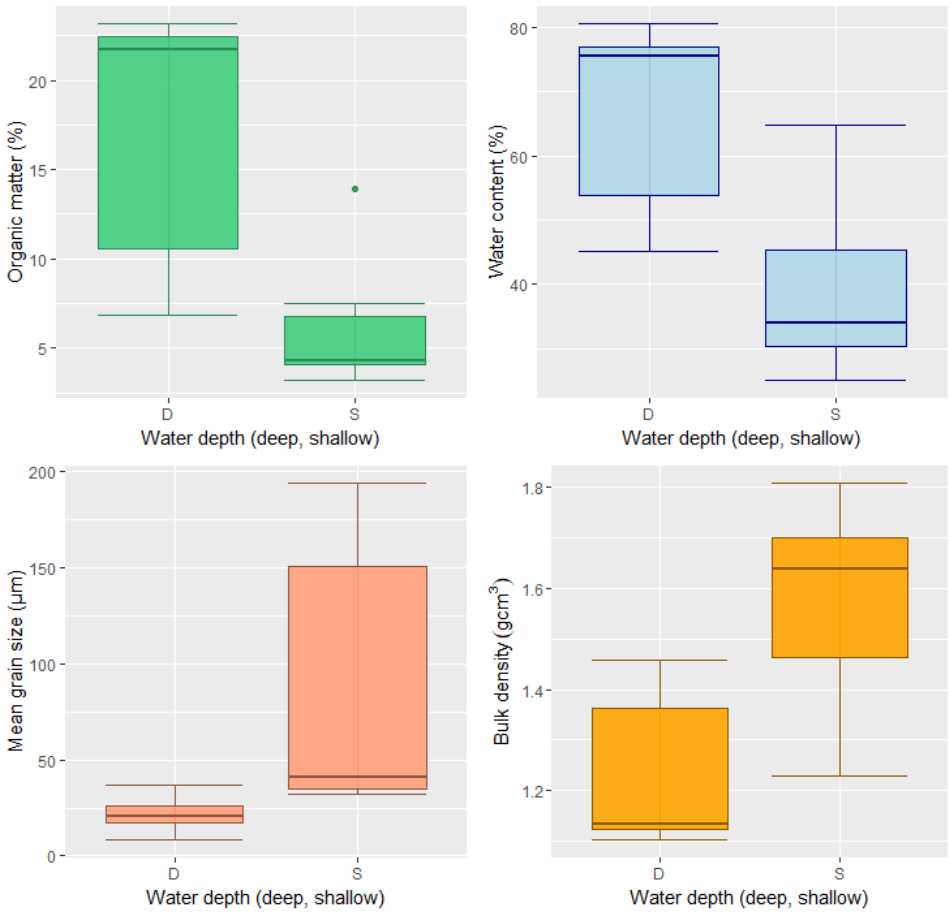

Figure 63. Differences in physical properties (organic matter, water content, mean grain size and bulk density) of sediments at Villa dei Yumpa from March to June 2021 in shallow (S; ≤0.6 m) and deep (D; > 0.6 m) water depths. Error bars show the range of all measurements, the top and bottom of the box show the 75th and 25th percentiles, respectively. The centre line within each box indicates the median. Additional data points outside of the error bars indicate outliers.

3.5.2 Wind parameters and water quality

Intensive single-point sampling (1–3 March 2021)

Total nitrogen (TN) concentrations were consistently greater than total phosphorus (TP) with a mean ratio of 32:1 (TN:TP). This ratio fluctuated throughout the course of the study (1–3 March 2021) with the highest ratio of 60:1 at 6am on 2 March and the lowest ratio of 13:1 at 10:15 pm on 1 March. Dissolved nutrient concentrations were unchanged from the beginning of the period, remaining consistently lower than minimum detection levels (< 0.005 mg/L for ammonium, < 0.003 mg/L for nitrate + nitrite and filterable reactive phosphorus). The wind was predominantly from the south and south-east (Figure 64). Mean wind speed was greater from the south (9.37 ± 0.09 m/s) and south-west (8.08 ± 0.13 m/s) than the east (1.53 ± 0.14 m/s) and south-east (3.42 ± 0.10 m/s).

Table 25. Summary statistics of the measured water quality variables during sampling at Villa dei Yumpa from 1–3 March 2021. Shown is the mean ± standard error (SE), maximum value, minimum value and number of samples (n).

VARIABLES	STATISTIC				
	UNITS	MEAN ± SE	MAX	MIN	N
Total nitrogen	mg/L	3.74 ± 0.05	4.17	3.17	19
Total phosphorus	mg/L	0.12 ± 0.01	0.24	0.06	19
Ammonium	mg/L	< 0.005 ± 0.00	< 0.005	< 0.005	19
Nitrate + nitrite	mg/L	< 0.003 ± 0.00	< 0.003	< 0.003	19
Filterable reactive phosphorus	mg/L	< 0.003 ± 0.00	< 0.003	< 0.003	19
Turbidity	NFU	17.39 ± 1.10	29.55	11.52	20
Wind speed	m/s	6.28 ± 0.15	12.23	0.92	517

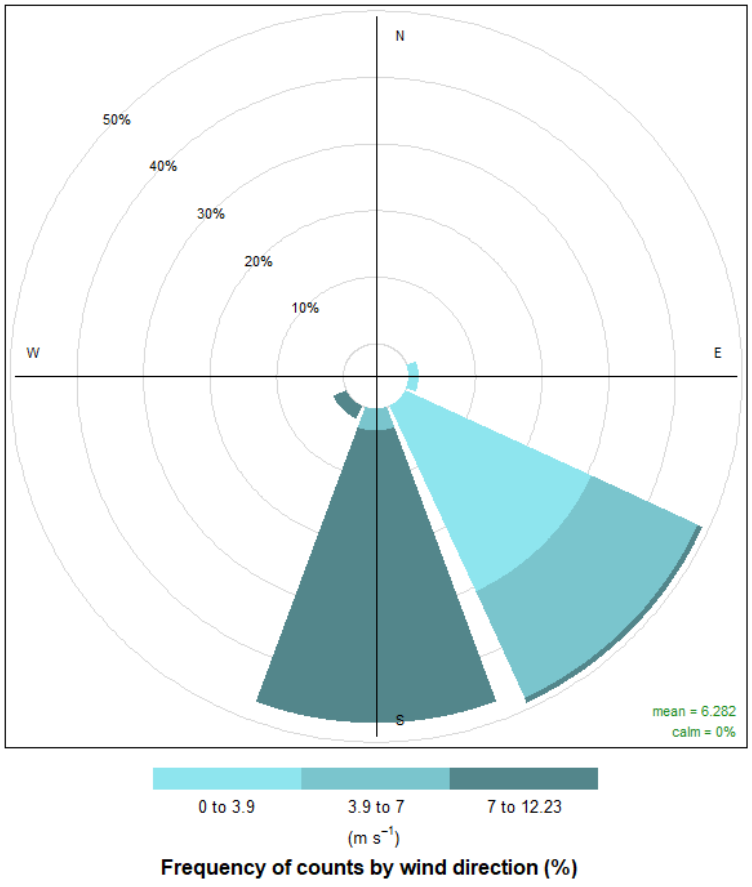

Figure 64. Frequency counts of wind speed from each wind speed category (light, 0-3.9 m/s; moderate, 3.9-7 m/s; strong, ≥ 7m/s) by wind direction (north, N: east, E; south, S; west, W) at Villa dei Yumpa during the sampling period from 1–3 March 2021.

Total nutrient concentrations (TN and TP) tended to fluctuate throughout the course of the study with TN moderately negatively correlated to wind speed (rho = -0.49, $p < 0.05$). Turbidity tended to increase throughout the study period, with the minimum and maximum values measured as the first and last records respectively. This is supported by the results of correlation analyses which revealed a significant and strong positive correlation between time and turbidity (rho = 0.84, $p < 0.0001$). No other significant correlations were found.

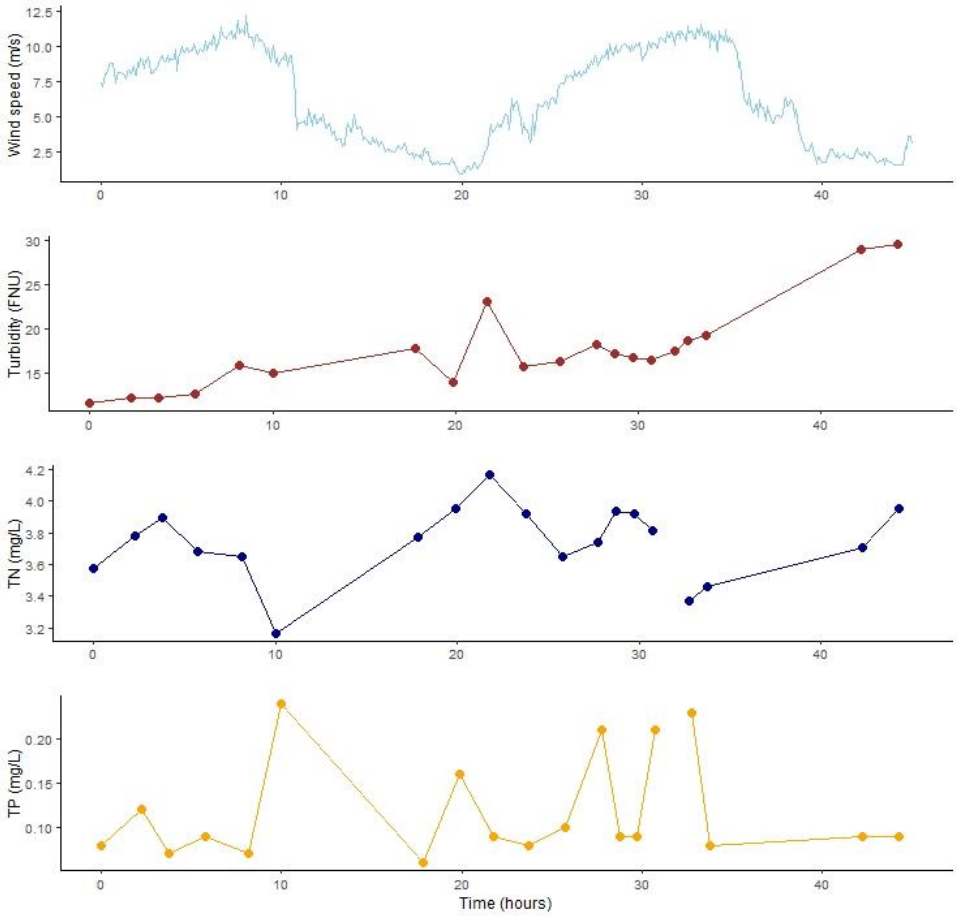

Figure 65. Time-series graphs of wind speed, turbidity, total nitrogen (TN) and total phosphorus (TP) during the sampling period at Villa dei Yumpa 1–3 March 2021.

Multi-point sampling (21–24 June 2021)

Surface water mean and maximum TN and TP were greater during 21–24 June 2021 than March 2021 (Table 26). In June 2021, TN concentrations were consistently greater than TP, with a mean ratio of 25:1 (TN:TP); lower than the March 2021 sampling. Maximum (46:1) and minimum (8:1) TN:TP were also lower than the March 2021 sampling. Of the 20 water samples taken in June 2021, 11 dissolved nitrogen (nitrate + nitrite) and 9 dissolved phosphorus (filterable reactive phosphorus) readings were above detectable levels (≥ 0.003 mg/L). However, as for the March 2021 sampling, ammonium was not recorded above the detectable level (< 0.005 mg/L). Mean and minimum turbidity were lower in June 2021 than in March 2021, albeit with a much greater maximum value recorded during the manual resuspension event at T3S1. Mean and maximum wind speeds were also lower in June 2021 compared to March 2021. The wind direction was predominantly from the north (Figure 66), with winds also recorded from the north-west and west. Mean wind speed was greatest from the west (8.75 ± 0.0001 m/s), followed by winds from the north (2.82 ± 0.14 m/s) and north-west (1.94 ± 0.06 m/s).

Table 26. Summary statistics of the measured water quality variables during sampling at Villa dei Yumpa from 21–24 June 2021. Shown is mean ± standard error (SE), maximum value, minimum value and number of samples (n).

VARIABLES	STATISTIC				
	UNITS	MEAN ± SE	MAX	MIN	N
Total nitrogen	mg/L	4.85 ± 0.72	16.52	2.77	20
Total phosphorus	mg/L	0.29 ± 0.10	2.02	0.08	20
Ammonium	mg/L	< 0.005 ± 0.00	< 0.005	< 0.005	20
Nitrate + Nitrite	mg/L	0.005 ± 0.001	0.016	0.003	11
Filterable reactive phosphorus	mg/L	0.004 ± 0.0004	0.006	0.003	9
Turbidity	NFU	12.63 ± 3.21	166.00	4.22	66
Wind speed	m/s	2.93 ± 0.19	8.75	1.57	66

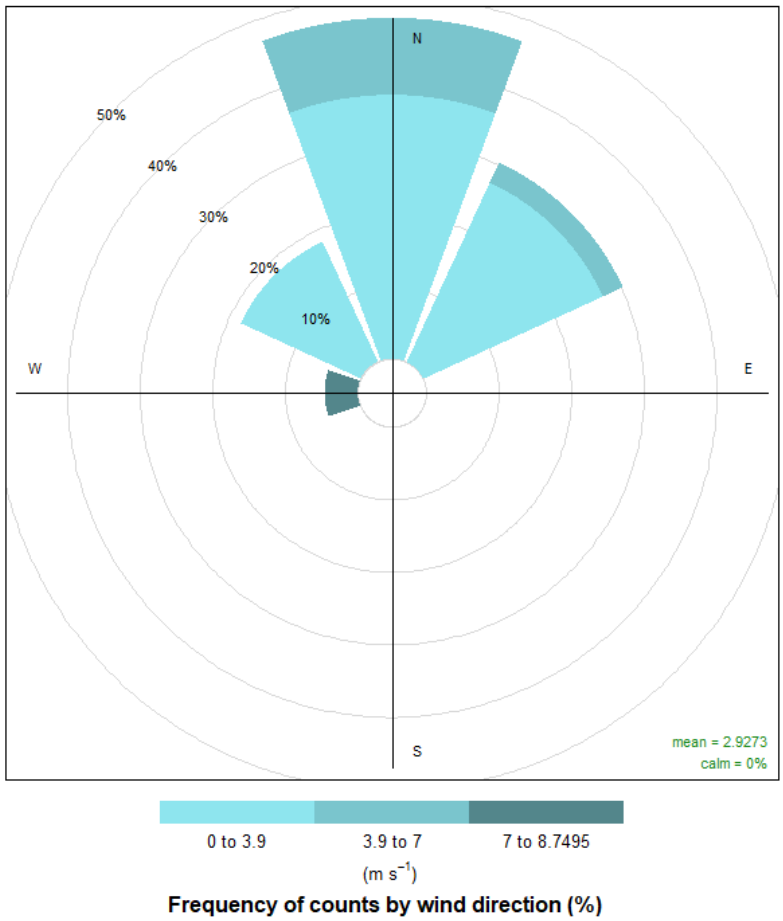

Figure 66. Frequency counts of wind speed from each wind speed category (light, 0-3.9 m/s; moderate, 3.9-7 m/s; strong, ≥ 7m/s) by wind direction (north, N: east, E; south, S; west, W) at Villa dei Yumpa during the sampling period from 21–24 June 2021.

Both TN and TP were significantly positively correlated with turbidity (TN rho = 0.52, $p < 0.05$; TP rho = 0.44, $p < 0.05$; Figure 67). TN and TP were significantly positively correlated with each other (rho = 0.71, $p < 0.001$; Figure 77). Nitrate + nitrite was marginally correlated with FRP (rho = 0.75, $p = 0.05$). No other significant correlations were found.

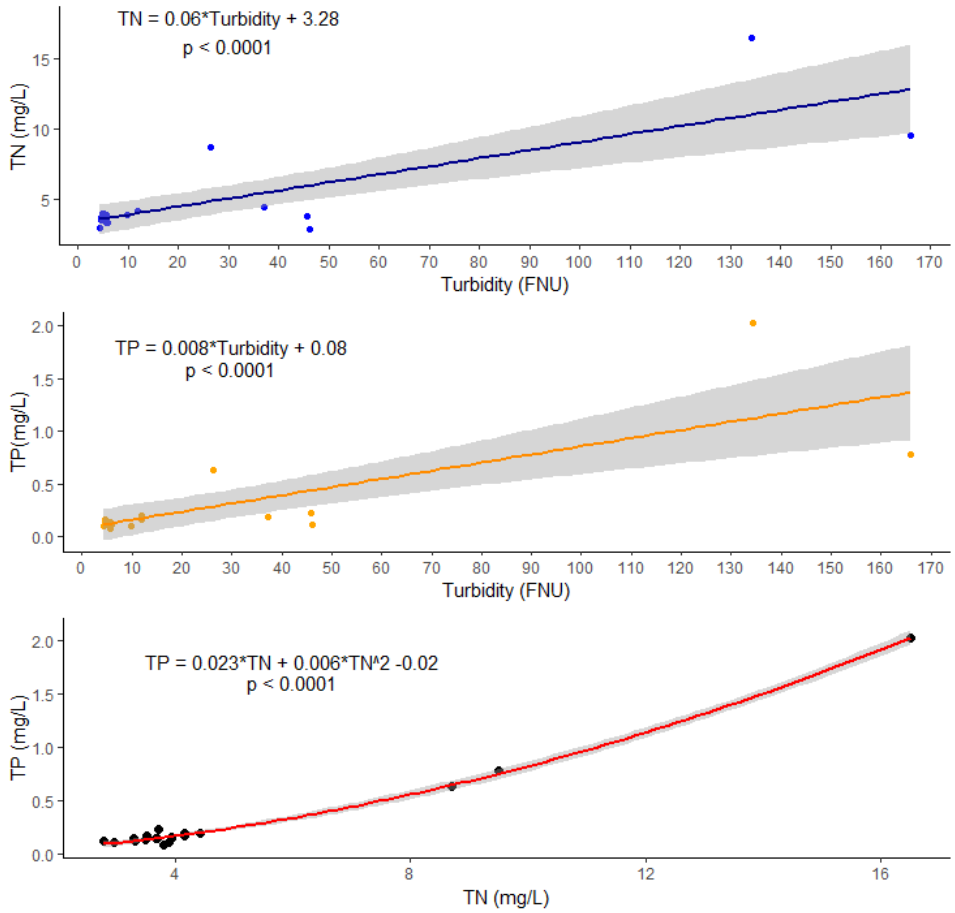

Figure 67. Scatterplots demonstrating the linear relationships between turbidity and total nitrogen (TN); turbidity and total phosphorus (TP); and TN and TP during 21-24 June 2021 sampling at Villa dei Yumpa. Equations of the fitted lines with *P*-values are labelled. Grey shaded areas denote 95% confidence intervals of the fitted line on all scatterplots.

Combined data from 1–3 March and 21–24 June 2021

Wind speeds were grouped into three categories: light (≤ 3.9 m/s), moderate (> 3.9 m/s, < 7 m/s) and strong (≥ 7 m/s). Turbidity significantly differed between categories (chi-squared = 30.54, p < 0.0001; Figure 68) with the greatest turbidity during strong winds (median = 16.70 FNU), followed by moderate (median = 6.85 FNU) and light (median = 5.08 FNU) winds. Post hoc testing revealed significant differences in turbidity between strong winds and light winds and between strong winds and moderate winds. Turbidity was significantly positively correlated with wind speed (rho= 0.43, p < 0.0001) and TN (rho = 0.35, p < 0.05; Figure 69). No other significant correlations were found.

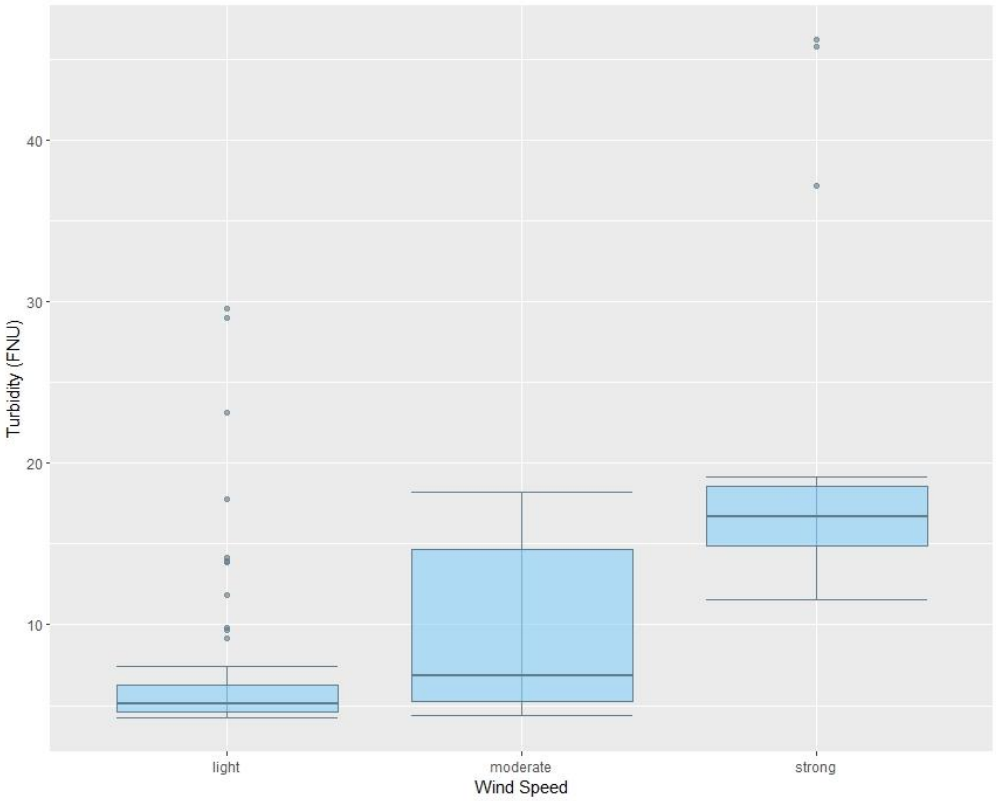

Figure 68. Differences in turbidity between three categories of wind speed during 21–24 June 2021 sampling at Vila dei Yumpa. Wind speeds categorised as light (≤ 3.9 m/s), moderate (> 3.9 m/s, < 7 m/s) and strong (≥ 7 m/s). Error bars show the range of all measurements. The top and bottom of the box show the 75th and 25th percentiles.

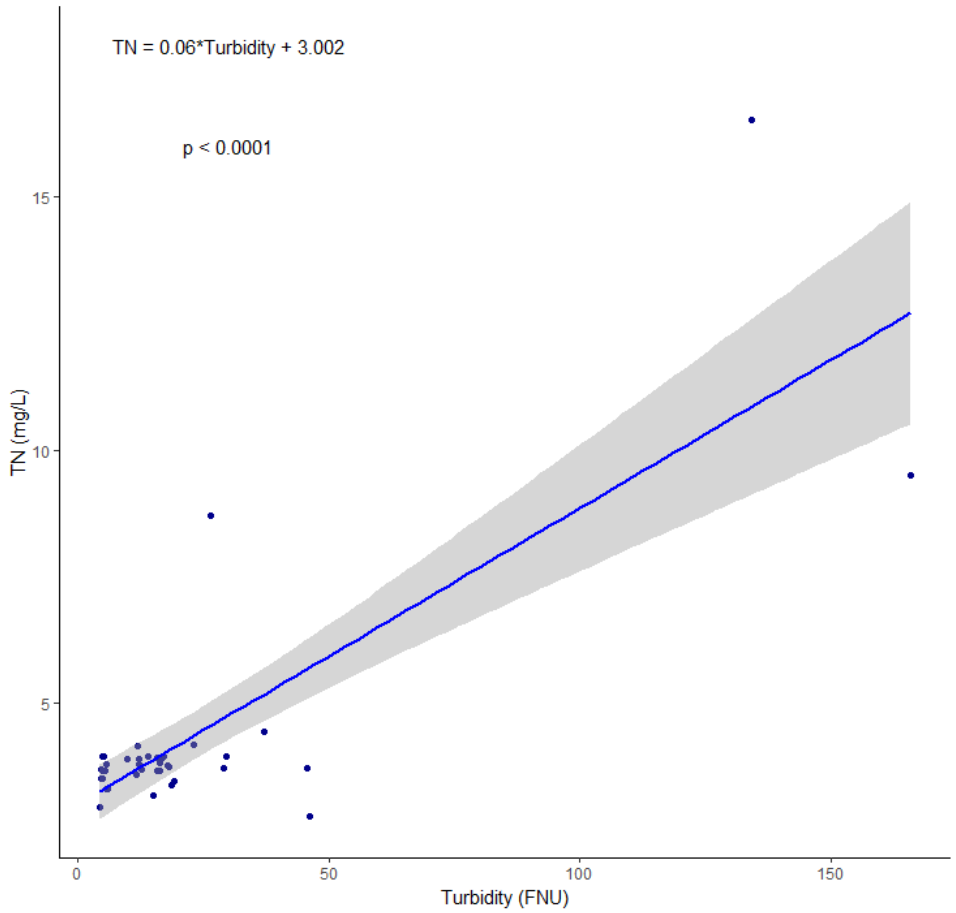

Figure 69. The relationship between turbidity and total nitrogen (TN) from 1–3 March and 21–24 June 2021 datasets at Villa dei Yumpa. A linear model smoothing line was fitted to the data with the equation and the *P*-value of the fitted line labelled. The grey shaded area denotes the 95% confidence intervals of the fitted line.

Continuous turbidity data

The continuous monitoring station at Woods Well (A4261209) showed several large spikes in turbidity over the sampling period (Figure 70), including several spikes in November 2020 that exceeded values corresponding to increased total nutrient concentrations observed during June 2021 sampling (Figures 67 and 69). A snapshot view of the turbidity and wind data from a nearby site (Parnka Point, A4260633) between October 2019 and February 2021 (Figure 70) shows that wind speeds > 7 m/s create resuspension events in the main lagoon water (muddy sediments with depth typically > 0.6 m) at Woods Well. This corresponds with observed significantly higher turbidity values when grouped into three wind speed categories (Figure 68). Correlation analyses showed the strongest positive correlation between turbidity and wind speed was when the wind speed reached 11 m/s or greater (rho = 0.51, $p < 0.05$).

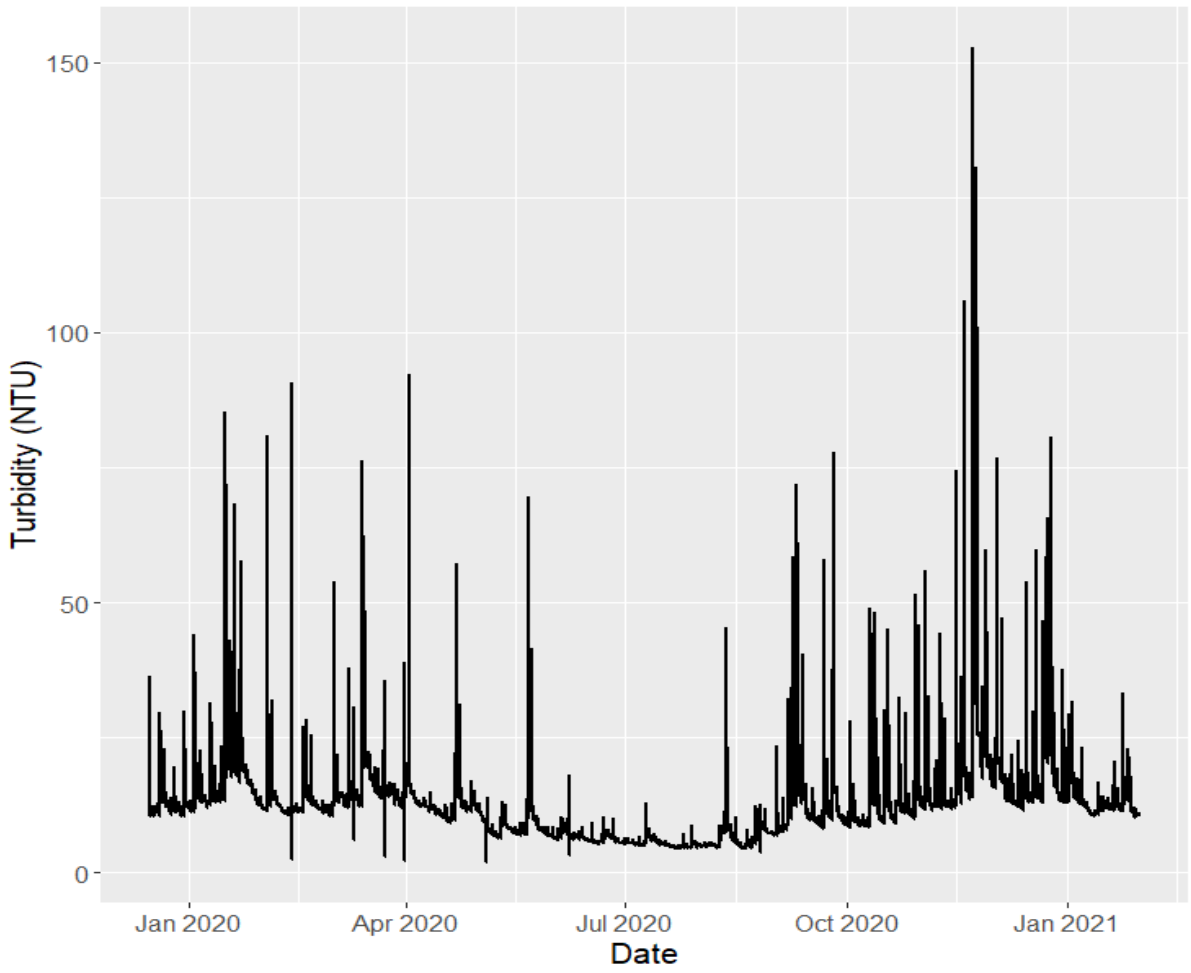

Figure 70. Continuous water column turbidity recorded at 5-minute intervals from 16 December 2019 to March 31 2021 in the Coorong South Lagoon near Woods Well (A4261209). (Source: DEW website, www.water.data.sa.gov.au)

4 Discussion

4.1 Nutrient cycling and fluxes

4.1.1 Deep permanent dark site sediments

The sediment quality and DGT/DET results confirmed that the sediments from deeper basin sites in the South Lagoon are in poor health. The sediments consisted of anoxic, black (due to presence of FeS) organic matter and nutrient enriched muds/oozes, with very high porewater ammonium, phosphate and sulfide concentrations and low dissolved ferrous iron. Sediment porewater ammonium concentrations ranged between 2800 (39,200 µg N/L) and 1400 µmol/L (19,600 µg N/L) in the sediments from the South of Salt Creek and Near Swan Island sites, respectively. Dissolved ammonium includes both dissolved ionised ammonium (NH_4^+) and un-ionised ammonia (NH_3). Dissolved ammonium can convert to un-ionised ammonia and vice versa, depending on the water pH, temperature and salinity, with ammonium being the dominant species at typical pH, temperature and salinity levels. Unionised ammonia is toxic at low concentrations, with concentrations of around 1.0 µmol/L known to be toxic to marine larvae, especially those of molluscs. In a review of acute and chronic toxicity effect data for marine waters and sediment pore waters, Simpson et al. (2013) proposed a new Australian threshold value for total ammonia-N in sediments of 4000 µg/L (approximately equal to 286 µmol/L). This was derived for slightly to moderately disturbed systems (95%

protection concentration, PC95) using species sensitivity distributions. At the South of Salt Creek and Near Swan Island sites, porewater dissolved ammonium concentrations were approximately ten and five times (respectively) higher than the guideline value. Additionally, based on the pH, temperature and salinity levels, the sediment porewater un-ionised ammonia concentrations were calculated to be approximately 1000 µg/L and 500 µg/L NH_3-N in sediments from the South of Salt Creek and Near Swan Island sites, respectively. These data are about ten times and five times higher than the Australian water quality guideline of 100 µg/L NH_3-N in marine water. Moreover, both deeper basin sites showed high levels of phosphate and sulphide in sediment porewater. At the South of Salt Creek and Near Swan Island sites, the maximum phosphate concentrations were 267 and 112 µmol/L in the sediment, respectively. The maximum sulfide concentrations in sediment were 87 and 93 µmol/L at the South of Salt Creek and Near Swan Island sites, respectively. Sulfide can be toxic to marine benthic invertebrates at low concentrations of 0.011 mg/L (approximately equal to 0.03 µmol/L) (Knezovich et al. 1996). The high salinity, high porewater ammonium and sulfide concentrations from the deep sites indicate that these sediments are an extremely harsh environment for fauna, explaining why no fauna have been found in these sediments (Remaili et al. 2018, Lam-Gordillo et al. 2022).

The high ammonium concentrations and steep concentration profiles of ammonium drove high ammonium effluxes from the sediment to the water column of 1074 ± 167 µmol/m^2/h and 503 ± 363 µmol/m^2/h at the South of Salt Creek and Near Swan Island sites, respectively. However, low nitrate and phosphate fluxes were found from the sediment to the water column. The low nitrate flux is likely to be because nitrification is inhibited in highly anoxic sediments despite high ammonium availability (Nizzoli et al. 2006). The low phosphate flux can be due to sediment resuspension, which oxides the dissolved ferrous irons in the sediment to iron oxide. The iron oxide can bind phosphate strongly, leading to low phosphate in the water column. Overall, the South Lagoon water column has been found to be phosphorus-limited (Mosley et al. 2020), which could be due to nitrogen oversupply, both of which are consistent with the results in this study.

4.1.2 Shallow water sediments

Sediments collected from different shallow photosynthetically active sites and in different seasons had variable in dissolved inorganic nutrients, dissolved ferrous iron and sulfide concentrations and profiles in the sediment porewater across depth and under light and dark conditions. There was high sediment pore water concentrations of ammonium and phosphate at sites in the South Lagoon. The ammonium concentration in the sediment at Policeman's Point in November 2020 was > 500 µmol/L (7,000 µg N/L). For sediment collected from Parnka Point and Policeman's Point in February 2021, the highest ammonium concentrations were about 220 (3,080 µg N/L) and 310 µmol/L (4340 µg N/L), respectively. The ammonium concentrations from the Policeman's Point were higher than the new Australian threshold value for total ammonia-N in sediments of 4000 µg/L. According to the pH, temperature and salinity levels at different sites, the sediment porewater un-ionised ammonia concentration was 225 µg N/L at Policeman's Point in November 2020. For the sediments collected from Parnka Point and Policeman's Point in February 2021, the un-ionised ammonia concentrations in sediment porewater were 100 and 71 µg N/L respectively. The un-ionised ammonia concentrations from the sampling sites were higher than the Australian water quality guideline of 100 µg/L NH_3-N in marine water, except for Policeman's Point in February 2021. The phosphate concentrations in the sediment porewater were less than 20 µmol/L from all the shallow sites. In contrast to ammonium, oxidised nitrogen (nitrate and nitrite) was barely detectable. This is likely symptomatic of the highly anoxic and sulfide-rich sediment in the South Lagoon, inhibiting healthy nutrient cycling (i.e. no nitrification to create nitrate). Internationally, coupled nitrification-denitrification has been found to be inhibited by sediment anoxia, with the relative importance of dissimilatory nitrate reduction to ammonium (DNRA) increasing (Kemp 1990, Hardison et al. 2015, Nizzoli et al. 2006).

In contrast to high dissolved nutrients in the sediment porewater, dissolved nutrients in the water column are typically low (often below detection limit) and mostly in organic form (Mosley et al. 2020). Furthermore the vast majority (>98%) of the total dissolved N and P is in the form of DON and DOP respectively (Priestley et al. 2022a), including at the Ruppia experiment site presented here. This is consistent with processes involving rapid uptake of nutrients released from the sediment by algae in the water column (Mosley et al. 2020, Priestley et al. 2022a,b). Recent data also suggests on average 40% of the total alkalinity is present as

organic alkalinity, with the remainder as dissolved inorganic carbon (DIC). However, calculations suggest the South Lagoon is calculated to be oversaturated with respect to calcium carbonate minerals, consistent with the findings of Shao et al. (2018, 2021).

The changes of dissolved ferrous iron and sulfide profiles at different depth in sediment porewater and under light and dark conditions can be caused by several processes. One is due to oxygen production by microphytobenthos promoting iron and sulfide oxidation in surficial sediments in the light, whereas dissolved ferrous iron and sulfide accumulate in the dark when there is no photosynthetic oxygen production. The second is *Ruppia* photosynthesis, with roots releasing more oxygen into the sediment under light conditions, which oxidises iron and sulfide. The third relates to benthic macrofauna and their activities which is less relevant to the South Lagoon under current conditions with no burrowing macro-invertebrates present (Lam-Gordillo et al. 2022a).

High sulfide concentrations were observed at all shallow sites under light and dark conditions except Noonameena in the North Lagoon under light incubation. The site at Noonameena showed lower porewater concentrations of ammonium, phosphate, dissolved iron and sulfide. This is likely due, at least in part, to reduced OM content of the sediment. However, it may also be related to the lower salinity in the Northern Lagoon, which allows colonisation of the sediments by bioturbating macroinvertebrates. Benthic macrofauna actively disperse, mix and modify the sediment via bioturbation and in doing so promote oxygen and nutrient exchange between the sediment and water column by bioventilation and bioirrigation processes, promoting solute movements and microbial activities which are ultimately responsible for organic matter mineralisation and nutrient cycling (Welsh 2003, Lohrer et al. 2004, Kristensen et al. 2012, Stief 2013, Remaili et al. 2018, Wyness et al. 2021). Benthic macrofauna and their activities increase sediment oxygenation and the overall volume of oxic sediments, resulting in the oxidation of dissolved ferrous iron and sulfide. The iron oxide can bind phosphate strongly, leading to lower phosphate concentrations. Redox fluctuations due to the benthic macrofauna and their activities can enhance nutrient cycling by providing the conditions and substrates for specific functional groups of bacteria responsible for nitrification and denitrification processes (Welsh 2003, Mermillod-Blondin and Rosenber 2006, Stief 2013, Bosch et al. 2015). Additionally, the animals themselves can be colonised by nitrifying and denitrifying bacteria and these populations can also significantly contribute to overall sediment rates of nitrification and denitrification (Welsh and Castadelli 2004, Heisterkamp et al. 2013, Welsh et al. 2015).

4.1.3 *Ruppia tuberosa* colonised sediments

Ex-situ core incubation

The sediments colonised by *Ruppia tuberosa* were a strong sink for water column oxygen during dark incubations which is typical of seagrass meadows (Ferguson et al. 2017; Welsh et al. 2000) where sediments are typically rich in OM. This occurs as the presence of the seagrass slows water currents, leading to increased entrapment and sedimentation of suspended particulate OM (Ferguson et al. 2017; Gacia et al. 2002), which in turn fuels higher rates of community respiration (Barrón et al. 2004). In contrast during light incubations, photosynthetic oxygen production exceeded community respiration rates and overall, there was a small net oxygen production. However, due to the much higher rates of oxygen consumption in the dark compared to oxygen production in the light, the seagrass meadow would have still been a substantial sink for water column oxygen over a daily diel light cycle. For example, for 12/12 hour light/dark cycle, the net effect equates to an oxygen consumption of 40.5 mmol $O_2/m^2/d$.

Changes in the physiology of the seagrass between light and dark conditions also influenced nutrient fluxes, sediment redox conditions, and porewater nutrient profiles. Seagrasses transport oxygen from their leaves to their roots and rhizomes via a system of air-filled lacunae, and part of this oxygen diffuses from the roots into the surrounding sediment (Frederiksen and Glud 2006; Pagès et al. 2012). This transport of oxygen is largely by diffusion and therefore the radial loss of oxygen from the roots occurs at much higher rates during the day when the plants are producing oxygen via photosynthesis (Connell et al. 1999; Frederiksen and Glud 2006; Jensen et al. 2005; Pedersen et al. 1998). Consequently, the thickness of the aerobic zone of sediment around individual roots is greater and the DO concentrations in the pore water are higher under light

compared to dark conditions (Elgetti Brodersen et al. 2016; Frederiksen and Glud, 2006a; Pedersen et al. 1998). Therefore, the generally lower porewater iron(II) and sulfide concentrations observed in the *R. tuberosa* rhizosphere during the light compared to dark conditions can be explained by higher rates of radial oxygen loss from roots and the light enhancing rates of chemical and microbiological oxidation of porewater sulfides and iron(II) relative to dark conditions (Pagès et al. 2012).

The observed light/dark shifts in ferrous iron(II) and sulfide can in turn explain the observed changes in porewater phosphate concentrations and sediment-water column fluxes. The oxidation of iron(II) to iron(III) associated with higher oxygen availability in the light would result in the precipitation of iron(III) oxyhydroxides, which are able to adsorb phosphate, reducing its porewater concentration and hence diffusion to the overlying water (Azzoni et al. 2001). Conversely, in the dark, rates of radial oxygen loss from the seagrass roots are lowered and the more anoxic conditions in the rhizosphere favour anaerobic metabolisms such bacterial iron and sulfate reduction (Kankanamge et al. 2020), which result in the reductive dissolution of iron(III) oxyhydroxide precipitates and the release of the absorbed phosphates to the sediment porewater (Azzoni et al. 2001; Pagès et al. 2012). Therefore, our results are consistent with diel shifts in radial oxygen loss playing a significant role in regulating phosphate concentrations in the sediment and sediment phosphate fluxes to the water column through its impact on the formation/dissolution of iron(III) oxyhydroxide precipitates, which act as a phosphate binding phase in the sediment.

Porewater ammonium concentrations were also higher in the *R. tuberosa* rhizosphere in light compared to dark incubations and although not significant there was an increase in ammonium efflux from the sediment in the light. Additionally, during the light incubations there was a large efflux of nitrate to the water that did not occur in the dark and in total the efflux of dissolved inorganic nitrogen (ammonium + nitrate) in the light incubations was approximately double that in the dark incubations. This increased production of inorganic nitrogen may reflect the higher rates of microbial activity that occur in the light compared to the dark (Blaabjerg et al. 1998; Moriarty et al. 1986), resulting in increased remineralisation of sediment organic nitrogen pools in the light and/or more complete mineralisation of the organic nitrogen with increased oxygen availability.

The occurrence of a nitrate efflux from the sediment in the light, however, demonstrates that nitrification was occurring where *R. tuberosa* was present, and that in these ammonium saturated sediments nitrification rates were regulated by oxygen and hence seagrass photosynthesis, as has been observed in other eutrophic sediments colonised by benthic microalgae (Dunn et al. 2012). The observation of active nitrification in this *R. tuberosa* meadow raises the possibility that these seagrass meadows may be “hot spots” for nitrogen loss in the lagoons via coupled nitrification-denitrification and/or anammox (anaerobic oxidation of ammonia by nitrite), and that efforts to remediate seagrass meadows in the South Lagoon could improve its eutrophication status. However, further studies are required to quantify rates of nitrogen loss in these seagrass beds, as any nitrate produced by nitrification could also be reduced back to ammonium via DNRA, especially as DNRA is known to be favoured over denitrification in eutrophic systems (Dunn et al. 2013; Erler et al. 2017).

In situ benthic chamber

The *in situ* profiles from the DET probes largely confirmed what has been found for the *ex situ* core incubations. For instance, the sediments colonised by *Ruppia tuberosa* had more oxidising conditions in the light when plants conducted photosynthesis and roots released more oxygen into the sediment. The *in situ* profiles provided more detail compared to the *ex situ* core incubations and showed these changes in the sediments were relatively slow and cyclical. For example, sediment slowly oxidised during the day and dissolved ferrous iron peaks moved deeper in the sediment profile. During the night, sediment slowly reduced and dissolved ferrous iron peaks shifted towards the sediment surface. The dissolved ferrous irons moved slightly further down the sediment profile when the sun rose on the second day. Despite these shifts, nutrient concentrations in sediment on the second morning were similar to those measured on the first morning.

The diurnal changes seen *in situ* in the sandy sediments that were generally more oxidised and had low OM contents were smaller than those in muddy, organic matter rich sediments or in the rhizosphere of *Z. capricornia* growing on muddy OM rich sediments (Pagès et al. 2012).

4.2 Microbial ecology

Hypersalinity putatively impairs the biogeochemical cycling processes required for a healthy estuary – particularly, denitrification. As an important mechanism by which eutrophication-driving forms of nitrogen are removed from aquatic systems, denitrification has attracted considerable research interest from a purely biogeochemical "process-focused" perspective. However, understanding the complex relationships between process-intermediary microbial communities, the factors which shape them, and the ensuing effect on biogeochemical processes is also critical for conservation efforts. This study analysed the diversity and composition of the Coorong's benthic prokaryotic communities using microbial DNA analysis, then inferred their functional roles, along with the presence and relative activity of a denitrification gene, *nirK*. Identification of key players in denitrification pathways and understanding how they respond to the prevailing salinity will aid the Coorong lagoons's recovery.

Salinity was identified as the most significant explanatory factor in overall community structure difference between sites, closely followed by DO. In South Lagoon sediments, there was a much higher level of *nirK* transcript:cell ratio than was observed at any other site. It is likely that this is due to the presence of halophilic "specialist" taxa with increased denitrification efficiency, or better adaptations to their niche. One such candidate taxon is the archaeal family, *Halobacteriaceae*.

Metagenome inference suggested a large shift in community functional roles along the salinity gradient. Benthic habitats of lower salinity close to the barrages, showed a functional "fingerprint" dominated by diverse metabolic pathways, indicating metabolic plasticity (ability to adapt to changes in nutrients) of the community, which likely responds to large nutrient inflows from the barrages. This inferred metagenomic plasticity is consistent with previously published metagenome data in the North Lagoon (Newton et al. 2018). As displayed in Figure 54, taxa in hypersaline sediments harboured pathways important for cell growth and protein biosynthesis, as well as transporters, which are vital in regulating intracellular solutes (osmoregulation) within salinity-resistant cells.

The present study has made the first steps into understanding sedimentary prokaryotic communities, their structure, potential functional roles and key taxa in a highly complex and degraded hypersaline environment. It has revealed the strong, negative impact of salinity and salinity-associated issues, such as anoxia, on the denitrifying community. Also discovered was a potentially beneficial ecological role of 'extremophile' taxa in regulating the nutrients in extreme habitats. This provides preliminary evidence for a path to recovery of the Coorong, through improved understanding of eutrophic regulation processes in the system.

Understanding where denitrification occurs and the rate that nitrogen can be lost as dinitrogen gas is important for determining how the Coorong processes nitrogen as part of the total nutrient budget. Determining a sustainable nutrient load to estuaries is challenging. On the one hand, nutrients are critical for supporting productivity, but on the other hand, it is desirable to avoid excessive productivity of problematic algal species. This work provides the first insight into the denitrifying community in the Coorong lagoons and further data analysis and comparison to other studies is in progress.

4.3 Influence of macroinvertebrates

The Experiment 1 results confirmed a very low abundance and diversity of benthic macroinvertebrate communities in the South Lagoon, consistent with previous studies (Dittmann et al. 2015, Tweedley et al. 2019, Lam-Gordillo et al. 2022a). The loss of macroinvertebrates is due to the salinity tolerances (< 60-65 PSU) of key species being persistently exceeded (Remailli et al. 2018, Dittmann et al. 2015; Dittmann et al. 2018). Loss of these benthic macroinvertebrates and their ecosystem functioning is likely to have contributed to the increasing eutrophication by favouring nutrient recycling over nutrient elimination/sequestration processes. This was supported by there being much more nitrate in sediments of the North Lagoon where invertebrates were present. This is indicative of more oxygenated sediments, whereas ammonium is the more dominant species of nitrogen under anoxic conditions common in the South Lagoon. Burrowing and bioturbating invertebrates oxygenate the sediment by reworking the sediment and dispersing OM, promoting the oxidation of sulfide (i.e. less anoxic black ooze), formation of iron oxides (which sequester

phosphate), and stimulating rates of coupled nitrification-denitrification promoting nitrogen loss as gaseous end-products (Welsh 2000, Stief 2013). Therefore, macroinvertebrates act as ecosystem engineers, altering the sedimentary environment which affects bacterial populations and changes microbially-driven nutrient cycling.

The *in situ* experiment (Experiment 2) revealed that colonisation of macrobenthic fauna was enabled by the translocation of sediment from a hypersaline site (PP) to a lower salinity site (LP), likely promoted by the sandy sediments readily facilitating the exchange and dilution of porewater with surface water thus producing favourable salinity levels (< 60 PSU) where many macrobenthic organisms can survive (Dittmann et al. 2015, Remaili et al. 2018, Lam-Gordillo et al. 2022). This *in situ* experiment also showed that restoration of the bioturbation functions of benthic macrofauna, in particular the polychaete *S. aequisetis*, modified the sediment biogeochemistry, promoting a healthier state (i.e. lower sulfide, ammonium and organic carbon concentrations) within a few weeks following creation of suitable salinity conditions. It has been suggested that biodiffuser and bioirrigator organisms, in combination with several feeding modes, promote microbial activities which are ultimately responsible for nutrient cycling and organic matter mineralisation (Welsh 2003, Braeckman et al. 2014, Bon et al. 2021). For example, organisms such as *S. aequisetis* and amphipods that build and inhabit burrows, are proposed to influence OM degradation rates by increasing oxygen transfer to the sediment by irrigating their burrows with the overlying water (Kristensen 2000, Welsh 2003, Volkenborn et al. 2012).

The experiments carried out in the Coorong demonstrate that the preservation, and potentially re-introduction of macrobenthic fauna communities, and therefore their functions should improve sediment conditions by reducing concentrations of ammonium and sulfide and promoting oxic conditions in the sediment. Macrobenthic fauna activities could thus provide a nature-based option for management actions to improve estuarine lagoons with anoxic-eutrophic-hypersaline conditions. Reducing salinity in the South Lagoon of the Coorong sufficiently (< 60 PSU), in combination with other mitigation and restoration activities, could allow recolonisation of the sediment by macrobenthic fauna, which in turn would improve sediment conditions and ecosystem functioning. However, larger scale mesocosm experiments across multiple locations (including hypersaline locations) would be beneficial to illustrate the potential pros and cons of interventions to reduce the salinity in the South Lagoon, and the response of macrobenthic fauna.

4.4 Sediment resuspension effects on water column nutrients

Evidence was found for the occurrence of wind-induced resuspension in the Coorong South Lagoon at the Villa dei Yumpa sampling site and at the Woods Well monitoring station through correlation analyses. The greater mean and minimum turbidity values recorded during the March 2021 sampling period than those recorded during the June 2021 sampling period are likely the result of greater mean and maximum wind speeds during March. However, there was only a significant positive correlation between wind speed and turbidity when using both sampling period datasets, in addition to the longer-term wind speed and turbidity data. This demonstrates and highlights the usefulness and need for long-term monitoring of environmental variables in the Coorong to better understand the processes that affect water quality and ecology.

There is some evidence for a threshold for initiation of sediment resuspension when wind speeds reach 7 m/s. However, while this relationship was evident from the June 2021 data, it was not evident from the intense sampling in March 2021. This is likely related to sediment type. The June 2021 sampling, in addition to the Woods Well data, included sampling over deeper, predominantly muddy sediments with high OM content and water content, and lower mean grain size and bulk density than the shallower predominantly sandy sediments over which the March 2021 sampling took place. Sediments with higher proportions of water and OM tend to be more readily resuspended into the water column, whereas sediments with a greater mean grain size and bulk density tend to be less susceptible to erosion (Grabowski et al. 2011). Therefore, the wind speed required to initiate resuspension in the predominantly sandy sediments is likely to be greater. Furthermore, other factors, such as the presence and abundance of aquatic plants (e.g. *R. tuberosa*) may be affecting this relationship by modifying the sediment physical structure and the near-sediment hydrodynamics, making the sediment less erodible (Adams et al. 2016). The *R. tuberosa* community tends to occur in the shallower predominantly sandy sediments in the Coorong South Lagoon (Paton et al. 2015). The

R. tuberosa community was not detected at the T1S2 site on either of the two sampling trips but was found within 50 m of the site in June 2021 and may have contributed to the lack of resuspension at this location in March 2021.

The significant positive correlation between turbidity and TN in the June 2021 dataset was stronger than in the combined March and June 2021 data. A significant positive correlation between turbidity and TP was only found for the June 2021 dataset. These results can likely be attributed to two factors. Firstly, the large turbidity values that were generated (mean = 108.85 ± 42.28, n = 3) from the manual resuspension event during the June sampling generated the two highest values for TN and TP concentration which influenced the dataset. Secondly, the sediment type over which the water samples were taken had an influence. The nutrient samples taken during the June 2021 sampling were over the predominantly muddy sediments which are richer in OM and nutrients (see Figure 18) than the predominantly sandy sediments. In addition, wind speed negatively correlated with TN when sampled over sandy sediments in March 2021. This demonstrates some evidence for increased flux of total nutrients (TN and TP) from resuspension primarily over muddy sediments with elevated nutrient concentrations combined with a physical structure more susceptible to erosion.

However, it is important to note that the manual resuspension events created using a boat may differ in the way they create resuspension compared to resuspension which is wind-induced (Hofmann et al. 2011). With removal of the manual resuspension data, positive correlations between turbidity and total nutrients (TN and TP) were observed for the 21-24 June dataset but were not statistically significant ($p > 0.05$). A positive correlation was only observed between turbidity and TN using the entire dataset but was also not statistically significant ($p > 0.05$). Therefore, the relationships established in figures 67 and 69 between turbidity and total nutrient concentrations may not accurately reflect relationships between total nutrients and turbidity as a result of wind forcing.

Wind-induced waves generate orbital velocities through a water column that are attenuated with depth. In sufficiently shallow water, these orbital velocities interact with benthic sediments by inducing a shear stress which can cause the resuspension of benthic sediments when a critical shear stress is exceeded (Bailey and Hamilton 1997). The critical shear stress required to resuspended predominantly muddy sediments is typically lower than the critical shear stress of sandy sediments, due to differences in physical factors (e.g., bulk density, mean grain size, water content, organic matter content) which affect their susceptibility to erosion (Grabowski et al. 2011). This was evident at Villa dei Yumpa in the Coorong South Lagoon. Shear stresses were unable to be calculated during this study, but a good direction for future research would be to apply the SWAN wave model and force it with measured site wind data to calculate shear stresses and investigate the relationship between shear stress and water column nutrient concentrations.

In summary, evidence for predominantly particulate nutrient flux from wind-induced resuspension events was found to occur primarily over muddy nutrient-rich sediments which are more susceptible to erosion than sandy sediments. The onset of resuspension appears to occur when wind speeds reach and exceed 7 m/s, with greater erosion of sediments as wind speed increases. Frequency of velocities experienced by the Coorong have not been analysed, but have for nearby Lake Alexandrina (see Skinner 2011). The cumulative frequency distribution of wind speeds measured on north-east Lake Alexandrina between 27 October 2009 and 24 March 2010 demonstrated that wind speeds reached ≥ 7 m/s approximately 65% of the time (Skinner 2011). A similar frequency distribution of wind speeds for the Coorong is expected. The diffusive sediment nutrient fluxes outlined above appear to be the dominant driver of bioavailable/dissolved nutrient supply to the water column in the Coorong, not resuspension.

5 Summary

Multiple lines of evidence confirm that the overall Coorong sediment quality and nutrient cycling processes are in an 'unhealthy' state due to a combination of factors. Key findings of the investigation that support this conclusion were:

- High total nutrient and organic carbon concentrations in the sediment and water of the South Lagoon and southern region of the North Lagoon
- High ammonium levels in sediment pore water and flux to the water column of the South Lagoon which provides the “fuel” for algal growth
- Limited nitrate availability and a lack of coupled nitrification-denitrification reactions, which remove nitrogen from the system (in gaseous form)
- High levels of sulfide in deeper sediments of the South Lagoon, indicative of highly anoxic conditions
- High sediment oxygen demand of the South Lagoon
- An absence of macroinvertebrates in the South Lagoon, which can burrow and oxygenate sediment due to hypersaline conditions (salinity > 60 PSU)
- Rapid (few weeks) recolonisation by burrowing invertebrates and a large improvement in sediment quality following an experimental translocation of hostile (hypersaline and sulfide-rich) sediment from the South Lagoon to the North Lagoon
- Resuspension and an increase in organic turbidity during strong wind events in the South Lagoon, while dissolved nutrient release was low.

Coupled with the limited flushing, the current nutrient cycling processes are promoting nutrient retention and eutrophication of the South Lagoon. However, there is evidence of improved sediment quality and nutrient cycling where *R. tuberosa* is present in the South Lagoon and macroinvertebrates are present in the North Lagoon. If overall water and habitat quality can be improved (e.g. via improved flushing and lowered hypersalinity), these ecosystem components have potential to help restore healthy nutrient cycling processes in the Coorong.

List of shortened forms and glossary

Anammox	Anaerobic oxidation of ammonia by nitrite
AVS	Acid Volatile Sulfur
Bioturbation	The disturbance of sediment by living organisms
CIIP	Coorong Infrastructure Investigations Project
CR	Community respiration
Denitrification	The microbial process in which nitrates and nitrites are reduced or removed from soil, water, or air by their conversion into nitrogenous gases
DET	Diffusive equilibrium in thin films
DGT	Diffusive gradients in thin films
DNRA	Dissimilatory nitrate reduction to ammonium
DF	Degrees of freedom
DO	Dissolved oxygen
DOC	Dissolved organic carbon
Efflux	Diffusion of compound from the sediment
Eluent	Solution after extracting samples
Eutrophication	Elevated supply of organic matter and nutrients
Euryarchaeaota	A phylum of Archaea, the third domain of life aside from Eukaryotes (complex organisms including all animals and plants) and bacteria. Archaea are unicellular organisms which often inhabit extreme environmental niches. Niche examples include: high salt concentrations, very high or very low temperatures, low or no oxygen, and high pressures
FNU	Formazin Nephelometric Unit
GAM	Generalised Additive Models
GPP	Gross primary production
Halophilic	A property of 'halophiles' - ‘salt-loving’ organisms which obligately require salt to grow
Heterotrophic	Consumer
HCHB	Healthy Coorong, Healthy Basin
MBO	Monosulfidic Black Ooze
Metabolic plasticity	The ability to use a range of different nutrients and different methods of processing nutrients.
Metagenome	A collection of genomes for all organisms within a given sample. In this instance all prokaryotic (bacterial and archaeal) genomes in an environmental sediment sample.
MDL	Method detection limit
Microphytobenthic	Relate to microphytobenthos: benthic microalgae, are microscopic primary producers living in association with benthic substrates
MS	Mean sum of squares

nirK	Nitrite reductase gene
nMDS	Non-Metric Multidimensional Scaling
NPP	Net primary production
Nitrification	The process by which bacteria in soil and water oxidise ammonia and ammonium ions and form nitrites and nitrates
OM	Organic matter
Osmoadaptation	Adaptation of cells to external osmotic pressure by controlling intracellular solute concentrations
PERMANOVA	Permutational analysis of variance
Prokaryotic	Describing microscopic single-celled organisms which have neither a distinct nucleus with a membrane nor other specialized organelles, including the bacteria and cyanobacteria
Residence time	The length of time a particular parcel of water remains in the Coorong (i.e. is not flushed out)
SS	Sum of squares
SWI	Sediment-water interface
T&I	Trials and Investigations
TN	Total nitrogen
TOC	Total organic carbon
TP	Total phosphorus
TSS	Total suspended solids

References

Adams MP, Hovey RK, Hipsey MR, Bruce LC, Ghisalberti M, Lowe RJ, Gruber, RK, Ruiz-Montoya L, Maxwell PS, Callaghan, DP, Kendrick GA and O'Brien KR (2016). Feedback between sediment and light for seagrass: Where is it important? *Limnology and Oceanography* 61: 1937–1955.

Almroth-Rosell E, Tengberg S, Andersson A, Apler A and Hall POJ (2012). Effects of simulated natural and massive resuspension on benthic oxygen, nutrient and dissolved inorganic carbon fluxes in Loch Creran, Scotland. *Journal of Sea Research* 72: 38–48.

American Public Health Association (1992) APHA standard methods for the examination of water and wastewater. Standard methods for the examination of water & wastewater. Washington, DC: American Public Health Association.

Anderson MJ, Gorley RN and Clarke KR (2008). PERMANOVA+ for PRIMER: Guide to Software and Statistical Methods. PRIMER-E, Plymouth, UK.

ANZG., 2018. Australian and New Zealand Guidelines for Fresh and Marine Water Quality. Australian and New Zealand Governments and Australian state and territory governments, Canberra ACT, Australia. Available at www.waterquality.gov.au/anz-guidelines.

Azzoni R, Giordani G, Bartoli M, Welsh DT and Viaroli P (2001). Iron, sulphur and phosphorus cycling in the rhizosphere sediments of a eutrophic *Ruppia cirrhosa* meadow (Valle Smarlacca, Italy). *Journal of Sea Research* 45(1), 15-26.

Bailey MC and Hamilton DP (1997). Wind induced sediment resuspension: A lake wide model. *Ecological Modelling* 99(2-3), 217-228.

Barrón C, Marbé N, Terrados J, Kennedy, H and Duarte, CM (2004). Community metabolism and carbon budget along a gradient of seagrass (Cymodocea nodosa) colonization. *Limnology and Oceanography* 49(5), 1642-1651.

Bennett WW, Teasdale PR, Welsh DT, Panther JG and Jolley DF (2012). Optimization of colorimetric DET technique for the *in situ*, two-dimensional measurement of iron (II) distributions in sediment porewaters. *Talanta* 88, 490-495.

Blaabjerg V, Mouritsen KN and Finster K (1998). Diel cycles of sulphate reduction rates in sediments of a Zostera marina bed (Denmark). *Aquatic Microbial Ecology* 15(1), 97-102.

Blott SJ and Pye K (2001). GRADISTAT: A grain size distribution and statistics package for analysis of unconsolidated sediments. *Earth Surface Processes and Landforms* 26: 1237–1248.

Bon M, Grall J, Gusmao JB, Fajardo M, Harrod C and Pacheco AS (2021). Functional changes in benthic macrofaunal communities along a natural gradient of hypoxia in an upwelling system. *Marine Pollution Bulletin*. 164: 112056. https://doi.org/10.1016/j.marpolbul.2021.112056.

Borum J, Sand-Jensen K, Binzer T, Pedersen O and Greve TM (2007). Oxygen Movement in Seagrasses. In: Seagrasses: biology, ecology and conservation. Springer, Dordrecht. https://doi.org/10.1007/978-1-4020-2983-7_10.

Bosch J, J Cornwell and Kemp W (2015). Short-term effects of nereid polychaete size and density on sediment inorganic nitrogen cycling under varying oxygen conditions. *Marine Ecology Progress Series* 524: 155–169.

Chen JJ, Erler DV, Wells NS, Huang J, Welsh DT and Eyre BD (2021). Denitrification, anammox, and dissimilatory nitrate reduction to ammonium across a mosaic of estuarine benthic habitats. *Limnology and Oceanography* 66(4), 1281-1297.

Clarke KR, Gorley RN, Somerfield PJ and Warwick RM (2014). Change in Marine Communities: An Approach to Statistical Analysis and Interpretation, 3rd edition. PRIMER-E Ltd, Plymouth, UK.

Cline JD (1969). Spectrophotometric determination of hydrogen sulfide in natural waters 1. *Limnology and Oceanography* 14(3), 454-458.

Connell EL, Colmer TD and Walker DI (1999). Radial oxygen loss from intact roots of Halophila ovalis as a function of distance behind the root tip and shoot illumination. *Aquatic Botany* 63(3), 219-228.

Davison W, Fones GR and Grime GW (1997). Dissolved metals in surface sediment and a microbial mat at 100-µm resolution. *Nature* 387(6636), 885-888.

Davison W, Grime G, Morgan J and Clarke K (1991). Distribution of dissolved iron in sediment pore waters at submillimetre resolution. *Nature* 352(6333), 323-325.

Dittmann S, Baring R, Baggalley S, Cantin A, Earl J, Gannon R, Keuning J, Mayo A, Navong N, Nelson M, Noble W and Ramsdale T (2015). Drought and flood effects on macrobenthic communities in the estuary of Australia's largest river system. *Estuarine, Coastal and Shelf Science* 165, 36-51. https://doi.org/10.1016/j.ecss.2015.08.023

Dittmann S, Rolston A and Baring R (2018). Estuarine and Lagoon Macro-Invertebrates- Patterns and Processes. In: Mosley, L., Ye., Q., Shepherd, S., Hemming, S., Fitzpatrick, R., eds. Natural History of the Coorong, Lower Lakes, and Murray Mouth Region (Yarluwar-Ruwe). Royal Society of South Australia. https://doi.org/10.20851/natural-history-cllmm-3.4.

Dunn RJ, Robertson D, Teasdale PR, Waltham NJ and Welsh DT (2013). Benthic metabolism and nitrogen dynamics in an urbanised tidal creek: Domination of DNRA over denitrification as a nitrate reduction pathway. *Estuarine, Coastal and Shelf Science* 131, 271-281.

Dunn RJ, Welsh DT, Jordan MA, Waltham NJ, Lemckert CJ and Teasdale PR (2012). Benthic metabolism and nitrogen dynamics in a sub-tropical coastal lagoon: microphytobenthos stimulate nitrification and nitrate reduction through photosynthetic oxygen evolution. *Estuarine, Coastal and Shelf Science* 113, 272-282.

Dzialowski AR, Wang SH, Lim NC, Beury JH and Huggins DG (2008). Effects of sediment resuspension on algal biomass and nutrient concentrations in reservoirs of the Central Plains. *Lake Reservoir Management* 24: 313–320.

Elgetti Brodersen K, Koren K, Lichtenberg M and Kühl M (2016). Nanoparticle-based measurements of pH and O_2 dynamics in the rhizosphere of Zostera marina L.: effects of temperature elevation and light-dark transitions. *Plant, cell & environment* 39(7), 1619-1630.

Erler DV, Welsh DT, Bennet WW, Meziane T, Hubas C, Nizzoli D and Ferguson AJ (2017). The impact of suspended oyster farming on nitrogen cycling and nitrous oxide production in a sub-tropical Australian estuary. *Estuarine, Coastal and Shelf Science* 192, 117-127.

Ferguson AJ, Gruber R, Potts J, Wright A, Welsh DT and Scanes P (2017). Oxygen and carbon metabolism of Zostera muelleri across a depth gradient–Implications for resilience and blue carbon. *Estuarine, Coastal and Shelf Science* 187, 216-230.

Frederiksen MS and Glud RN (2006). Oxygen dynamics in the rhizosphere of Zostera marina: a two-dimensional planar optode study. *Limnology and Oceanography* 51(2), 1072-1083.

Gacia, E, Duarte CM and Middelburg JJ (2002). Carbon and nutrient deposition in a Mediterranean seagrass (Posidonia oceanica) meadow. *Limnology and Oceanography* 47(1), 23-32.

Grabowski RC, Droppo IG and Wharton G (2011). Erodibility of cohesive sediment: The importance of sediment properties. *Earth-Science Reviews* 105: 101–120.

Håkanson L and Jansson M (1983). Principles of Lake Sedimentology. Springer, Berlin.

Hallett CS, Valesini FJ, Kilminster K, Wells NS and Eyre BD (2019). A rapid protocol for assessing sediment condition in eutrophic estuaries. *Environmental Science: Processes Impacts* 21, 1021. DOI: 10.1039/c9em00141g

Heisterkamp IM, Schramm A, Larsen LH, Svenningsen NB, Lavik B, de Beer D and Stief P (2013). Shell biofilm associated nitrous oxide production in marine molluscs: processes, precursors and relative importance. *Environmental Microbioly* 15:1943-1945.

Huang J, Bennett WW, Welsh DT, Li T and Teasdale PR (2016). Development and evaluation of a diffusive gradients in a thin film technique for measuring ammonium in freshwaters. *Analytica Chimica Acta* 904, 83-91.

Huang J, Franklin H, Teasdale PR, Burford MA, Kankanamge NR, Bennett WW and Welsh DT (2019). Comparison of DET, DGT and conventional porewater extractions for determining nutrient profiles and cycling in stream sediments. *Environmental Science: Processes & Impacts* 21(12), 2128-2140.

Jensen SI, Kühl M, Glud RN, Jørgensen LB and Priemé A (2005). Oxic microzones and radial oxygen loss from roots of Zostera marina. *Marine Ecology Progress Series* 293, 49-58.

Kankanamge NR, Bennett WW, Teasdale PR, Huang J and Welsh DT (2020). A new colorimetric DET technique for determining mm-resolution sulfide porewater distributions and allowing improved interpretation of iron(II) co-distributions. *Chemosphere* 244: 125388.

Kankanamge NR, Bennett WW, Teasdale PR, Huang J and Welsh DT (2017). Comparing *in situ* colorimetric DET and DGT techniques with *ex situ* core slicing and centrifugation for measuring ferrous iron and dissolved sulfide in coastal sediment pore waters. *Chemosphere* 188, 119-129.

Knezovich JP, Steichen DJ, Jelinski JA and Anderson SL (1996). Sulfide tolerance of four marine species used to evaluate sediment and pore-water toxicity. *Bulletin of environmental contamination and toxicology 57*(3), 450-457.

Kristensen E, Penha-Lopes G, Delefosse M, Valdemarsen T, Quintana CO and Banta GT (2012). What is bioturbation? The need for a precise definition for fauna in aquatic sciences. *Marine Ecology Progress Series* 446: 285–302.

Kristensen E (2000). Organic matter diagenesis at the oxic/anoxic interface in coastal marine sediments, with emphasis on the role of burrowing animals. *Hydrobiologia* 426: 1–24.

Krom M, Davison P, Zhang H and Davison W (1994). High-resolution pore-water sampling with a gel sampler. *Limnology and Oceanography* 39(8), 1967-1972.

Lam-Gordillo O, Mosley, LM, Simpson SL, Welsh DT and Dittmann S (2022a). Loss of benthic macrofauna functional traits correlates with changes in sediment biogeochemistry along an extreme salinity gradient in the Coorong lagoon, Australia. *Marine Pollution Bulletin* 174: 113202. https://doi.org/10.1016/j.marpolbul.2021.113202.

Lam-Gordillo O, Huang J, Barceló A, Kent J, Mosley LM, Welsh DW, Simpson SL and Dittmann S (2022b). Restoration of benthic macrofauna promotes biogeochemical remediation of hostile sediments; an *in situ* transplantation experiment in a eutrophic estuarine-hypersaline lagoon system, Australia. Science of the Total Environment.

Langille MG, Zaneveld J, Caporaso JG, McDonald D, Knights D, Reyes JA, Clemente JC, Burkepile DE, Thurber RLV, Knight R, Beiko RG and Huttenhower C (2013). Predictive functional profiling of microbial communities using 16S rRNA marker gene sequences. *Nature biotechnology*, *31*(9), 814-821.

Lohrer AM, Thrush SF and GibbsM MM (2004). Bioturbators enhance ecosystem function through complex biochemical interactions. *Nature* 431: 1092– 1095.

McDonald D, Price MN, Goodrich J, Nawrocki EP, DeSantis TZ, Probst A, Andersen GL, Knight R and Hugenholtz P (2012). An improved Greengenes taxonomy with explicit ranks for ecological and evolutionary analyses of bacteria and archaea. *The ISME journal*, *6*(3), 610-618.

Mermillod-Blondin F and Rosenberg R (2006). Ecosystem engineering: the impact of bioturbation on biogeochemical processes in marine and freshwater benthic habitats. *Aquatic Science* 68: 434-442.

Moriarty D, Iverson R and Pollard P (1986). Exudation of organic carbon by the seagrass Halodule wrightii Aschers. and its effect on bacterial growth in the sediment. *Journal of Experimental Marine Biology and Ecology* 96(2), 115-126.

Mosley LM, Ye Q, Shepherd S, Hemming S and Fitzpatrick R (2018). Natural History of the Coorong, Lower Lakes, and Murray Mouth Region (Yarluwar-Ruwe). Royal Society of South Australia. https://doi.org/10.20851/natural-history-cllmm-3.4.

Mosley LM, Priestley S, Brookes J, Dittmann S, Farkaš J, Farrell M, Ferguson AJ, Gibbs M, Hipsey M, Huang J, Lam-Gordillo O, Simpson SL, Teasdale PR, Tyler JJ, Waycott M and Welsh DT (2020). Coorong water quality synthesis with a focus on the drivers of eutrophication. Goyder Institute for Water Research Technical Report Series No. 20/10.

Mosley LM, Brookes J, Dittmann S, Huang L, Lam-Gordillo O, Priestley S, Simpson S, Welsh D, and Waycott M (2022). A scientific evaluation to inform nutrient removal options for the Coorong. Goyder Institute for Water Research Technical Report Series No. 22/06.

Newton K, Jeffries TC, Smith RJ, Seymour JR, Seuront L and Mitchell JG (2018). Taxonomic and metabolic shifts in the Coorong bacterial metagenome driven by salinity and external inputs. *Journal of Oceanology and Limnology 36*(6), 2033-2049.

Niemestö J and Lund-Hansen LC (2019). Instantaneous effects of sediment resuspension on inorganic and organic benthic nutrient fluxes at a shallow water coastal site in the Gulf of Finland, Baltic Sea*. Estuaries and Coasts* 42: 2054–2071.

Niemestö J, Kononets M, Ekeroth E, Tallberg P, Tengberg A and Hall POJ (2018). Benthic fluxes of oxygen and inorganic nutrients in the archipelago of Gulf of Finland, Baltic Sea: Effects of sediment resuspension measured *in situ*. *Journal of Sea Research* 135: 95–106.

Nizzoli D, Bartoli M, Cooper M, Welsh DT, Underwood GJ and Viaroli P (2007). Implications for oxygen, nutrient fluxes and denitrification rates during the early stage of sediment colonisation by the *polychaete Nereis spp*. in four estuaries. *Estuarine, Coastal and Shelf Science* 75(1-2), 125-134.

Nizzoli D, Welsh DT, Fano EA and Viaroli P (2006). Impact of clam and mussel farming on benthic metabolism and nitrogen cycling, with emphasis on nitrate reduction pathways. *Marine Ecology Progress Series 315*, 151-165.

O'Meara T, Gibbs E and Trush SF (2017). Rapid organic matter assay of organic matter degradation across depth gradients within marine sediments. *Methods in Ecology and Evolution* 1-9. https://doi.org/10.1111/2041-210X.12894.

Oksanen J, Blanchet FG, Friendly M, Kindt R, Legendre P, McGlinn, et al. (2019). vegan: Community Ecology Package. R package version 2.5-6. https://CRAN.R-project.org/package=vegan.

Pagès A, Welsh DT, Robertson D, Panther JG, Schäfer J, Tomlinson RB and Teasdale PR (2012). Diurnal shifts in co-distributions of sulfide and iron (II) and profiles of phosphate and ammonium in the rhizosphere of Zostera capricorni. *Estuarine, Coastal and Shelf Science* 115, 282-290.

Pant HK and Reddy KR (2001). Phosphorus sorption characteristics of estuarine sediments under different redox conditions. *Journal of Environmental Quality* 30: 1474–1480.

Paton DC, Paton FL and Bailey CP (2015). *Ecological character description for Ruppia tuberosa in the Coorong*. The University of Adelaide, South Australia.

Pedersen MO and Kristensen E (2015). Sensitivity of Ruppia maritima and Zostera marina to sulfide exposure around roots. *Journal of Experimental Marine Biology and Ecology 468*, 138-145.

Pedersen MO, Borum J, Duarte CM and Fortes MD (1998). Oxygen dynamics in the rhizosphere of Cymodocea rotundata. *Marine Ecology Progress Series* 283-288.

Priestley S, Mosley L, Farkas J, Tyler J, Shao Y, Shanafield M, Banks E, Wong WW, and Leyden E (2022a). Sources and transport of nutrients in the Coorong. Goyder Institute for Water Research Technical Report Series No. 22/01.

Priestley SC, Tyler J, Liebelt SR, Mosley LM, Wong WW, Shao Y, Woolston Z, Farrell M, Welsh DT, Brookes JD and Collins AS (2022b). N and C Isotope Variations Along an Extreme Eutrophication and Salinity Gradient in the Coorong Lagoon, South Australia. Front. *Earth Sci*, *9*, 727971.

R Development Core Team (2018). R: a language and environment for statistical computing. R Foundation for Statistical Computing, Vienna, Austria.

Rayment GE and Lyons DJ, (2011). Soil chemical methods: Australasia, 3. CSIRO publishing.

Reese BK, Finneran DW, Mills, HJ, Zhu MX and Morse JW (2011). Examination and refinement of the determination of aqueous hydrogen sulfide by the methylene blue method. *Aquatic geochemistry* 17(4), 567-582.

Remaili TM, Simpson SL and Jolley DF (2017). Effect of enhanced bioturbation intensities on the toxicity assessment of legacy-contaminated sediments. *Environmental Pollution* 226, 335–345. https://doi.org/10.1016/j.envpol.2016.11.038.

Remaili TM, Simpson SL, Bennett WW, King JJ, Mosley LM, Welsh DT and Jolley DF (2018). Assisted natural recovery of hypersaline sediments: salinity thresholds for the establishment of a community of bioturbating organisms. *Environmental Science: process and impacts* 20, 1244-1253. https://doi.org/10.1039/C8EM00092A.

Ritchie RJ (2008). Universal chlorophyll equations for estimating chlorophylls a, b, c, and d and total chlorophylls in natural assemblages of photosynthetic organisms using acetone, methanol, or ethanol solvents. *Photosynthetica* 46:115– 126. https://doi.org/10.1007/s11099-008-0019-7.

Robertson D, Teasdale PR and Welsh DT (2008). A novel gel-based technique for the high resolution, two-dimensional determination of iron (II) and sulfide in sediment. *Limnology and Oceanography: methods* 6(10), 502-512.

Sarkar D (2008). Lattice: Multivariate Data Visualization with R. Springer, New York. ISBN 978-0-387-75968-5.

Schallenberg M and Burns CW (2004). Effects of sediment resuspension on phytoplankton: teasing apart the influences of light, nutrients, and algal entrainment. *Freshwater Biology* 49: 143–159.

Seeberg-Elverfeldt J, Schluter M, Feseker T and Kölling M (2005). Rhizon sampling of porewaters near the sediment-water interface of aquatic systems. *Limnology and Oceanography Methods* 3, 361–371. https://doi.org/10.4319/lom.2005.3.361

Shao Y, Farkas J, Holmden C. Mosley L, Kell-Duivestein I, Izzo C, Reis-Santos P, Tyler J, Torber P, Fryda J, Taylor H, Haynes D, Tibby J and Gillanders BM (2018). Calcium and strontium isotope systematics in the lagoon estuarine environments of South Australia: Implications for water source mixing, carbonate fluxes and fish migration. *Geochimica et Cosmochimica Acta* 239: 90-108. https://doi.org/10.1016/j.gca.2018.07.036

Shao Y, Farkaš J, Mosley L, Tyler J, Wong H, Chamberlayne B, Raven M, Samanta M, Holmden C, Gillanders BM, Kolevica A, Eisenhauer A (2021). Impact of salinity and carbonate saturation on stable Sr isotopes ($\delta^{88/86}$Sr) in a lagoon-estuarine system. *Geochimica et Cosmochimica Acta* 293: 461-476.

Simpson SL, Batley GE and Chariton AA (2013). Revision of the ANZECC/ARMCANZ sediment quality guidelines., Revision of the ANZECC/ARMCANZ sediment quality guidelines), CSIRO Land and Water Science Report 08/07. Lucas Heights, NSW Australia.

Simpson SL and Batley GE (2016). Sediment Quality Assessment: A Practical Guide. CSIRO Publishing, Melbourne, Victoria. 359 pp.Gee and Bauder (1986) in Methods of Soil Analysis. Part 1 Agron. Monogr. 9 (2nd Ed). Klute, A., American Soc. of Agronomy Inc., Soil Sci. Soc. America Inc., Madison WI: 383-411.

Skinner D (2011). Sediment resuspension during declining water levels in Lake Alexandrina. PhD Thesis, The University of Adelaide, South Australia.

Stief P (2013). Stimulation of microbial nitrogen cycling in aquatic ecosystems by benthic macrofauna: mechanisms and environmental implications. *Biogeosciencs* 10: 2829–2846. https://doi.org/10.5194/bgd-10-11785-2013.

Sullivan L, Ward N, Toppler N and Lancaster G. (2018). National acid sulfate soils guidance: national acid sulfate soils identification and laboratory methods manual, Department of Agriculture and Water Resources, Canberra, ACT. CC BY 4.0.

Tweedley JR, Warwick RM, Valesini FJ, Platell ME and Potter IC (2012). The use of benthic macroinvertebrates to establish a benchmark for evaluating the environmental quality of microtidal, temperate southern hemisphere estuaries. *Marine Pollution Bulletin* 64, 1210–1221.

Volkenborn N, Meile C, Polerecky L, Wethey, DS and Woodin, SA (2012). Intermittent bioirrigation and oxygen dynamics in permeable sediments: An experimental and modelling study of three tellenid bivalves. *Journal of Marine Research* 70: 794-823. https://doi.org/10.1357/002224012806770955

Welsh DT (2003). It's a dirty job but someone has to do it: the role of marine benthic macrofauna in organic matter turnover and nutrient recycling to the water column. *Chemistry and Ecology* 19: 321−342. https://doi.org/10.1080/0275754031000155474

Welsh DT, Bartoli M, Nizzoli D, Castaldelli G, Riou SA and Viaroli P (2000). Denitrification, nitrogen fixation, community primary productivity and inorganic-N and oxygen fluxes in an intertidal Zostera noltii meadow. *Marine Ecology Progress Series* 208, 65-77.

Welsh DT and Castadelli G (2004). Bacterial nitrification activity directly associated with isolated marine animals. *Marine Biology* 144, 1029–1037.

Wyness AJ, Fortune I, Blight AJ, Browne P, Hartley M, Holden M, and Paterson DM (2021). Ecosystem engineers drive differing microbial community composition in intertidal estuarine sediments. PlOS One 16: e0240952. https://doi.org/10.1371/journal.pone.0240952

GOYDER INSTITUTE FOR WATER RESEARCH

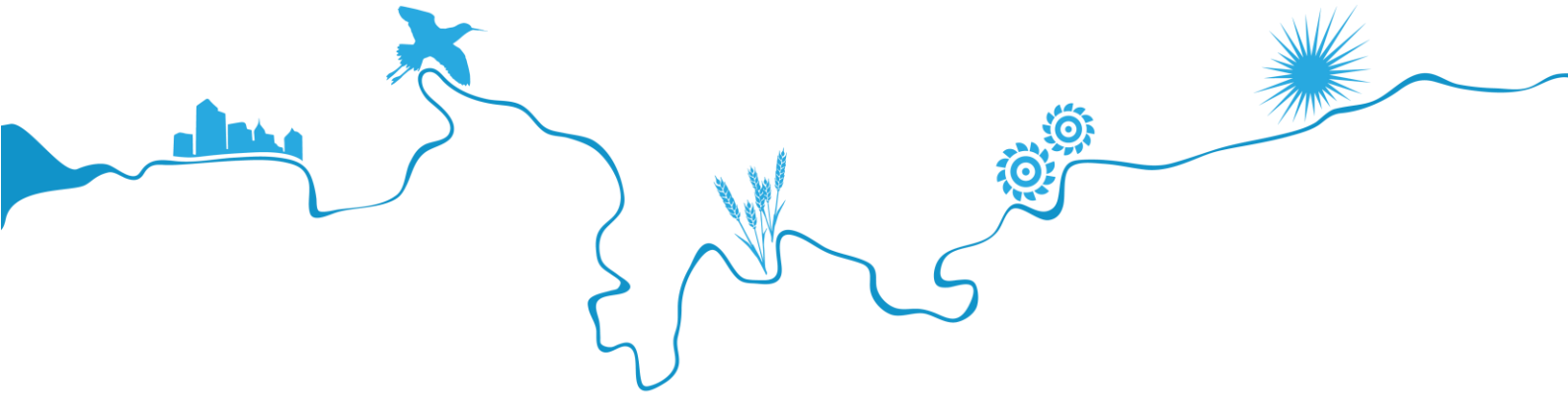

Government of South Australia
Department for Environment and Water

CSIRO

Flinders University

THE UNIVERSITY of ADELAIDE

University of South Australia

The Goyder Institute for Water Research is a research alliance between the South Australian Government through the Department for Environment and Water, CSIRO, Flinders University, the University of Adelaide and the University of South Australia.